THE CONDUCTIVITY, DIELECTRIC CONSTANT, MAGNETORESISTIVITY, 1/*f* NOISE AND THERMOELECTRIC POWER IN PERCOLATING RANDOM GRAPHITE--HEXAGONAL BORON NITRIDE COMPOSITES

JUNJIE WU

A thesis submitted to the Faculty of Science, University of the Witwatersrand, Johannesburg, in partial fulfilment of the requirements for the degree of Doctor of Philosophy.

Johannesburg, January 1997

DECLARATION

I DECLARE THAT THIS THESIS IS MY OWN, UNAIDED WORK. IT IS BEING SUBMITTED FOR THE DEGREE OF DOCTOR OF PHILOSOPHY IN THE UNIVERSITY OF THE WITWATERSRAND, JOHANNESBURG. IT HAS NOT BEEN SUBMITTED BEFORE FOR ANY DEGREE OR EXAMINATION IN ANY OTHER UNIVERSITY

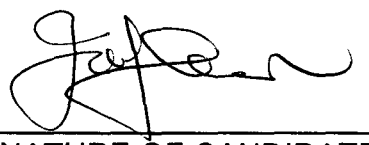

(SIGNATURE OF CANDIDATE)

23 DAY OF January 1997

ACKNOWLEDGMENTS

I would like to express my sincere thanks to my supervisor, Professor David S. McLachlan, for providing support, guidance and encouragement. I owe special thanks to Dr. A. Albers, not only for helpful discussions and suggestions, but also for his assistance in set-up the data acquisition system and in writing the computer program for the magnetoresistance and Hall coefficient measurements. I am particularly grateful to Professors M. J. R. Hoch and J. D. Comins for their constant support in the Physics Department.

I wish to extend my thanks to many people who helped me to produce this thesis. Mr. A. Voorvelt and Mr. C. J. Sandrock contributed to the design and construction of electronic circuits and apparatus used in this project. The staff of the mechanical workshop in the Physics Department produced numerous pieces of experimental apparatus. Professor L. Schöning assisted in the interpretation of the X-ray results, obtained by Mrs. J. Salemi. Professor Harahan of the Electrical Engineering Department lent me the HP3562A signal analyzer that made the $1/f$ noise experiments possible. Professor M. H. Moys and Mr. M. Van Nierop of the Chemical Engineering Department made the results of grain size distributions available. Professor D. Chandler of the Mechanical Engineering Department assisted with the work on the universal testing machine. Many of the figures in chapter three have benefitted from the excellent artwork of R. Smith. Fellow students Mr. D. Dube and Mr. C. Chiteme helped me to prepare the powder samples for some grain shape experiments on the scanning electron microscope, and to correct grammar and punctuation.

Most of all, however, I wish to express my deep gratitude to my wife Sijia and my daughter Tianshu. Without their indispensable support, tireless enthusiasm, and great patience through the years of this project, none of the works presented in this thesis would have been possible.

ABSTRACT

Percolation phenomena involving the electrical conductivity, dielectric constant, Hall coefficient, magnetoconductivity, relative magnetoresistivity, $1/f$ noise and thermoelectric power are investigated in graphite (G) and hexagonal boron-nitride (BN) powder mixtures. Two kinds of systems are used in the experiments: highly compressed discs and parallelepipeds, cut from these discs, as well as 50%G-50%BN and 55%G-45%BN powder mixtures undergoing compression.

The measured DC conductivities follow the power-laws $\sigma(\phi,0) \propto (\phi-\phi_c)^t$ $(\phi > \phi_c)$ and $\sigma(\phi,0) \propto (\phi_c-\phi)^{-\bar{s}}$ $(\phi < \phi_c)$, and the low frequency (100Hz & 1000Hz) dielectric constant varies as $\varepsilon(\phi,\omega \approx 0) \propto (\phi_c - \phi)^{-s}(\phi < \phi_c)$, where ϕ_c is the percolation threshold, t and $\bar{s}$ are the conductivity exponents, and s is the dielectric exponent. Near the percolation threshold and at high frequencies, the AC conductivity varies with frequency as $\sigma(\phi,\omega) \propto \omega^x$ and the AC dielectric constant varies as $\varepsilon(\phi,\omega) \propto \omega^{-y}$, where the exponents x and y satisfy the scaling relation $x + y = 1$. The crossover frequency ω_c scales with DC conductivity as $\omega_c \propto \sigma^q(\phi,0)$ $(\phi > \phi_c)$, while on the insulating side, $\omega_c \simeq 1$, resulting in $q \simeq 0$ for the three G-BN systems. The loss tangent $\tan\delta(\phi,\omega)$ $(\phi < \phi_c)$ is found to have a global minimum, in contrary to the results of computer simulations.

The Hall constant could not be measured using existing instrumentation. The measured magnetoconductivity and relative magnetoresistivity follow the power-laws $-\triangle\sigma \propto (\phi - \phi_c)^{3.08}$ and $\triangle R/R \propto (\phi - \phi_c)^{0.28}$ respectively. These two exponents,

3.08 and 0.28, are not in agreement with theory.

The $1/f$ noise was measured for the conducting discs and parallelepipeds. The normalized $1/f$ noise power varies as $S_V/V^2 \propto R^w$ with the exponents $w = 1.47$ and 1.72 for the disc and parallelepiped samples respectively. Furthermore, the normalized noise power near the percolation threshold is, for the first time, observed to vary inversely with the square-root of sample volume.

Based on the Milgrom-Shtrikman-Bergman-Levy (MSBL) formula, thermoelectric power of a binary composite is shown to be a linear function of the Wiedeman-Franz ratio. A scaling scheme for the Wiedeman-Franz ratio for percolation systems is proposed, which yields power-law behavior for the thermoelectric power. The proposed power-laws for the thermoelectric power can be written as $(S_m - M_1) \propto (\phi - \phi_c)^{h_1}$ for $\phi > \phi_c$ and as $(S_m - M_1) \propto (\phi_c - \phi)^{-h_2}$ for $\phi < \phi_c$, where S_m is the thermoelectric power for the composites, M_1 is a constant for a given percolation system, and h_1 and h_2 are the two critical exponents. The experimental thermoelectric power data for the G-BN conducting parallelepipeds was fitted to the above power-law for $\phi > \phi_c$. A least squares fit yielded the exponent $h_1 = -1.13$ and parameter M_1=9.51$\mu V/K$ respectively.

Contents

List of the Figures

List of the Tables

Chapter 1

INTRODUCTION

Percolation theory deals with both macroscopically and microscopically disordered systems. The origin of percolation theory is attributed to Broadbent and Hammersley (1957), who introduced lattice models for the flow of a fluid through a static random medium, and showed, using geometrical and probabilistic concepts, that no fluid will flow if the concentration of active medium is smaller than some nonzero threshold value — a percolation threshold. Since the 70s, percolation models have involved the concepts of scaling, which emphasizes particularly the so-called critical phenomena. Percolation theory has become one of few theoretical techniques that is available to describe strongly disordered materials.

Percolation theory is marked by the fact that it provides a well-defined, simple, and intuitively satisfying model for granular binary composites, in which the relevant physical properties of the individual components differ widely. To be specific, consider compacted random binary mixtures of conducting (metallic) and insulating (dielectric) components, for which only an average grain size and overall composition are known. Then, if the concentration of dielectric is not too large, electrons can move through the sample via an "infinite" metallic cluster, resulting in conducting sample. As the dielectric concentration increases the infinite metallic cluster becomes less dense, and eventually breaks into isolated clusters embedded in dielectric matrix, resulting in insulating sample. Denoting the volume fraction of the conducting

component in the sample by ϕ, percolation theory predicts that there is a critical value fraction ϕ_c, called a percolation threshold, at which an infinite metallic cluster spanning whole sample first appears, and the system undergoes a percolative metal-insulator transition (MIT). This percolation transition is the most fundamental and striking feature of the percolation model, and makes percolation a natural model for describing a diversity of physical processes.

In many aspects, the percolation transition is an analogue of second order phase transition in thermodynamic systems. Near the percolation threshold, the percolation quantity Q follows a power-law given by

$$Q \propto |\phi - \phi_c|^{\alpha}, \tag{1.1}$$

where α is a critical exponent characterizing the asymptotic behavior of Q as ϕ_c is approached from below or above. Scaling laws relate the different exponents which occur in a given percolation system, which means that the critical exponents appeared in a percolation system are not independent of each other. The exponent α can be positive or negative depending on what physical property is under study in the percolation system. The values of α, found from computer simulations, are dependent only on the dimensionality of system [Stauffer and Aharony 1994]. Exponents of this nature are described as universal. Recent experimental and theoretical results show that, in three dimensional continuum systems, the values of the same exponent could differ considerably from system to system[Carmona et al. 1984, Kogut and Straley 1979, Feng et al. 1987, Balberg 1987a, and Nan 1993 and references therein]. It has been shown that the particle size distribution, shape and orientation can influence the percolation threshold ϕ_c [Kusy 1977, Balberg 1987b, and Dovzhenko and Zhirkov 1995]. Note that the power-law (1.1) is expected to hold only close to the percolation threshold and then only if the investigated physical properties of the two components are drastically different. If it is not the case, a variety of effective-medium theories can be employed to model the properties of the composites.

The electrical transportation properties which have been studied experimentally on continuum percolation systems include: electrical conductivity, dielectric constant, $1/f$ noise, Hall constant, magnetoconductivity, and thermoelectric power (thermopower). In addition the critical current density and critical field have also been investigated, using a percolation approach, for inhomogeneous superconductors [Deutscher and Rappaport 1979; Grave, Deutscher and Alexander 1982]. For percolation systems, the electrical conductivity and the dielectric constant are the most extensively studied quantities. Some of the continuum percolation systems that have been previously investigated include: amorphous carbon-teflon composites [Song et al. 1986], carbon-epoxy composites [McLachlan et al. 1990, Lee et al. 1993], nickel-polypropylene composites [Chen and Johnson 1991], carbon-wax mixtures [Chen and Chou 1985; Chou and Jaw 1988; Chakrabarty et al. 1993], carbon-polymer composites [Michels et al. 1989], carbon-PVC composites [Balberg and Bozowski 1982], polyethylene gels-conducting polymer system [Fizazi et al. 1990], carbon fibers-polymer composites [Carmona et al. 1984], Ag-KCl composites [Grannan et al. 1981], glass-iron balls mixtures [Benguigui 1985], plain and silver-coated glass microbead mixtures [Laugier 1982, Laugier et al. 1986], glass-In mixtures [Lee et al. 1986], $PrBa_2Cu_3O_7$-Ag composites [Lin 1991], sintered silver beams [Deptuck et al. 1985], thin gold films [Laibowitz and Gefen 1984; Hundley and Zettl 1988], granular Sn-Ar films [Rohde and Micklitz 1989], thick bismuth ruthenate films [Nitsch et al. 1990], thick glass-RuO_2 films [Pike 1978], and microemulsions [Van Dijk 1985, Van Dijk et al. 1986, Moha-Ouchane et al. 1987, Peyrelasse et al. 1988, and Clarkson and Smedley 1988].

The Hall constants of only two percolation systems has been studied: Al-Ge films [Dai et al. 1987] and Sn-Ar films [Rohde and Micklitz 1989]. The latter reference also reported the investigation of the magnetoconductivity and relative magnetoresistivity.

The $1/f$ noise is a sensitive probe of the microstructure of the infinite clusters in percolation systems [Rammal, Tannous and Tremblay 1985]. Percolation systems, in which $1/f$ noise has been investigated, include: carbon-wax mixtures [Chen and Chou 1985], copper particle-polymer composites [Pierre et al. 1990], Al_2O_3-Pt cer-

mets [Mantese and Webb 1985 and Mantese et al. 1986], thin gold films [Williams and Burdett 1969 and Koch et al. 1985], silver films [Octavio et al. 1987], thin Al, In, and Cr foils [Garfunkel and Weissman 1985], and AgPt-TFE mixtures [Rudman et al. 1986].

The percolation behavior of the thermoelectric power in Al-Ge films was investigated by Hurvits et al. (1993).

The experimental results obtained from the above-mentioned continuum percolation systems have verified many aspects of percolation theory and provide a significant experimental data for the application of percolation models. However, some discrepancies between theory and experiment still exist, and, therefore more experiments are necessary to further advance the development of theoretical models, especially for non universal exponents.

It should be noted that in most previous studies of a single continuum percolation system only one or two of the physical percolation properties were measured, discussed, and compared with other experimental results and theoretical predictions. In many cases, other percolation phenomena could have been measured on the same system. This situation makes it difficult to compare and correlate the different exponents that have been obtained from experiments done on various percolation systems. It should also be noted that for the Hall coefficient, magnetoresistivity and thermoelectric power only one or two previous sets of experimental data are available.

The primary objective of the study presented in this thesis is to observe as many of these percolation phenomena as possible in a single reliable continuum percolation system. The measured critical exponents and percolation thresholds are then used to, where possible, test various theoretical models and the exponents are compared with those obtained from other previous experiments. This full spectra of critical exponents, all from the same system, should help to provide a more complete understanding of percolation theory.

Various mixtures of graphite (G) and hexagonal boron-nitride (BN) powders, undergoing compression in the appropriate cell, compacted discs and the parallelepipeds cut from these discs, were chosen as the subject of this study. In these systems the graphite powder is the conducting component, while the hexagonal boron-nitride is the insulating component. The reasons for choosing these systems are as follows. Firstly, the insulating and conducting components have a very small conductivity ratio $\approx 1\times10^{-17}$. Secondly, they have the same densities, 2.25g/cm^3, and nearly the same unit hexagonal cell dimensions at room temperature: $a = b = 2.464$Å and $c = 6.736$Å for graphite, while $a = b = 2.504$Å and $c = 6.661$Å for hexagonal boron-nitride [Lide 1994] . These properties made the two components indistinguishable by the usual X-ray methods and easy to mix together to form random composites. Thirdly, single crystals of G and BN show very similar stress-strain relationships along either the c-axis or the a-b layer planar [Lynch and Drickamer 1966]. These properties of two components appear to make the G-BN powder mixtures nearly ideal percolation systems, on which the critical volume fractions and many of the exponents that appear in the percolation equations can be measured.

No previous investigation on the G-BN percolation systems has been reported in the literature. Phenomena studied at room temperature include the DC conductivity, AC conductivity and dielectric constant, magnetoconductivity or relative magnetoresistivity, $1/f$ noise and thermoelectric power. It was not possible to measure the Hall coefficient at room temperature or at liquid nitrogen temperature.

In Chapter two the various theoretical percolation equations, relevant to the measurements made on the G-BN percolation systems, are presented. The topics include the geometric phase transition, where the basic concepts and elementary results are introduced, the percolation equations for the various electrical transportation properties, $1/f$ noise and thermoelectric power for a binary continuum medium, as well as recent progresses in the understanding of the nonuniversality of the critical exponents. Chapter three describes the experimental techniques and apparatus used in this study. The results for the disc porosity, grain orientation, grain size distribution,

and the comparative strength of the interparticle bonds are given here. The various powder cells employed for measuring the DC and AC conductivities and dielectric constant in the axial (along the direction of compression) and transverse (perpendicular to the direction of compression) directions for 50%G-50%BN and 55%G-45%BN powders and powder pouring methods are described in detail. The principles of measurement, schematic diagrams and electrical circuits are given for the apparatus and techniques used to measure the electrical conductivity, dielectric constant, Hall constant, magnetoconductivity, $1/f$ noise and thermoelectric power. Chapter four presents the experimental results of the electrical conductivity, dielectric constant and magnetoconductivity. Chapter five presents the experimental $1/f$ noise results obtained from the compressed conducting disc and parallelepiped samples near the percolation threshold. In Chapter six, power-laws to describe the Wiedeman-Franz ratio in continuum percolation systems are proposed, which in turn lead to new power-laws for the thermoelectric power near the percolation threshold. Measured thermoelectric power data for the G-BN parallelepipeds, on the conducting side of percolation threshold, is presented and fitted using one of the new power-laws for the thermoelectric power, developed in this chapter. In all cases, the experimental results are illustrated using a large number of graphs, while the observed or fitted parameters, obtained from various theoretical expressions, namely the critical volume fractions and exponents, are given in tables or the text where appropriate. Where possible, comparisons between the present experimental results and those obtained from other continuum percolation systems are made. Chapter seven of the thesis summarizes and discusses the main results, and makes several suggestions for the further investigations.

In order to look for signs of weak localization near percolation threshold, the temperature dependences of the resistances were studied using conducting G-BN parallelepipeds at temperatures from 1.8K to 300K, using a DIP system [Albers 1994]. Some of these samples, which had ϕ values very near the percolation threshold, were also measured at temperatures from 1.4K to 30K and in magnetic fields up to 8.5T. Since these experimental results were inconclusive, they are not included in this thesis.

Chapter 2

THEORY

2.1 Introduction

This chapter deals with the percolation theory of a number of phenomena in heterogeneous conductor-insulator composites. A fairly complete overview of the theoretical developments in this field is given. Some relevant numerical and experimental results will also be discussed in this section, but only when it is necessary to prove or to supplement the line of the theoretical arguments.

Since the 70s, percolation theory and its applications have been the subject of a large number of review articles and some books. Some of the review articles quoted here in chronological order are by Kirkpatrick (1973), Essam(1980), Deutscher et al. (Ed., 1983), Clerc et al. (1990), Bergman and Stroud(1992), and Nan (1993). Stauffer and Aharony's revised textbook (1994) provides the most recent complete review of geometrical aspects of the percolation problem, with emphasis on cluster statistics, renormalization group techniques, and numerical algorithms.

This chapter is organized as follows. Section 2.2 contains a detailed presentation of the geometrical percolation problem, with emphasis on the critical exponents and scaling laws. Section 2.3 presents the application of percolation theory to the measurements of various physical quantities measured in this thesis, and again emphasizes

the critical volume fraction and the existence of scaling laws. The microstructures leading to different ϕ_cs are presented first. The percolation equations, describing the electrical conductivity, dielectric constant, magnetoresistance, Hall coefficient, $1/f$ noise, and thermoelectric power, are then discussed. In addition, the GEM equation, which interpolates between the two percolation equations, is discussed in this section. The chapter ends with Section 2.4, in which the current models accounting for the nonuniversality of the conductivity exponent are reviewed.

2.2 Geometric Percolation

The geometric phase transition can be studied, either as a bond or as a site percolation problem. The bond percolation problem may always be converted into its dual site percolation problem [Fisher, 1961]. The converse is however not true: not every site percolation problem corresponds to a bond percolation problem. For this reason, the site process is considered to be more fundamental. In this section, the basic concepts and elementary results of geometric percolation are illustrated using the site percolation model, which is also the most appropriate one for continuum systems.

A site percolation system, using a 50×50 square lattice, is shown in Fig. 2.1. Each site is occupied (black squares) at random with probability p or empty (white squares) with the complementary probability (1-p). The neighboring squares are called **nearest neighbours** if they have one side in common but not if they touch only at one corner. A group of occupied squares, connected through nearest neighbours, is called a cluster. A s-site cluster is a cluster containing s sites. When p is small, most occupied squares are isolated or form very small clusters. The occupied squares become more interconnected and form larger clusters as p is increased. At **percolation threshold** p_c, an infinite cluster spanning the entire lattice appears. For all $p < p_c$, there is no infinite cluster, and for $p > p_c$ the infinite cluster co-exists with smaller finite clusters, which join the infinite one as p is further increased.

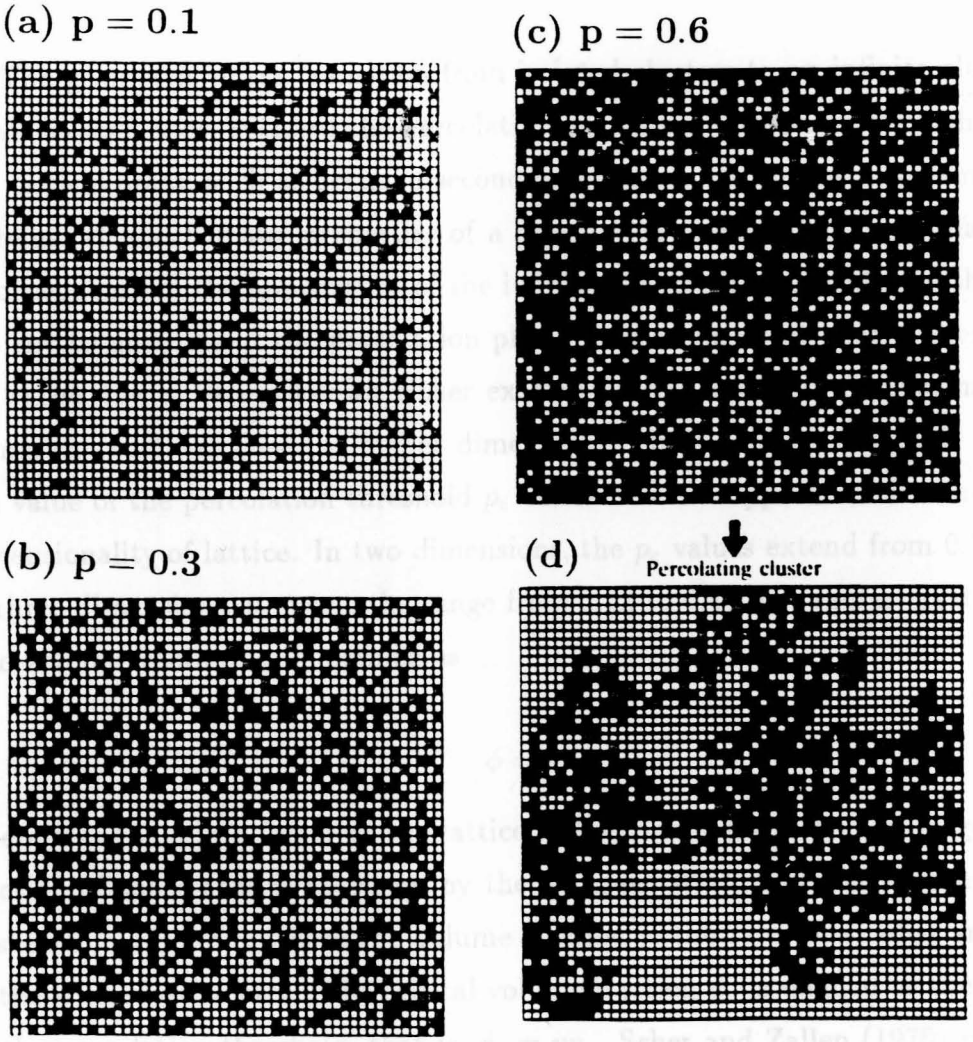

Fig. 2.1 Percolation network on a 50×50 square lattice for three values of p is shown in the figures. Occupied and empty sites are represented by black and white squares, respectively. The 'infinite' (percolating) cluster near the percolation threshold p_c =0.59 is also shown. The arrow indicates that (d) is obtained from (c) by deleting all clusters except for the percolating one. (Reproduced from Smilauer 1991)

The geometric phase transition from isolated clusters to an infinite cluster, plus small isolated ones, is called the percolation transition. The percolation threshold p_c is a critical point, such as occur in second-order phase transitions in thermodynamic systems, at which many properties of a percolation system change dramatically, as a consequence of the appearance of the infinite cluster. The percolation threshold is the key to understand the percolation phenomena of many physical systems. Table 2.1 shows the p_c values known either exactly (in one and two dimensions) or from numerical work (in three or higher dimensions). It is evident from this table that the value of the percolation threshold p_c varies with the type of lattice and with the dimensionality of lattice. In two dimensions, the p_c values extend from 0.35 to 0.70; in three dimensions, p_c spans the range from 0.12 to 0.43 for regular crystal lattices. The volume fraction, ϕ, is defined as

$$\phi = vp, \tag{2.1}$$

where v is the filling factor of the lattice. The volume fraction ϕ is, in general, the fraction of space that is taken up by the occupied sites. The two dimensional case is shown in Fig. 2.1, where the volume fraction is the ratio of shaded area to that of the whole lattice area. The critical volume fraction ϕ_c is defined as the value of ϕ at the percolation threshold, that is, $\phi_c = vp_c$. Scher and Zallen (1970) pointed out that ϕ_c, in contrast to p_c, is remarkably insensitive to lattice structures with the same dimensionality. This is seen by comparing the fourth and eighth columns of Table 2.1. To within a few percent, the critical area or volume fraction for site percolation is 0.45 in two dimensions and 0.16 in three dimensions. The approximate dimensional invariance of the critical volume fraction ϕ_c suggests that ϕ_c is a more fundamental quantity than p_c, in site lattice percolation problems. For this reason, p_c is used only to present lattice percolation models, while ϕ_c will be used in all future discussions on continuum percolation systems, both theoretical and experimental.

In addition to the percolation threshold p_c or critical volume fraction ϕ_c, six other basic quantities or concepts are used to describe the geometrical properties and

Table 2.1 The bond (p_c^{bond}) and site (p_c^{site}) percolation thresholds on a variety of lattices (after Zallen 1983).

Dimensionality d	*Lattice or Structure*	p_c^{bond}	p_c^{site}	*Coordination z*	*Filling Factor v*	zp_c^{bond}	$vp_c^{site} \equiv \phi_c$
1	Chain	1	1	2	1	2	1
2	Triangular	0.3473	0.5000	6	0.9069	2.08	0.45
2	Square	0.5000	0.593	4	0.7854	2.00	0.47
2	Kagomé	0.45	0.6527	4	0.6802	1.80	0.44
2	Honeycomb	0.6527	0.698	3	0.6046	1.96	0.42
						2.0 ± 0.2	0.45 ± 0.03
3	fcc	0.119	0.198	12	0.7405	1.43	0.147
3	bcc	0.179	0.245	8	0.6802	1.43	0.167
3	sc	0.247	0.311	6	0.5236	1.48	0.163
3	Diamond	0.388	0.428	4	0.3401	1.55	0.146
						1.5 ± 0.1	0.16 ± 0.02
4	sc	0.160	0.197	8	0.3084	1.3	0.061
4	fcc		0.098	24	0.6169		0.060
5	sc	0.118	0.141	10	0.1645	1.2	0.023
5	fcc		0.054	40	0.4653		0.025
6	sc	0.094	0.107	12	0.0807	1.1	0.009

statistics of clusters in a percolation lattice [Stauffer and Aharony 1994, and references therein]. These additional concepts are: the correlation length, cluster size, order parameter, density-density correlation function, scaling law and universality, and fractal structures. Before discussing these six concepts, the distribution function of cluster size should be introduced.

The cluster number n_s is defined as the density of finite clusters, consisting of s occupied and connected sites. It is nothing but the number of such clusters per unit volume in the thermodynamic limit [Clerc et al. 1990]. Near the percolation threshold p_c, the distribution of cluster numbers is assumed to follow the scaling form

$$n_s(p) \propto s^{-\varsigma} f(z), \tag{2.2}$$

where $z = |p - p_c|\, s^{\eta}$, ς and η are both critical indices, and $f(z)$ is a universal scaling function, where $f(0) = 1$. Equation (2.2) is fundamental in the scaling theory of percolation phenomena, as will be seen below. Consider the k-th moment of the site number s in a cluster, which is given by $\sum_s s^k n_s$. For p near p_c, the singular part of this k-th moment can be calculated by replacing the sum with an integration. This replacement is valid since only large clusters are responsible for singularity. Direct calculation [Stauffer and Aharony 1994] yields

$$\sum_s s^k n_s = \int_0^\infty s^k n_s ds = q_o \int_0^\infty s^{k-\varsigma} f\left[|p - p_c|\, s^{\eta}\right] ds$$

$$= \frac{q_o}{\eta} |p - p_c|^{(\varsigma-1-k)/\eta} \int_0^\infty |z|^{(1+k-\varsigma)/\eta} z^{-1} f(z) dz, \tag{2.3}$$

Evaluation of the integral on the right-hand side of the above equation gives

$$\sum_s s^k n_s \propto |p - p_c|^{(\varsigma-1-k)/\eta}. \tag{2.4}$$

(1) **The correlation length ξ**

Mathematical calculations show that the correlation length measures the mean distance between two sites belonging to the same cluster, which contributes to the divergences of the k-th moment of the site number. As the percolation threshold is approached, large clusters join, becoming larger and larger, and the correlation length diverges according to the power-law

$$\xi \propto |p - p_c|^{-\nu}, \tag{2.5}$$

where ν is a constant. ξ is measured in units of the site length a_o, implying that the correlation length is actually $a_o\xi$. Computer simulations [See Table I of Harris 1983] yield ν=1.35 and 0.88 in two and three dimensions respectively.

(2) **The cluster size**

The number of sites within the largest cluster near p_c is s_ζ, which diverges as

$$s_\zeta \propto |p - p_c|^{-1/\eta}. \tag{2.6}$$

The average size $s_{av.}$of the clusters near p_c, derived from Equation (2.4), is

$$s_{av.} = \frac{\sum_s s n_s}{\sum_s n_s} \propto |p - p_c|^{-\gamma}, \tag{2.7}$$

where γ is an exponent.

(3) **The order parameter $\mathbf{P}_\infty$**

$\mathbf{P}_\infty$ is defined as the probability that any occupied site, chosen at random, belongs to the infinite cluster. At $p < p_c$ there is no infinite cluster and $P_\infty = 0$; at $p = 1$, all sites are connected together, therefore $P_\infty = 1$. In general P_∞ can be expressed, according to its definition, as

$$P_\infty = 1 - \frac{1}{p}\sum_s s n_s. \tag{2.8}$$

Near the percolation threshold p_c, P_∞ follows the power-law

$$P_\infty \propto (p - p_c)^\beta. \tag{2.9}$$

(4) **The density-density correlation function g(l)**

This function g(l) gives the probability for two occupied sites separated by distance l to belong to the same cluster, and can be written as

$$g(l) = \xi^{-\frac{\beta}{\nu}} F(l/\xi), \tag{2.10}$$

where F(u) denotes a scaling function with F($u << 1$)$\sim u^{-\beta/\nu}$ and F($u >> 1$)$\simeq$1.

(5) **The scaling laws and universality**

The exponents in Equations (2.5) to (2.9) are called critical exponents in the study of percolation phenomena. From (2.4) it is clear that these exponents are not independent of each other. Comparing (2.4) with (2.5) — (2.9), one obtains the following scaling laws

$$2 - \alpha = (\varsigma - 1)/\eta,\ \beta = (\varsigma - 2)/\eta,\ -\gamma = (\varsigma - 3)/\eta, \tag{2.11}$$

and

$$2 - \alpha = \gamma + 2\beta,\ \nu d = \beta + 1/\eta, \tag{2.12}$$

where d is the Euclidean spatial dimensionality of the lattice. From these scaling laws it can be shown that only two of these exponents are independent. Universality in the percolation transition requires that these exponents depend only on the lattice dimensionality, and not on the local structure of the lattices. The scaling laws and universality provide one of the most compelling arguments to apply lattice percolation theory to continuum percolation systems, to test whether these concepts hold for continuum systems

(6) **The fractal structure**

The geometry of the percolation cluster near ϕ_c is described by irregular geometric fractals, or statistically self-similar fractals, within the length scale L such that $a_o <<$

$L << \xi$. For $L >> \xi$, the percolation cluster appears homogeneous and the detailed structure of the percolation network is unimportant in determining the network's physical properties. Combining equations (2.5) and (2.7), one obtains

$$s_{av} \propto \xi^{d_f} \propto (p - p_c)^{-d_f \nu}, \tag{2.13}$$

where the exponent d_f is the fractal dimension of the percolation cluster. The scaling laws relate the fractal dimension d_f to other critical exponents and the lattice dimensionality d ($d < 6$) as

$$d_f = d - \beta/\nu. \tag{2.14}$$

This fractal dimension d_f is found to be 1.9 in two dimensions and about 2.5 in three dimensions [Stauffer and Aharony 1994]. Since $\beta/\nu > 0$, the finite clusters at the percolation threshold are fractals such that their fractal dimension d_f is smaller than their lattice dimension d.

2.3 Percolation in Binary Continuum Composites

A binary continuum percolation system is a topologically disordered mixture of two components with drastically different physical properties, e.g. conductor-insulator, conductor-superconductor, and sol-gel. In this section, only conductor-insulator composites will be discussed, as this is the subject of the thesis. Conductor-insulator composites consist of a conductor, with conductivity σ_c, and an insulator, with conductivity σ_i and dielectric constant ε_i, such that $\sigma_i/\sigma_c << 1$. The conducting volume fraction ϕ is defined, by analogy to the site lattice problem, as the fraction of the volume taken up by the conducting component. Such systems undergo a metal-insulator transition at a critical conducting volume fraction ϕ_c, at which the conducting component first forms a continuously connected infinite cluster through the sample. In this infinite cluster, the current is carried only by the backbone, which is obtained from the infinite cluster by removing all the dead or "dangling" ends,

which do not participate in the conduction.

The underlying concept of topological disorder is important in distinguishing continuum percolation systems from the lattice problem. In lattice percolation, the structural starting point is that of a regular geometrical object—a periodic lattice. Disorder is introduced by superimposing on the sites or bonds of such a lattice, a randomly assigned two-state property (empty/occupied). The bimodal statistical variable, imposed on a regular geometrical structure, gives rise to a stochastic-geometry situation [Frisch and Hammersly, 1963]. The situation in the continuum system, however, represents a higher order of stochastic geometry, because the disorder-generating statistical variable (conductor/insulator) is superimposed on a structure that is itself topologically disordered.

The universality and scaling laws discussed in the previous section suggest that one may apply lattice results to continuum percolation systems. Recent developments in understanding the continuum system have revealed many special features of such systems, that make this branch of percolation studies attractive and practical in its own right. One of these aspects, the nonuniversality of critical exponents, or so called "continuum correction", will be discussed in Section 2.4.

Scaling theory predicts that many physical properties of percolation systems will scale with the conducting volume fraction ϕ as a power-law with the form $|\phi - \phi_c|^{\alpha}$, where the critical exponent α can be positive or negative depending upon the property being studied, and ϕ_c is the critical conducting volume fraction. The critical exponents used in this thesis are:

ν, correlation length exponent
t, DC conductivity exponent on the conducting side
$\bar{s}$, DC conductivity exponent on the insulating side
s, dielectric constant exponent
κ and w, $1/f$ noise exponents

g, Hall coefficient exponent

t_m, magnetoconductivity exponent

h_1, thermoelectric exponent on the conducting side

h_2, thermoelectric exponent on the insulating side

The following subsections will discuss the critical volume fraction and the various percolation equations, which will be used to describe the percolation phenomena associated with the G-BN percolation systems.

2.3.1 Critical Volume Fraction

The introduction of the critical volume fraction marked a milestone in the study of lattice percolation systems because ϕ_c, as was discussed in the last section, is a lattice invariant. Recognizing that the random-close-packed structure is another form of lattice [Zallen 1983], one expects that the continuum parameter $(\phi - \phi_c)$ should play the same role as the lattice parameter $(p - p_c)$. It must be emphasized that in the lattice percolation problem the empty sites and occupied ones are equal in size and shape. This is hardly the case for all continuum systems. In fact the percolation thresholds for binary composites can vary from less than 0.01 to greater than 0.5, depending upon the structural parameters such as relative size, shape and distribution of two component grains [Malliaris and Turner 1971, Kusy 1977, Balberg et al. 1984, McLachlan 1991, and Dovzhenko and Zhirkov 1995].

The conductor and the insulator are assumed to consist of spherical or near spherical grains, where l_c and l_i are the radii of the conductor and the insulator grains. When $l_c \simeq l_i$, the critical metal volume fraction ϕ_c obtained is about 0.16 in agreement with Scher and Zallen's invariant, as was discussed in the previous section. In the case $l_c \neq l_i$, the ϕ_c values will deviate from the invariant value of about 0.16. For $l_c << l_i$, the conducting grains coats the surface of and/or fills the interstitial space between the insulator grains. An example of this is that a conducting liquid fills the pores in a sedimentary rock. An early model is due to Malliaris and Turner (1971),

who assumed that each insulator grain is covered completely, with a monolayer of the conductor grains at ϕ_c. Under this assumption they calculated ϕ_c, as a function of the ratio of l_i and l_c, to be

$$\phi_c = \frac{50p_c}{1 + (\frac{a}{4})(\frac{l_i}{l_c})}, \tag{2.15}$$

where a = 1.11, 1.27, and 1.38 and p_c =0.38, 0.50 and 0.67, respectively, for coordination numbers, in two dimensions, of 6 (hexagonal), 4 (square), and 3 (triangular). The ϕ_c values calculated using Equation (2.15) are often several times smaller than the observed experimental ones, as Kusy (1977) noted. This is due to the fact that many of the conducting grains can be trapped in voids between the large insulator grains where they are unable to contribute to the percolation backbone. Kusy (1977) considered the situation where the conducting grains do not have to cover completely the insulating grains in order to form a conducting network. In this case a two dimensional percolation network is formed on the surfaces of the insulating grains at ϕ_c, which is about one-half of that needed for Malliaris and Turner's model. He also derived ϕ_c as a function of the ratio l_i/l_c, which can be written, only in the case of cubic symmetry, as

$$\phi_c = \frac{1}{1 + (\frac{a}{4X_c})(\frac{l_i}{l_c})}, \tag{2.16}$$

where a=1.27 and X_c=0.42 for a cubic lattice. The ϕ_c values predicted by this model are in good agreement with the many experimental results for $l_i/l_c \geq$2.0, as shown in Fig. 2.2.

It should be noted that the two models discussed above do not account for any " interactions", such as attractions and repulsions, between two grains and do not apply to nonspherical grains.

A further development in the modeling of the critical volume fraction ϕ_c was the introduction of the concept of the excluded volume in continuum percolation systems [Balberg 1987b and references therein]. The excluded volume is defined as the volume around an object $\hat{V}_{ex}$ into which the centre of another object is not allowed to

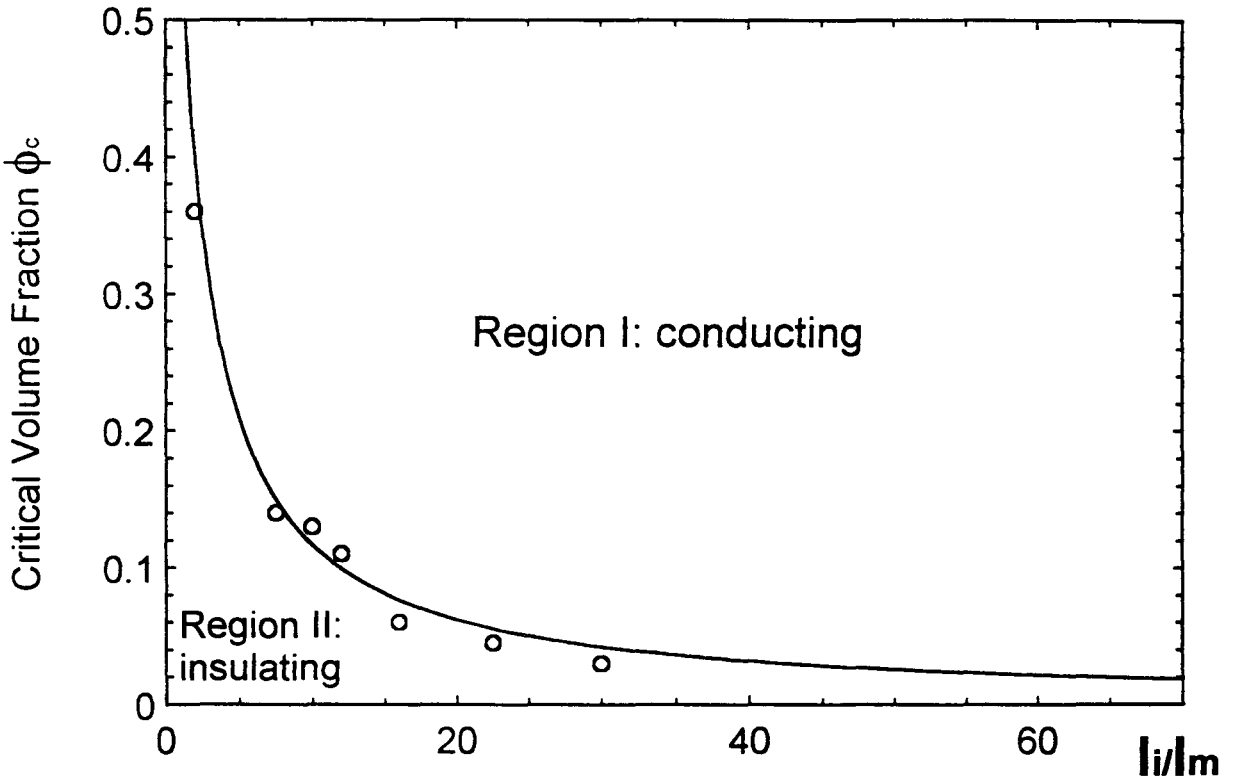

Fig. 2.2 Relationship between the critical volume fraction ϕ_c and the ratio l_i/l_m predicted by the equation (2.16) using a=1.27 and X_c=0.42 for the cubic lattice. The experimental data were taken from Kusy's table I [Kusy 1977].

enter, if overlap of these two permeable objects is to be completely avoided. Using the excluded volume concept, ϕ_c has been derived as

$$\phi_c = 1 - \exp\left[-\left(B_c \hat{V} / < \hat{V}_{ex} >\right)\right], \tag{2.17}$$

where $\hat{V}$ is the grain volume, $< \hat{V}_{ex} >$ the proper average of the objects' excluded volumes, and B_c the $Z \rightarrow \infty$ limit value of $p_c Z$, where Z is the coordination number of the lattice (see Table 2.1). B_c turns out to be invariant for a given object shape. For example, the numerical values of B_c and $\hat{V}/\hat{V}_{ex}$ are B_c=2.7 and 4.5, and $\hat{V}/\hat{V}_{ex}$=1/8 and 1/4, for spheres (3d) and disks (2d), respectively. Consequently from Equation (2.17) ϕ_c=0.286 and 0.675 for spheres (3d) and discs (2d) with excluded volume effects, respectively. Note that this is a "soft" overlapping sphere model in contrast to the hard sphere model which gives $\phi_c = 0.16$.

The excluded volume theory predicts that the percolation threshold also depends on any macroscopic anisotropy of a system. The anisotropy considered arises from the orientation distribution (partially or completely parallel to a certain direction or plane) of nonspherical grains in space. In this case ϕ_c is generally larger than its counterpart in the situation with completely random orientation, and depends both on the aspect ratio of the particles and orientation states [Nan 1992 and references therein].

2.3.2 Electrical Conductivity and Dielectric Constant

As in lattice percolation problems, the critical behavior of physical properties of binary continuum percolation systems is always controlled by the single correlation length ξ, which diverges as ϕ_c is approached from both sides, and is given by

$$\xi \approx a_o \left|\phi - \phi_c\right|^{-\nu}, \tag{2.18}$$

where a_o is the mean grain size, and ν is the critical exponent.

The DC conductivity of a binary conductor-insulator composite behaves in a singular fashion near the critical conducting volume fraction ϕ_c, at which the first electrical conducting path spanning the whole samples is formed, if σ_i is zero. The DC conductivity $\sigma(\phi,0)$ of conductor-perfect insulator composites vanishes as ϕ_c is approached from the conducting side ($\phi > \phi_c$) as

$$\sigma(\phi,0) \propto (\phi - \phi_c)^t, \tag{2.19}$$

where t is the conductivity exponent, which depends only on the dimensionality of system in lattice and ideal continuum systems. Computer simulations give t=1.1 — 1.3 in two dimensions and t = 1.6 — 2.0 in three dimensions [Stauffer and Aharony 1994]. On the other hand, $\sigma(\phi,0)$ diverges as ϕ approaches ϕ_c from below, if σ_c is infinite, as

$$\sigma(\phi,0) \propto (\phi_c - \phi)^{-\bar{s}}, \tag{2.20}$$

where the exponent $\bar{s}$ describes the divergence behavior of conductivity on the insulating side. The numerical calculations suggest $\bar{s}$=1.1 — 1.3 in two dimensions and $\bar{s}$=0.7 — 1.0 in three dimensions [Nan 1993 and reference therein]. When the conductivity ratio of real continuum conductor-insulator percolation systems is finite, the so-called crossover (critical) region is defined as

$$|\phi - \phi_c| \leq (\frac{\sigma_i}{\sigma_c})^{\frac{1}{t+\bar{s}}}. \tag{2.21}$$

Here the DC conductivity can be shown to be constant [Straley 1977 and Kirkpatrick 1979], as

$$\sigma(\phi,0) = \sigma_i^{\frac{t}{t+\bar{s}}} \sigma_c^{\frac{\bar{s}}{t+\bar{s}}}. \tag{2.22}$$

The low frequency dielectric constant $\varepsilon(\phi,0)$ of percolation systems diverges as

$$\varepsilon(\phi,0) \propto (\phi_c - \phi)^{-s}, \tag{2.23}$$

where s is the dielectric exponent, and $\phi_c \geq \phi$. The scaling ansatz predicts $s = \overline{s}$ [Nan 1993].

The AC conductivity $\sigma(\phi,\omega)$ and dielectric constant $\varepsilon(\phi,\omega)$ for a percolation system have been studied using the scaling ansatz with a complex AC conductivity $\Sigma(\phi,\omega) = \sigma(\phi,\omega) + j\omega\varepsilon(\phi,\omega)$ [Efros and Shklovskii 1976, Bergman and Imry 1977, Straley 1977, Stephen 1978, Webman 1981, Stroud and Bergman 1982, Wilkinson et al. 1983, and Clerc et al. 1990]. The form of this scaling equation is

$$\Sigma(\phi,\omega) \propto |\phi - \phi_c|^t g_{\pm}\left(\frac{j\omega}{\omega_c}\right), \tag{2.24}$$

where $j = \sqrt{-1}$, g_+ and g_- are two different scaling functions for above and below ϕ_c respectively, and ω_c is the critical frequency given by

$$\omega_c = \frac{\sigma_c}{2\pi\varepsilon_i}|\phi - \phi_c|^{t+s} \propto \sigma(\phi,0)^q. \tag{2.25}$$

Here q is an exponent, expected to be $(t+s)/t$ on the conducting side and to be $-(t+s)/\overline{s}$ on the insulating side of percolation. At $\phi = \phi_c$ and at low frequencies, (2.24) reduces to

$$\Sigma(\phi_c,\omega) \propto \left(\frac{j\omega}{\omega_c}\right)^x, \tag{2.26}$$

where

$$x = \frac{t}{s+t}. \tag{2.27}$$

Defining

$$y = \frac{s}{s+t}. \tag{2.28}$$

The analytic properties of Equation (2.26) then lead to

$$\sigma(\phi_c,\omega) \propto \omega^x, \tag{2.29}$$

and

$$\varepsilon(\phi_c,\omega) \propto \omega^{-y}, \tag{2.30}$$

where x and y are critical exponents. It is easily to see from (2.27) and (2.28) that the critical exponents x and y satisfy the following scaling relation

$$x + y = 1. \tag{2.31}$$

Another important and elegant result derived from Equation (2.26) is the universal loss angle. A loss angle δ for a materials with a complex AC conductivity $\Sigma(\phi,\omega)$ is defined by

$$\tan\delta(\phi,\omega) = \frac{\sigma(\phi,\omega)}{\varepsilon(\phi,\omega)}. \tag{2.32}$$

Clerc et al. (1990 and references therein) noted that Equation (2.26) yields a universal loss angle δ_c given by

$$\delta_c = \frac{\pi}{2}(1-x) = \frac{\pi}{2}\frac{s}{s+t} \tag{2.33}$$

at low frequencies near the percolation threshold, when $\omega << \omega_o \equiv \sigma_c/2\pi\varepsilon_i$. Note that δ_c depends only on the dimensionality of systems, when s and t have their universal values. From (2.32) it is seen that δ is a function of the conductor volume fraction ϕ and frequency ω for $\phi \neq \phi_c$. However, in the critical region where ϕ differs slightly from ϕ_c, the universal value of δ_c should still be observed in a frequency range $\omega_c << \omega << \omega_o$. Clerc et al. (1990) have performed numerical calculations of the universal loss angle δ_c using an effective-medium theory, the transfer-matrix method, and the decorated deterministic fractal lattice. Their results indicated that $\tan\delta_c$=1.0 in two dimensions and $\tan\delta_c$=0.54 in three dimensions.

The AC conductivity and dielectric constant of percolation systems have previously been studied using two different physical models, namely (1) the intercluster po-

larization model [Bergman and Imry 1977], also known as R—C model [Clerc et al. 1990] and (2) the anomalous diffusion model [Gefen et al. 1983]. Although these two theories are based on different starting assumptions, they both predict the scaling relations (2.29), (2.30) and (2.31) but differ in the expressions they predict for the exponents x and y.

In the intercluster polarization model, the conducting component is considered as "pure" conductor while the insulating component is identified as perfect dielectric. Within the framework of intercluster polarization, Efros and Shkolovskii (1976), Bergman and Imry (1977), Stroud and Bergman (1982), Webman (1981), and Wilkinson et al. (1983), derived the relations (2.27) and (2.28). In fact the percolation equations for the electrical conductivity, dielectric constant and dielectric loss, discussed above, all belong to the intercluster polarization picture.

In the anomalous diffusion model, the transport properties of the percolation structure is formulated as a random-walk or Brownian-motion problem on the percolating cluster. Anomalous diffusion occurs because of the fractal nature of the infinite percolation network. The mean-square distance traveled randomly on the backbone by the random walker will scale with the travel time t in the form

$$< r^2(t) > \propto t^{\frac{2}{2+\chi}}, \tag{2.34}$$

where χ is related to the previously defined critical exponents via $\chi=(t-\beta)/\nu$. The χ term in the equation (2.34) characterizes the self-similar geometry of the infinite cluster. For a nonfractal system, $\chi = 0$ and the mean-square displacement scales linearly with t, as expected for a nonfractal, Euclidean system. By performing a Fourier transform and replacing the time in Equation (2.34) by the frequency ($t \Rightarrow 1/\omega$), Equation (2.34) becomes

$$\hat{L}(\omega) \propto \omega^{\frac{-1}{2+\chi}}. \tag{2.35}$$

By relating this diffusion length $\hat{L}$ to the conductivity, via the Einstein diffusion rela-

tion, and averaging over the contributions of the charge carriers in different clusters, Gefen et al. (1983) calculated the dispersion for electrical conductivity and dielectric constant, and obtained

$$x = \frac{t}{2\nu - \beta + t}, \tag{2.36}$$

$$y = \frac{2\nu - \beta}{2\nu - \beta + t}. \tag{2.37}$$

Note that these exponents x and y also obey the scaling relation (2.31), because a single time scale for both resistance and capacitance is assumed in the calculation. More recently, (2.36) and (2.37) have been derived using, instead of the generalized Einstein relation, the Miller-Abrahams equivalent network which has the same electrodynamic behavior as the random-walk system [Schirmacher 1994]. No model exists which unifies the intercluster polarization and anomalous diffusion mechanisms.

2.3.3 GEM Equation

In Subsection 2.3.2, separate equations, (2.19) and (2.20), have been used to describe the DC conductivities of a percolation system on each side of critical volume fraction. McLachlan (1986 and 1996) developed a generalized effective media (GEM) equation, which can, however, be used to fit the conductivity data obtained from percolation systems. This equation can be written as

$$\frac{(1-\phi)(\sigma_i^{1/s} - \sigma^{1/s})}{\sigma_i^{1/s} + \frac{1-\phi_c}{\phi_c}\sigma^{1/s}} + \frac{\phi(\sigma_c^{1/t} - \sigma^{1/t})}{\sigma_c^{1/t} + \frac{1-\phi_c}{\phi_c}\sigma^{1/t}} = 0, \tag{2.38}$$

where the symbols have their usual meaning. This equation is a continuous interpolation between the two percolation equations (2.19) and (2.20), which describe the divergent behavior of conductivity near the percolation threshold. When σ_i=0, the GEM equation reduces to

$$\sigma = \sigma_c(\frac{\phi - \phi_c}{1 - \phi_c})^t, \tag{2.39}$$

and when $\sigma_c=\infty$, it reduces to

$$\sigma = \sigma_i(\frac{\phi_c - \phi}{\phi_c})^{-\bar{s}}. \tag{2.40}$$

Both of these equations have the mathematical form of the percolation equations. Letting $\phi_c = 0$ in Equation (2.39) and $\phi_c = 1$ in (2.40), one arrives at the Bruggeman asymmetric equations. Furthermore, in the case of $t=\bar{s}=1$, the GEM equation reduces to the Bruggeman symmetric equation.

The GEM equation has been used to accurately fit the conductivity data for a number of binary percolation composites [McLachlan et al. 1990 and references therein]. It has also been shown [Deprez et al. 1988] that the electrical conductivity, thermal conductivity and permeability can all be fitted to the GEM equation with the same two morphology parameters ϕ_c and $t=\bar{s}$.

2.3.4 Hall Coefficient and Magnetoresistance

The magnetoresistance and Hall coefficient of percolation systems involve the coupling of electrical and magnetic fields, and have been less thoroughly investigated than the electrical conductivity and dielectric constant. For the magnetoresistance, Bergman (1987) calculated, using the scaling ansatz, the magnetoconductivity $\triangle\sigma\,(H)$ and the relative magnetoresistance $[R(H)-R(0)]/R(0)$ in low magnetic fields, near the critical volume fraction. Bergman's is the only theory for magnetoresistivity and as only the transverse magnetoresistances of the G-BN conducting parallelepiped samples are measured in this thesis, the critical behavior of the transverse magnetoresistance in conducting regime is quoted first. Bergman (1987) gave

$$\frac{\triangle R}{R} = \frac{R(H) - R(0)}{R(0)} \propto (\phi - \phi_c)^{t_m - t}, \tag{2.41}$$

and

$$-\triangle\sigma = -[\sigma(H) - \sigma(0)] \propto (\phi - \phi_c)^{t_m}, \tag{2.42}$$

where t_m is the critical exponent describing the critical behavior of the second order Hall contribution to the low field magnetoresistance, and H is the magnetic field. Bergman (1987) also made the prediction that $t = t_m$, implying that the relative magnetoresistance $[R(H) - R(0)]/R(0)$ is constant near the percolation threshold.

Many authors [Skal and Shklovskii 1974, Levinshtein et al. 1975 and Straley 1980] have predicted that the Hall coefficient R_H of a percolation system diverges, as the critical volume fraction ϕ_c is approached from the conducting side of the percolation transition, as

$$R_H \propto (\phi - \phi_c)^{-g}. \tag{2.43}$$

Here g is the "Hall" critical exponent with predicted values of 0.5 — 0.6 in three dimensions and $g = 0$ in two dimensions. However, according to Bergman and Stroud (1985), the effective Hall coefficient R_H of conductor-insulator composite on the conducting side can be described by scaling theory, as

$$R_H \propto R_c(\phi - \phi_c)^{-g} + R_i\left(\frac{\sigma_i}{\sigma_c}\right)^2(\phi - \phi_c)^{-2t}, \tag{2.44}$$

where R_c and R_i are the Hall coefficients of the conductor and insulator respectively and t is the conductivity exponent defined in Subsection 2.3.2. The theoretical values of the exponent g in Equation (2.44) are g=0 in two dimensions and g=0.3~0.8 for three dimensional systems. The second term dominates the right-hand side of (2.44) only when ϕ is close enough to ϕ_c for the condition

$$(\phi - \phi_c) < \left[\left(\frac{R_i}{R_c}\right)\left(\frac{\sigma_i}{\sigma_c}\right)\right]^{\frac{1}{2t-g}} \tag{2.45}$$

to be satisfied. Dai et al. (1987) investigated experimentally the exponents t and g for the Al-Ge films and found that the measured values of t=1.75 and g =3.8 ($\simeq 2t$) and 0.38, close to the threshold of Al and the threshold of Ge respectively, are in good agreement with Equation (2.44).

2.3.5 $1/f$ (flicker) Noise

The voltage drop across almost any resistor fluctuates about its average value with or without a constant current flowing through it. In the absence of a driving current, these voltage fluctuations are known as Johnson or Nyquist noise, which originates from the thermal motion of the charge carriers. In an equilibrium situation this thermal motion has an average energy $3/2k_BT$, where k_B is the Boltzman's constant and T is the absolute temperature. The power spectrum $S_V(f)$ (f=frequency) of the voltage fluctuations is related to its resistance R, through a fluctuation-dissipation theorem, by

$$S_V(f) = 4k_BTR. \tag{2.46}$$

Since the relaxation time of thermal motion is extremely fast, τ=10^{-12}s, the Johnson noise is frequency independent (or white) at low frequencies ($< 10^{12}Hz$).

When a DC current is passing through a resistor two "excess" noises, depending upon the magnitude of the DC current, are often observed. The first of these is shot noise. Its spectral density $S_I(f)$ of the current fluctuations is also "white" or constant at low frequencies and is given by

$$S_I(f) = 2eI, \tag{2.47}$$

where e is the electronic charge, and I is the DC current flowing through the sample. The shot noise arises because of the finite size of the electrical charge carriers which leads to current pulses at the electrodes of the sample. In practice, the shot noise is large only at low current where the discreteness of the electrical charge carriers is important. The details of the transport processes of the charge carriers have no influence on the shot noise, provided there is no interaction between them and their statistics are close to Boltzman [Hooge et al. 1981].

At sufficiently low frequencies, the "$1/f$" or "flicker" noise is the dominant excess noise. Unlike the Johnson noise and the shot noise, which are well understood, the

source of $1/f$ noise has been the subject of innumerable controversies [Dutta and Horn 1981, Hooge, Kleinpeening, and Vandamme 1981 and Weissman 1988]. Hooge (1969) proposed an empirical formula for the $1/f$ noise in homogeneous samples, which in terms of the voltage fluctuations can be written in a general form as:

$$S_V(f) = \frac{\alpha V^{\vartheta}}{N^{\eta} f^{\gamma}}, \tag{2.48}$$

where, in Hooge's original paper, α is a dimensionless constant, with a value of about 2×10^{-3} for III-V compound semiconductors and not greatly dependent on the temperature, ϑ=2 for ohmic samples, η=1, γ is a number close to unity over a wide frequency range typically from $10^{-2}Hz$ to $10^{4}Hz$, and N the total number of charge carriers; usually proportional to the sample volume. In more recent years, the observed value of α has been found to vary from 10^{-5} to 10^{-1} in small volume metallic samples [Testa et al. 1988] and to be as high as 10^{3} to 10^{7} in granular high T_c superconductors [Song et al. 1990]. Although the relation between the noise power and DC voltage is usually given by the square-law, i.e., ϑ=2, for most electrical $1/f$ noise systems, a linear dependence of $S_V(f)$ on V, for a limited DC current range, has very recently been observed in superconductors [Kang et al. 1994]. The exponent γ is usually found to be 1.0±0.1 over six or more decades of frequency. However, a great controversy over the factor N still exists. The inverse dependence on N was postulated by Hooge (1969) to unify the noise process in metals and semiconductors with $\alpha \simeq 2\times10^{-3}$. The physical idea behind this postulate is that independent fluctuations are occurring on each of the mobile carriers, that is, the noise process for each carrier is independent.

For an ohmic resistor, the voltage fluctuation δV under a constant bias current arises from resistance fluctuations δR, and $\delta V = I\delta R$. In this case, the normalized spectrum is independent of the type of stimulation, e.g. constant current or voltage, and [Hooge et al. 1981]

$$\frac{S_V(f)}{V^2} = \frac{S_R(f)}{R^2} = \frac{S_I(f)}{I^2} = \frac{\alpha}{N^{\eta} f^{\gamma}}. \tag{2.49}$$

The problem of $1/f$ noise in percolation systems has lead to a number of theoretical and experimental investigations. The problem is potentially very interesting because the noise power is a more sensitive probe of inhomogeneities in the conductor than the resistance. In fact, the total resistance R of an inhomogeneous system is a moment of order 2 of the local currents i_λ flowing through the conduction paths λ, which are characterized by their resistances r_λ. The total resistance R can be written as

$$R = \frac{\sum_\lambda i_\lambda^2 \, r_\lambda}{I^2}, \tag{2.50}$$

where I is the total current through the sample. In contrast, the resistance fluctuations are a moment of order 4 in the current i_λ, and

$$S_R(f) = \frac{\sum_\lambda i_\lambda^4 \, S_\lambda(f)}{I^4}, \tag{2.51}$$

where $S_\lambda(f)$ is the noise power spectrum for resistor r_λ [Rammal et al. 1985b].

Rammal, Tannous, Breton and Tremblay (1985) have introduced a new scaling exponent, κ, different from and unrelated to any of the previously defined exponents for percolation, to describe the divergence of normalized noise power spectrum $S_V(f)/V^2$, near the critical volume fraction ϕ_c, on the conducting side of percolation through the power law

$$\frac{S_V(f)}{V^2} \propto (\phi - \phi_c)^{-\kappa}. \tag{2.52}$$

Recalling that the DC resistances diverge with critical exponent t as ϕ_c is approached from the conducting side, and combining Equations (2.19) and (2.52) gives a unique prediction for the normalized $1/f$ noise spectrum as a function of the resistance. This can be written as

$$\frac{S_V(f)}{V^2} \propto R^w, \tag{2.53}$$

where the exponent $w = \kappa/t$. Equation (2.53) is more convenient for fitting experimental data because the experimental determination of the critical volume fraction ϕ_c is not always reliable.

The resistance R of a fractal lattice has an anomalous size-dependence [Alexander and Orbach 1982 and Rammal and Toulouse 1983], given by

$$R(L) \propto L^{-\beta_L}, \tag{2.54}$$

where L is the size of lattice and $\beta_L = \frac{d_f}{d}(d-2)$ is an exponent characterizing the transport properties on the lattice considered. Here d_f and d are the fractal and spatial dimensions of the structure respectively. Motivated by Equation (2.54), Rammal et al. (1985b) showed, using scaling arguments, that the noise power $S_V(f)/V^2$ of a fractal structure should follow the scaling relation

$$\frac{S_V(f)}{V^2} \propto L^{-b}, \qquad (L >> 1) \tag{2.55}$$

where b appears as a new exponent, not related to any previously introduced exponents, and is bounded as

$$-\beta_L \leq b \leq -2\beta_L - \frac{1}{\nu}, \tag{2.56}$$

where ν is the correlation length exponent. The exponents β_L and b have been calculated for a variety of lattices, using various numerical methods, and the results give β_L=0.97 and 1.16, and b=1.16 and 1.26 in two and in three dimensions respectively [Rammal et al. 1985a and Tremblay et al. 1986]. Note that L is measured in terms of the site or grain size. Rammal et al. (1985b) also used Equations (2.54) — (2.56) to study percolation systems involving a fractal geometry for the infinite cluster.

2.3.6 Thermoelectric Power (Seebeck Coefficient)

The thermoelectric effect provides a useful tool for characterizing the transport properties of conductors and semiconductors. Herring (1960) was probably the first

to study this problem for composites, but only where the differences in the physical quantities between the various components were assumed to be small. Webman et al. (1977) studied the thermal conductivity and the thermoelectric power of binary inhomogeneous materials consisting of conductor and nonconductor components with electrical conductivities σ_c and σ_i, thermal conductivities K_c and K_i, and Peltier coefficients P_c and P_i respectively. They derived a self-consistent effective-medium approximation for the thermoelectric power, which can be written as

$$S_m = \frac{6K_m < S'D' >}{1 - 3 < K'D' >}, \tag{2.57}$$

where

$$D' = \frac{\sigma'}{(K' + 2K_m)(\sigma' + 2\sigma_m)} \tag{2.58}$$

and

$$S' = \frac{P'}{\sigma'}. \tag{2.59}$$

Here the subscript m refers to composite materials having a thermoelectric power S_m, an effective electrical conductivity σ_m and an effective thermal conductivity K_m. P', σ' and K' are the local Peltier coefficient, electrical conductivity and thermal conductivity, respectively; and the average $< - >$ was taken over all space or over all local configurations around a given point.

Equation (2.57) exhibits two interesting features. First, in the case where $\sigma_i \ll \sigma_c$ and $P_i \ll P_c$, it reduces to

$$S_m(\phi) = S_c, \tag{2.60}$$

where $\phi > \phi_c + 0.1$, that is, well above the percolation threshold, $S_m(\phi)$ is independent of ϕ.

Second, in the insulating region, $\phi < \phi_c$, $S_m(\phi)$ shows a pronounced rise with decreasing ϕ, given by

$$S_m(\phi) = \left(\frac{S_i}{\phi_c}\right)(\phi_c - \phi), \tag{2.61}$$

provided that $\sigma_i \ll \sigma_c$, $S_i \gg S_c$, and $K_i \simeq K_c$. In summary, $S_m(\phi)$ is proportional to $\sigma^{-1}(\phi)$ below ϕ_c and is constant above it.

More recently Milgrom and Shtrikman (1989) and Bergman and Levy (1991) made theoretical studies of thermoelectric properties of binary composites, using the field decoupling transformation discovered by Straley (1981). They obtained an expression for the effective thermoelectric power of binary composites, given by

$$\frac{S_c - S_m}{S_c - S_i} = \frac{\frac{K_m}{K_c}/\frac{\sigma_m}{\sigma_c} - 1}{\frac{K_i}{K_c}/\frac{\sigma_i}{\sigma_c} - 1}, \tag{2.62}$$

where the symbols have the meanings already given in this section. Starting from this equation, the thermoelectric power S_m of composites can be expressed in a form showing an explicit interpolation between the thermoelectric power values of the metallic component S_c and insulating component S_i, which is

$$S_m = S_c + (S_i - S_c)\frac{\frac{K_m}{K_c}/\frac{\sigma_m}{\sigma_c} - 1}{\frac{K_i}{K_c}/\frac{\sigma_i}{\sigma_c} - 1}. \tag{2.63}$$

The behavior of S_m near a percolation threshold has been studied in detail, using the scaling arguments, by Levy and Bergman (1992). In their scaling scheme, both K_i/K_c and σ_i/σ_c are assumed to be very small compared to unity. Furthermore, the dependence of S_m upon both the electrical conductivity ratio σ_i/σ_c and the thermal conductivity ratio K_i/K_c, which can sometimes be described by qualitatively different expressions of ϕ, can make the scaling behavior very complex, in contrast to the familiar simple power-law for the electrical conductivity. It is surprising that the coupling of electric and temperature fields does not cause the appearance of any new exponent, necessary to describe the critical behavior of thermoelectric power, as Levy and Bergman could use only the exponents t and s to achieve their objectives. For graphite and hexagonal boron-nitride, one has $K_i \geq K_c$ [Lide 1994]. Therefore Levy and Bergman's scaling scheme for thermoelectric power of percolation systems is not

applicable to the G-BN systems. New power-laws for the thermoelectric power near percolation threshold are proposed in this thesis and will be presented in Chapter six.

2.4 The Nonuniversality of Critical Exponents

The applications of the scaling laws of lattice percolation to continuum systems, as discussed in Section 2.3, are probably attributed to the concept of the universality of the scaling behaviors, i.e. they depend only on the dimension of the percolation system, and do not on the details of geometric structure or the interactions between the conducting particles. For the critical exponents s and t, the most widely accepted universal values in three dimensions are 0.87 and 2.0 respectively. Although many computer simulations and experiments support this belief, some experimental results on continuum systems have shown that the value of exponent t can be 3 or even larger [Pike 1978, Carmona et al. 1984, Chen and Chou 1985, and McLachlan et al. 1990], which implies that the critical exponents are not necessarily universal in some continuum systems.

Kogut and Straley (1979) first realized that peculiar conductance distributions in an infinite percolation resistor network could yield nonuniversal conductivity exponents. Consider a network where the conductances of the occupied sites are distributed according to the distribution function $h(G) \sim G^{-\alpha}$ as $G \to 0$ for $G < G_c$, where $0<\alpha<1$. The value G_c is defined as the minimum conductance in a subset of conductances, which give rise to percolation when the conductances are placed into the lattice in descending order. Since close to the percolation threshold, the resistance of the sample is determined by the intercluster links, and the total resistance of a link is determined largely by a series connection of the resistors G^{-1}, the average conductance of the system is given by

$$G_{sample} \propto \ < G^{-1} >^{-1} (\phi - \phi_c)^t \ \propto \ (\phi - \phi_c)^{t+\frac{\alpha}{1-\alpha}} . \tag{2.64}$$

Therefore the universal exponent t should be replaced by

$$t' = \begin{cases} t & if \quad \alpha < 0 \\ t + \frac{\alpha}{1-\alpha} & if \quad 0 < \alpha < 1. \end{cases} \tag{2.65}$$

Note that this model does not allow t' to be smaller than the accepted universal values of t. The first percolation system found, that yielded a theoretical distribution function of the $G^{-\alpha}$ class, leading to nonuniversal behavior of the conductivity, was the 'Swiss-cheese' (or random-void) model [Halperin et al. 1985]. In this system, uniformly-sized overlapping insulating spheres are placed randomly in a uniform conducting matrix. Near the percolation threshold ϕ_c, the resistance behavior of the Swiss-cheese model is dominated by the narrow conducting necks which join the larger regions of the conducting medium. The local conductance G of these narrow necks depends on their neck 'width' δ as $G \sim \delta^{y+1}$, where $y = \alpha/(1-\alpha)$. For $y \geq 0$ or $0<\alpha \leq 1$, the critical exponent is in the range

$$Max[y + 1 + (d-2)\nu,\ t] \ \leq \ t' \ \leq \ t + y. \tag{2.66}$$

For $y \leq 0$ or $\alpha \leq 0$, i.e. in the inverted Swiss-cheese model, the roles of the two components are interchanged. A similar argument, analogous to the Swiss-cheese model, can then be made. However, in this case the conductance distribution does not result in any correction to the conductivity exponents.

Balberg (1987a) suggested another system which gives nonuniversal behaviour. In this system, the conducting particles are embedded in an insulating matrix, similar to the inverted Swiss-cheese model, but where the inter-particle conduction mechanism is tunneling and the particles are arranged onto a percolating network. In this model, the tunneling conductance between two hard spherical conducting particles of radius b_o, separated by a distance r ($>>b_o$), is given by

$$G \propto exp(-r/l), \tag{2.67}$$

where l is the tunneling distance (typically 10$\sim$100$\AA$). To find the conductance

distribution, a distribution function for the distance between the surfaces of two adjacent particles, $h(r)$, was proposed. This is

$$h(r) \propto \left(\frac{r}{a_o}\right) e^{-\frac{r}{a_o}}, \tag{2.68}$$

where a_o is the average closest distance between two particles. Using the relation in elementary probability theory $h(G) = h(r) \cdot dr/dG$, for large values of r, Equations (2.67) and (2.68) give rise to the distribution $G^{(\frac{l}{a_o})^{-1}} = G^{-\alpha}$ for small G, yielding a nonuniversal critical exponent

$$t' = t + (\frac{a_o}{l})(1 - \frac{l}{a_o}). \tag{2.69}$$

The nonuniversality of the conductivity exponent t has also been found in percolation systems with macroscopic anisotropy [Yoon and Lee 1990; Carmona et al., 1984]. More recently, Lin (1991) found in the $PrBa_2Cu_3O_7$-Ag percolation system, that the conductivity exponent t increases monotonically from 1.48 to 1.91 with increasing conductivity ratio σ_c/σ_i, from $3.2\text{x}10^4$ to $2.2\text{x}10^{11}$. The mechanisms for the breakdown of the universality of t in these last two cases are not well understood.

Chapter 3

APPARATUS AND EXPERIMENTAL METHODS

3.1 Sample Fabrication

All the samples studied in this thesis are mixtures of Graphite powder (G: Lonza, KS75) as the conducting component and hexagonal Boron-Nitride powder (BN: Advanced Ceramic Corporation) as the insulating component. Since the actual bulk resistivity of the graphite and BN powders, and the actual dielectric constant of the BN powder, used in the present study, are not known, they had to be measured experimentally, as will be described in this chapter. Compressed pellets of the BN have a resistivity of $10^{16}\Omega - cm$ in the axial direction and $4.2\times10^{14}\Omega - cm$ in the transverse direction, and a relative dielectric constant of 2.8 in the axial direction. Similar compressed Graphite pellets have a resistivity of $0.12\Omega - cm$ and $2.9\times10^{-3}\Omega - cm$ in the axial and transverse directions respectively. This measured axial resistivity is consistent with that of $0.15 \sim 0.25\Omega - cm$ along the c-axis observed in a good single graphite crystal at room temperature, while the measured transverse resistivity is close to that of $4.2\times10^{-5}\Omega - cm$ in the a-b plane [Reynolds 1968]. Therefore the measured bulk graphite resistivity is thought to be mainly bulk resistivity of graphite grains and not intergrain contacts.

Two classes of powder mixtures were made using these materials: the first, compressed discs and parallelepipeds cut from the discs, and the second, a powder mixture undergoing compression. In this section, the relevant details of the method of sample preparation and fabrication are discussed.

A predetermined amount of graphite and BN powder was weighed out with the appropriate weight percentage of the two components. This weight percentage is equal to the relative volume percentage, since these two constituents have the same densities: 2.25gms/cm^3 [Lide 1994]. The preweighted amounts of G and BN powder were then put into an agate container, together with agate balls, and ground and mixed in a planetary mill. At the end of this process, the powders had become a random mixture of grains, since the two constituents are mechanical isomorphs, with the same crystal structure (hexagonal) and almost the same crystal structure parameters, as discussed in Chapter one. Carefully poured 50%G-50%BN and 55%G-45%BN powder mixtures, with a total weight of 35gms each, were used in this form for conductivity and dielectric constant measurements, in the appropriate sample cell. To make the compressed discs, about 3gms of the appropriate powder mixture was poured into a die of 26mm diameter and compressed into a disc using a pressure of 200MPa. The discs were typically about 2.5mm thick. Bar shaped samples (50x5x5mm) were also made, using a square cylinder with a cross-section of 50x5mm and a pressure of 200MPa, perpendicular to the 50x5mm surface.

For the measurements of the axial conductivity, dielectric constant and $1/f$ noise, silver colloid paste was painted on two surfaces of the discs, forming both the electrodes and capacitor plates. During this procedure a circle of thin copper wire, with a diameter of about 16mm for the current/voltage contacts, was embedded in the electrodes. For samples with a resistance less than 100Ω, a separate wire near the centre of the disc, for a separate voltage contact, was also embedded in the electrodes. When all the measurements in the axial direction were finished, the silver paste was stripped off the faces of the discs and the discs were cut and polished into 24(length)x8(width)x2(thickness)mm and 18x3x2mm parallelepipeds. The former,

using silver paste and embedded copper wire on the two 8x2mm surfaces as electrical contacts, were used for the measurements of the transverse DC conductivity, Hall coefficient, $1/f$ noise and thermoelectric power. The smaller parallelepipeds, with the electrical contacts on the two 18x2mm opposite surfaces, were used only for the transverse magnetoresistance measurements, which are described in Section 3.4.

Because of the slow relaxation after mechanical compression, it was found that the resistance of the disc samples, especially those near the percolation threshold, increased with time, so that an aging period was allowed before performing the various measurements on these samples. In an effort to determine the correct aging time, the resistance of the sample with ϕ =0.156 was measured twice daily for a period of 35 days. The results are plotted in Fig. 3.1, in which the solid curve is a best fit to the data using the following equation

$$R(t) = R_1 + R_2(1 - e^{-\frac{t}{\tau}}), \tag{3.1}$$

where R_1 is the initial (t=0) resistance, t is time, and τ is the relaxation time. For this particular sample, a least squares fit gave R_1 =73.7$k\Omega$, R_2 = 38.4$k\Omega$ and τ = 20.5days. For 99% accuracy of the final resistance $R(t = \infty)$, a simple calculation based on Equation (3.1) shows that minimum aging time $t_{\text{min}} = 3.5\tau$ = 72days is required. All the measurements reported in this thesis were made on disc samples that had aged for at least three months. Samples measured a year later were found to have altered by less than 1%.

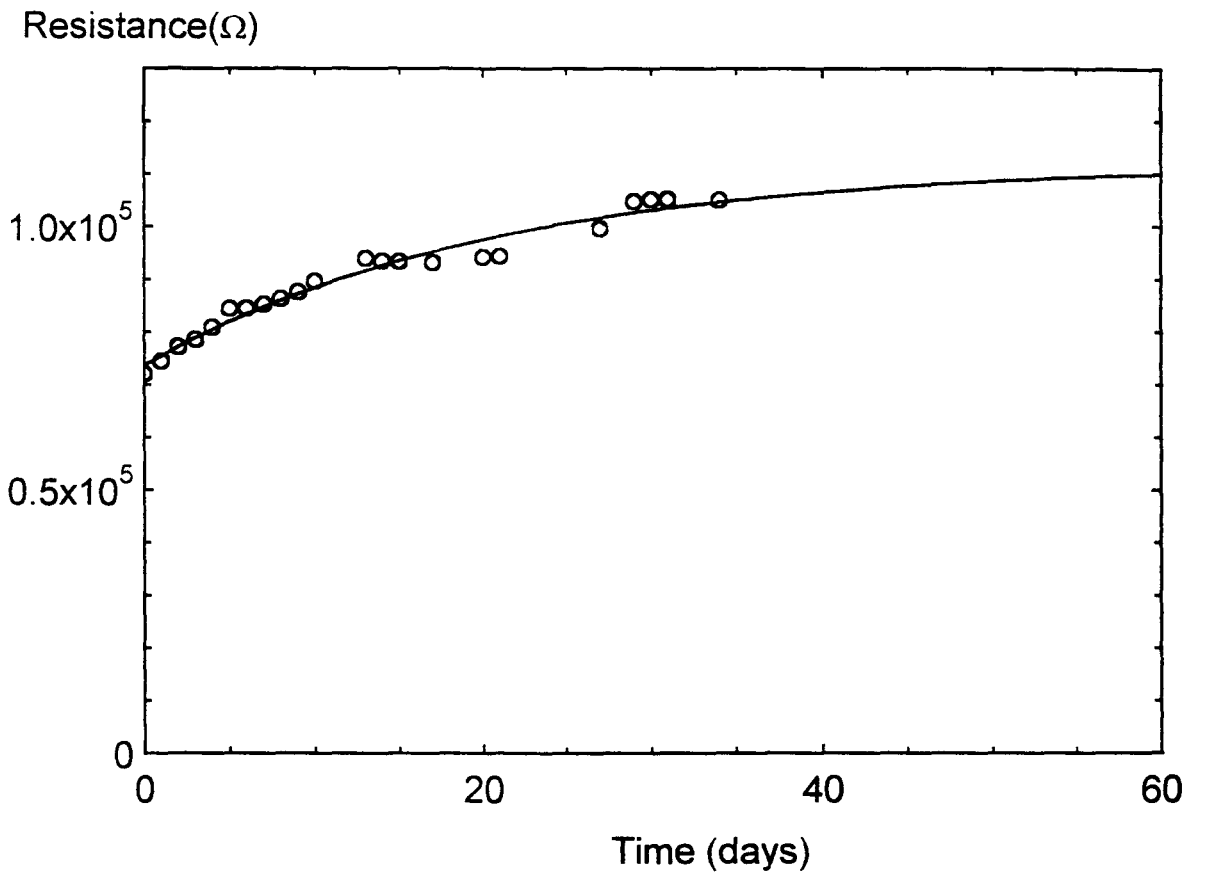

Fig. 3.1 The resistance against time(days) for the disc sample with $\phi = 0.156$. The solid curve is a least squares fit of the relation $R(t) = R_1 + R_2(1\text{-}e^{-\frac{t}{\tau}})$ to the data. The best fit parameters are given in the text.

3.2 Sample Characterization

3.2.1 Porosity of the Disc Samples

The apparent densities of disc samples were obtained by measuring their mass and thickness only, as their diameters were constant (26.0mm). The porosity of the discs is calculated using the formula

$$porosity = 1 - \frac{\frac{W}{\rho}}{\pi r^2 \cdot \triangle}$$

$$= 1 - 0.0838\frac{W}{\triangle} \tag{3.2}$$

where

W= the mass of disc, grams;

ρ= the density of disc without porosity, 2.25g/cm^3;

r= the radius of disc, 1.30cm;

Δ = the thickness of disc, cm.

Fig. 3.2 shows the results of these measurements in the form of disc porosity against the volume fraction of graphite. As the mass of the discs can be measured with uncertainty of $\pm$0.1mg in the total mass of about 2.5g, the experimental error in porosity comes mainly from the thickness measurements which have 2% relative error. Therefore the error bars for the porosity data in Fig. 3.2 are all less than the size of the symbols. It is seen from this plot that the average porosity is about 18% for all the compressed disc samples, this is consistent with previous results on pure graphite measured using a similar method [Reynolds 1968]. Furthermore, near the percolation threshold ϕ_c=0.150 (see Chapter 4) there is a small peak of porosity. This could possibly be attributed to the fractal structure of the infinite percolation

cluster in the samples if one images that there are more interstitial spaces within the percolation cluster which the BN grains cannot fill in due to their finite sizes.

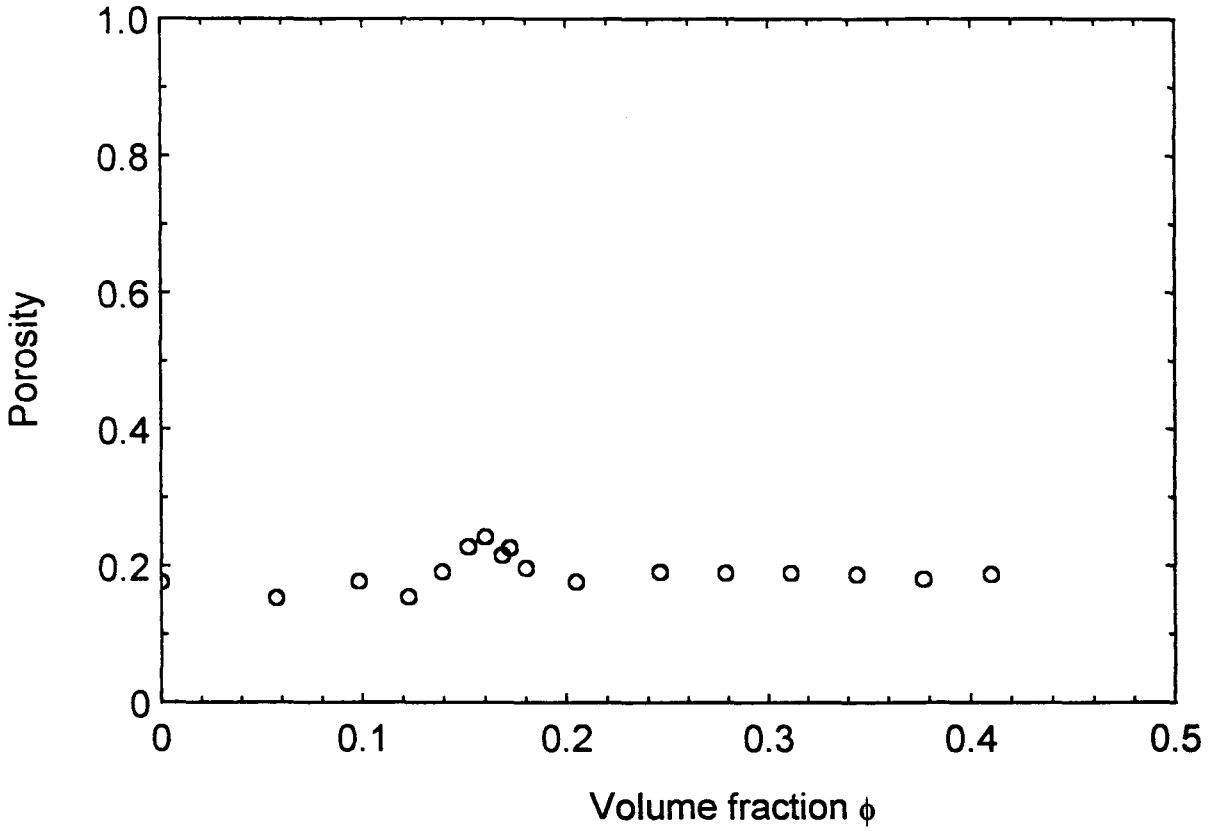

Fig. 3.2 The porosity against the graphite volume fraction for the disc samples. There is a small porosity peak associated with the critical volume fraction ϕ_c= 0.150 (see Section 4.2).

3.2.2 X-ray diffraction

X-ray diffraction (XRD) was principally used to examine the grain orientation in the discs. A Phillips *PW* 1010 X-ray diffraction spectrometer was used and operated at 40kv, 20ma, and a scanning rate of 1°/minute. A nickel filter was placed in position so as to produce nearly monochromatic radiation from a copper source. The results are shown in Fig. 3.3. As graphite and hexagonal BN have the same crystal structure and nearly the same parameters and density, they are indistinguishable by the usual X-ray methods. Therefore, any detectable impurity should show up as unexpected peaks in the traces of graphite and/or BN. The traces in Fig. 3.3 show that no significant contamination was introduced during sample preparation.

To monitor the grain orientation or anisotropy in the powders and discs, a powder mixture was poured into a copper cup of 26mm in diameter and 4mm in depth. The powder always filled the cup and the X-rays scanned the flat upper surface. Different densities of powder in the cup were obtained by pressing the top surface using a piston with the same diameter as that of the copper cup. A filling and pressing process was repeated until the desired density was obtained. The relative intensity of peaks changed accordingly with the apparent density of the powder in the cup, as shown in Fig. 3.4. The X-ray trace of a lightly poured and unpressed powder was treated as the reference, i.e. grains distributed randomly without any orientation. The anisotropy of discs with the same compositions was determined by comparison with the reference. The results and calculations indicate that the Graphite and BN crystals in the discs have about 80% of their c-axis within 1° of the direction of the pressure or axis of the disc. This orientation effect is later qualitatively confirmed from the very anisotropic resistivity measured in the compressed samples.

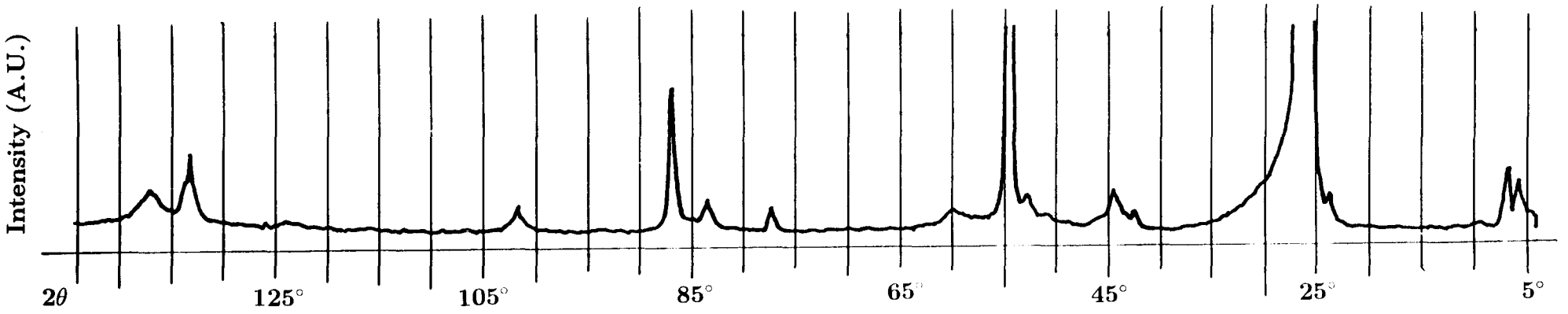

(a) $\phi = 0.00$

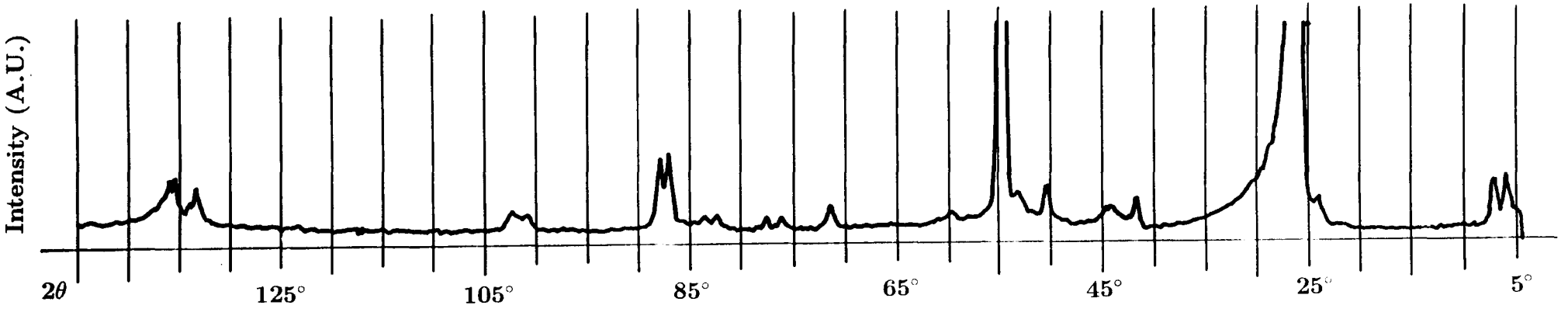

(b) $\phi = 0.82$

Fig. 3.3 X-ray scattering data on the disc samples with the graphite volume fractions indicted on each curve.

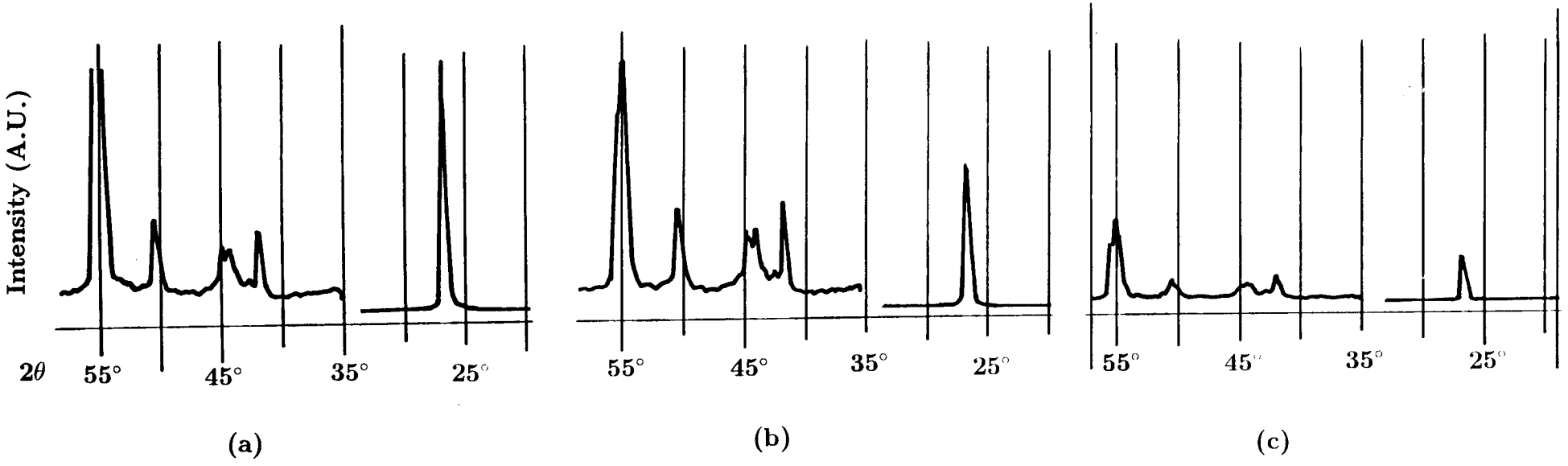

Fig. 3.4 Comparison of X-ray scattering data of the G-BN powder with decreasing pressure from (a) to (c). The densities of the samples from (a) to (c) are 1.81g/cm^3, 0.76g/cm^3 and 0.34g/cm^3 respectively.

3.2.3 Stress-Strain Tests

The stress-strain relationships in the disc making process for graphite, BN and 50%G-50%BN mixture, were investigated. Fig. 3.5 shows the typical results, which were obtained using a universal testing machine. There was always the same amount, $3gm$, of powder inside the die. Typically, a very small stress was observed until a packing fraction of about 0.45, after which the stress increased rapidly, indicating an increasing resistance to inter-particle slipping. At packing fraction of about 0.62 the stress begins to rise very rapidly, indicating plastic deformation. This plastic flow must lead to fairly large contact areas between neighboring grains, and hopefully to a more uniform pressure inside the die, which would yield a more uniform density within the disc samples.

Another stress-strain experiment was made to compare the strength of pressure bonds among the G-G, G-BN and BN-BN contacts. Compressed bars of 50x5x5mm dimension, consisting of pure graphite, 50%G-50%BN and pure BN, were used for this purpose. The bar was supported at the two ends, about 20mm from its centre, and a load applied in the middle of the bar. The bar was oriented so that the load stress was in the same direction as the pressure during sample preparation. The results are illustrated in Figs. 3.6a, b and c. One important feature of all these curves is that a force between 3.5 and 8.5N was needed to break the bars, showing that the strength of the G-G, G-BN and BN-BN pressure bonds between grains are all approximately the same. From these observations, it seems that the mechanical relaxation would be about the same for all discs for the full range of graphite volume fractions. If this is so, one would expect that the aging time obtained for the one sample described in the previous section is similar to those that would have been obtained for all the others.

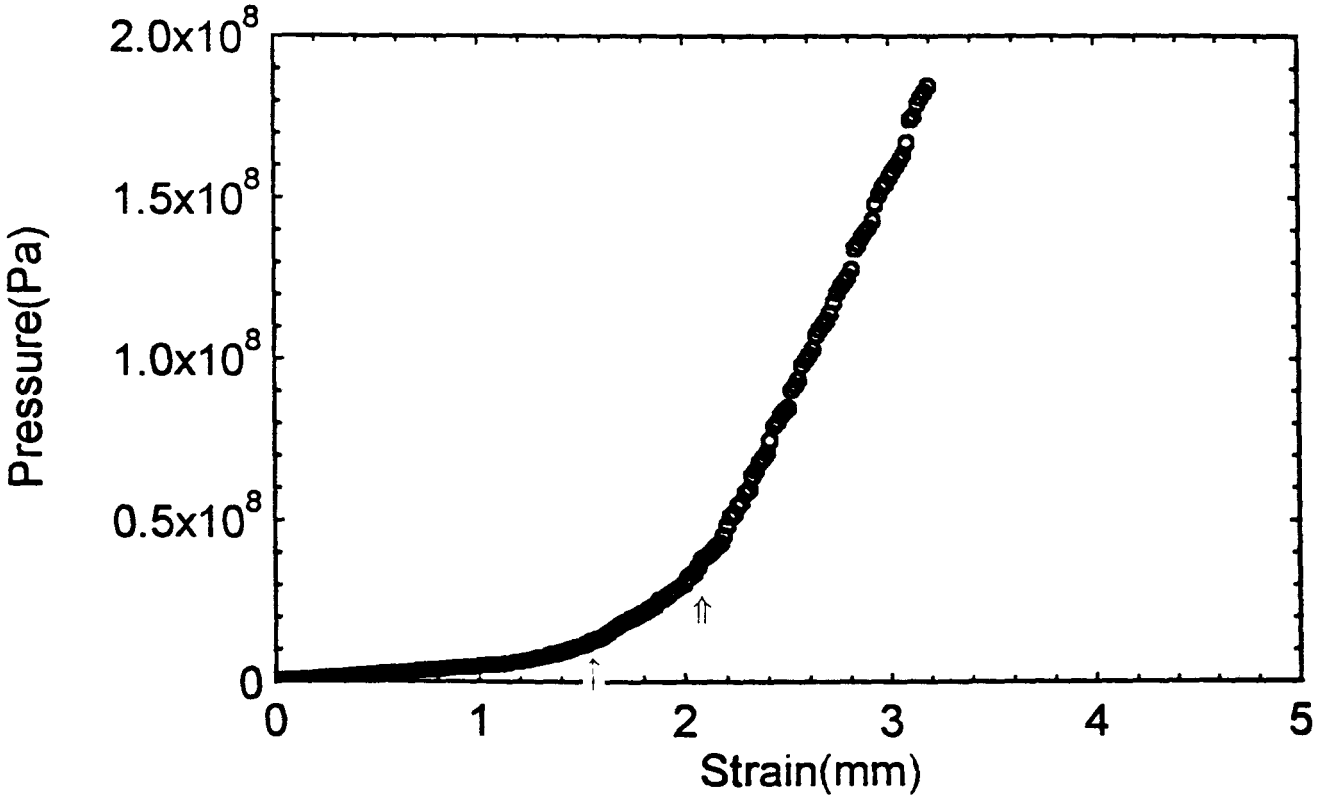

Fig. 3.5 A typical relationship of stress-strain in the disc making process. ↑: the packing fraction=0.45; ⇑: the packing fraction =0.62.

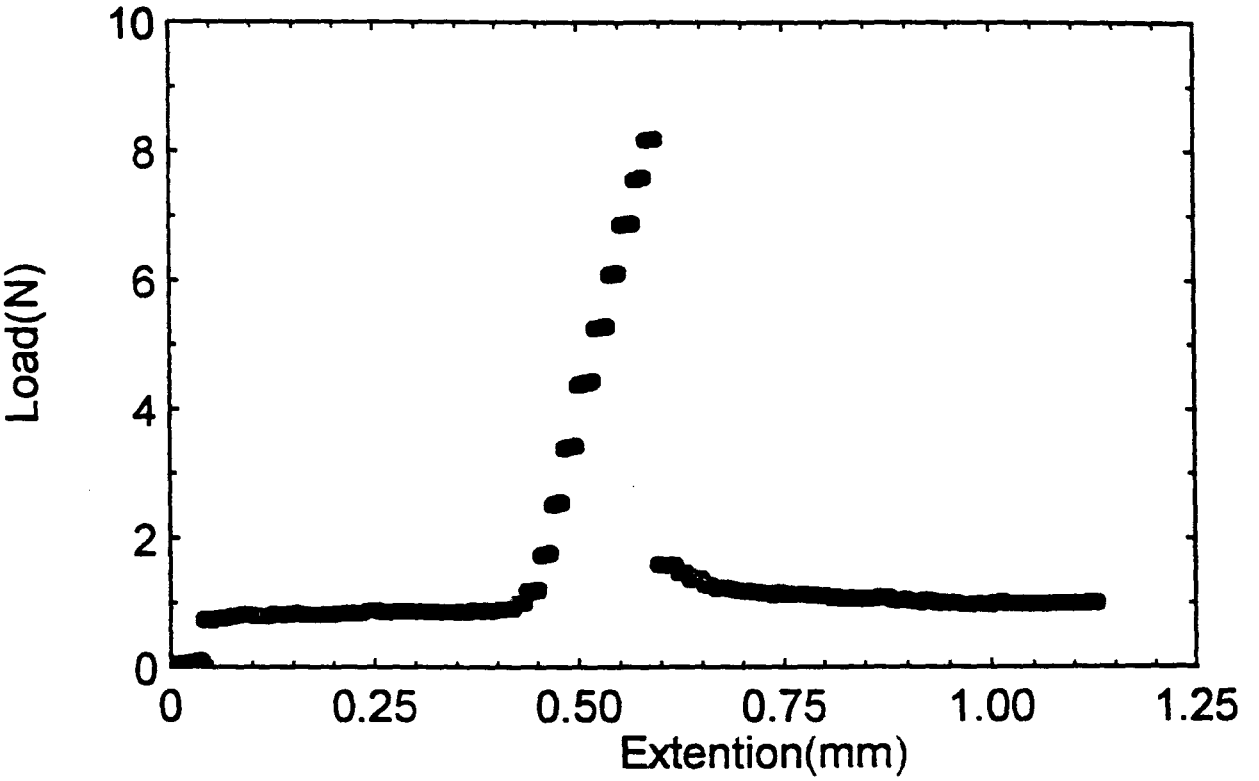

Fig. 3.6a The bond strength tests for a compressed graphite bar.

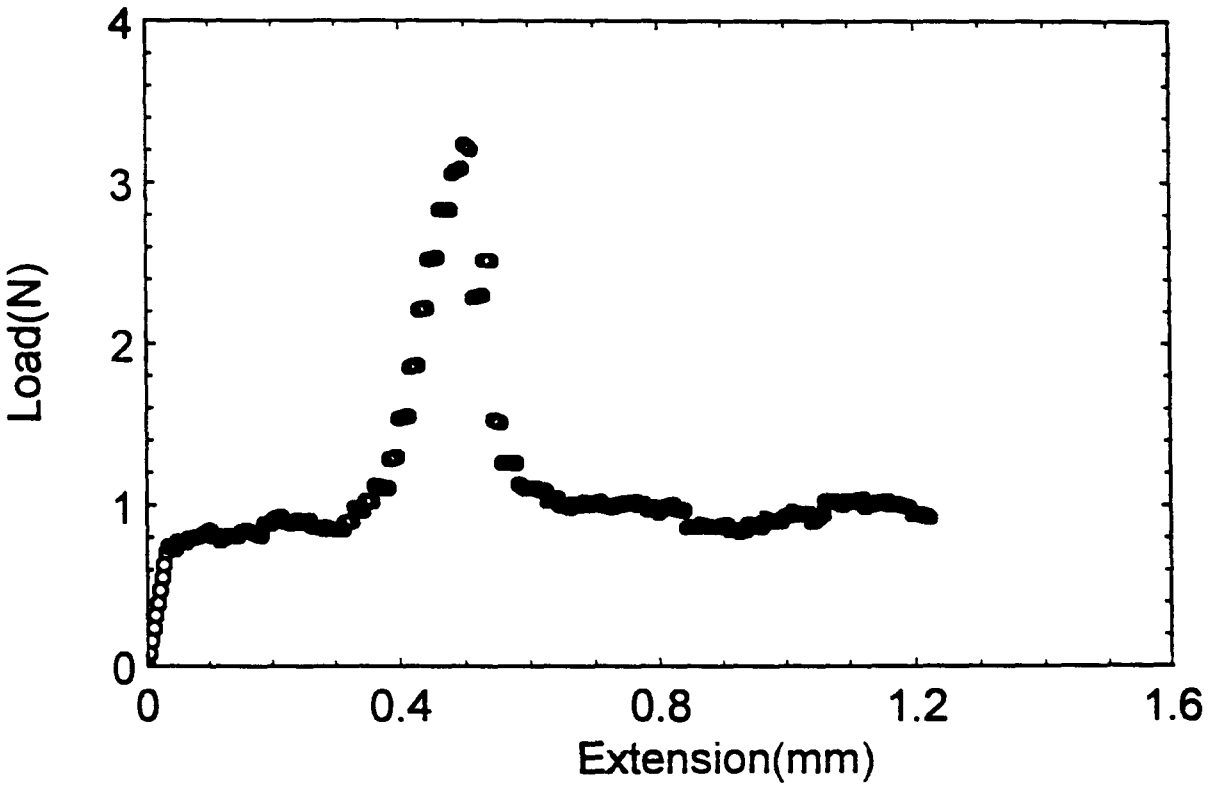

Fig. 3.6b The bond strength tests for a compressed 50%G-50%BN bar.

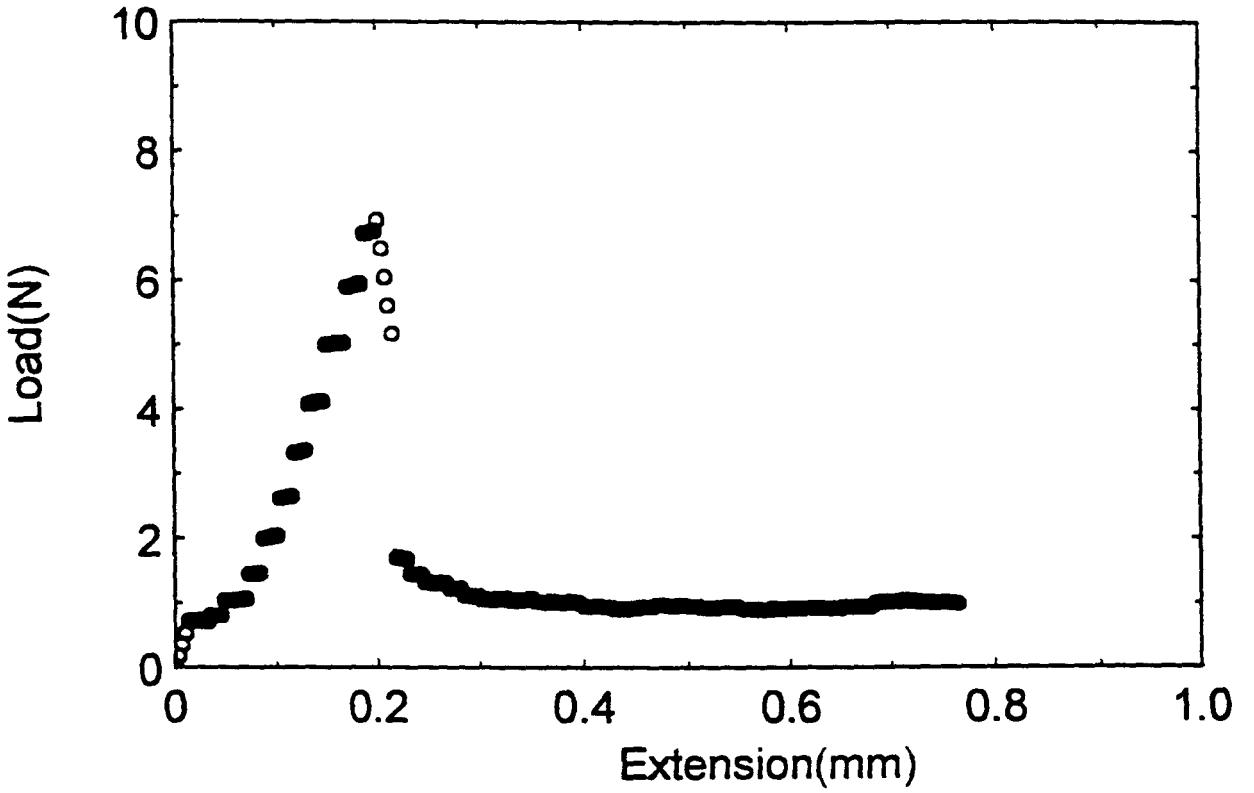

Fig. 3.6c The bond strength tests for a compressed BN bar.

3.2.4 Grain Size Distribution and Shape

The grain size distributions of composites were investigated using the Mastersizer (Malvern Instruments) and the "paste sampling" method. This instrument employs a low angle laser scattering technique, using a He-Ne gas laser of wave length 0.63μm, and has high resolution, differentiating up to 100 size classes in the range of 0.1 — 80μm. The ground powder was mixed with water and stirred thoroughly. Then the powder-water mixture was pumped through (in a transparent plastic pipe) the laser beam of length 2.2mm, and a diffraction pattern was obtained from all grains. A volume distribution was generated directly by the instrument. This is equal to the weight distribution since the density of the two components in this case is constant. Over 2000 measurement sweeps were averaged to obtain the final results. Figs. 3.7a, b, c, and d show some results of the grain size distributions obtained for G, BN, 18.7wt%G and 20wt%G powders. This data shows that the particle size distributions of the powders are a log-normal or Gaussian, as expected. The average grain diameters are found to be 18.8±2.5μm (G), 12.4±1.8μm (BN), 16.0±2.4μm (ϕ = 0.153), and 12.6±2.0μm(ϕ=0.164) respectively. Note that the diameter used above, to specify a grain diameter, is the volume equivalent spherical diameter. For example, the volume equivalent spherical diameter for a cylinder of 200μm height and 20μm in diameter is 49.3μm. This means that one cannot relate the grain sizes (diameters), obtained from the grain-size distribution experiment, to their true shapes. As a result, the grain shapes have to be obtained using other methods. This was done using both an optical microscope and an electron scanning microscope. In Fig. 3.8 are optical micrographs of the grain in powders with ϕ =0.158 and 0.41. It is clear that the graphite and BN grains have an irregular shape, but are definitely not "rod" or "disc" shaped. A reasonably good approximation for the shapes is spherical or near spherical.

Upper Size	% in	Lower Size	% under	Upper Size	% in	Lower Size	% under	Result source = Sample Sample: G
		180	100	10.3	6.1	8.48	16.0	Focal length = 100
180	0.4	149	99.6	8.48	4.6	7.01	11.4	Presentation=stand
149	0.5	123	99.2	7.01	3.2	5.79	8.2	Volume distribution
123	0.7	102	98.5	5.79	2.2	4.79	6.0	Beam length = 2.2
102	1.2	83.9	97.3	4.79	1.5	3.95	4.5	Obscuration = 0.1826
83.9	2.1	69.3	95.2	3.95	1.0	3.27	3.4	Volume Conc. = 0.0339 %
69.3	3.3	57.3	91.9	3.27	0.7	2.70	2.7	Residual =0.306%
57.3	4.7	47.3	97.3	2.70	0.5	2.23	2.2	Model indp
47.3	6.0	39.1	81.3	2.23	0.4	1.84	1.7	
39.1	7.0	32.3	74.3	1.84	0.3	1.52	1.4	D(v,0.5) = 18.83 µm
32.3	7.8	26.7	66.4	1.52	0.3	1.26	1.1	D(v,0.9) = 53.00 µm
26.7	8.7	22.0	57.7	1.26	0.2	1.04	0.9	D(v,0.1) = 6.44 µm
22.0	9.3	18.2	48.4	1.04	0.2	0.86	0.7	D(4,3) = 24.20 µm
18.2	9.6	15.1	38.8	0.86	0.2	0.71	0.5	D(3,2) = 13.86 µm
15.1	9.0	12.4	29.8	0.71	0.2	0.59	0.3	Span = 2.5
12.4	7.8	10.3	22.1	0.59	0.2	0.48	0.2	Spec. surf. area 0.5525 sq.m./cc.

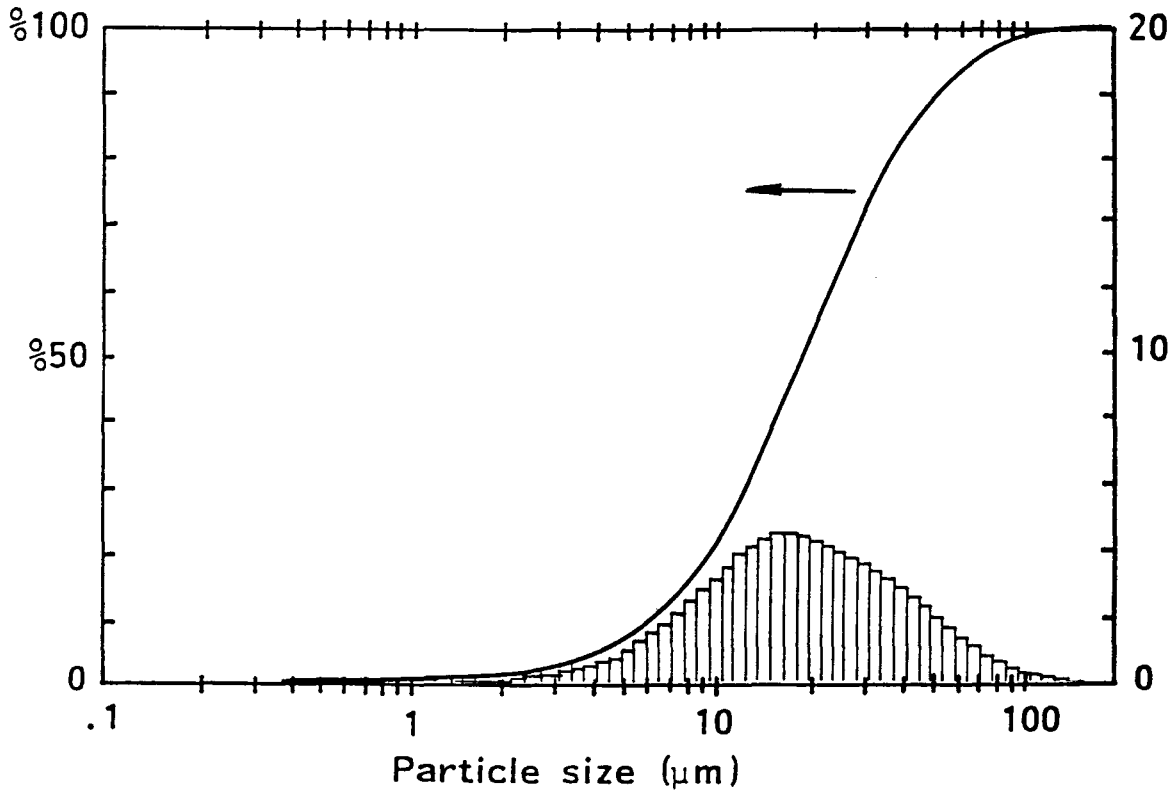

Fig. 3.7a The grain size distribution for $\phi = 0.82$ (pure G). The average grain size is 18.8μm.

Upper Size	% in	Lower Size	% under	Upper Size	% in	Lower Size	% under	Result source = Sample Sample:BN
		180	100	10.3	9.0	8.48	29.7	Focal length = 100
180	0.0	149	100	8.48	7.0	7.01	22.7	Presentation=stand
149	0.0	123	100	7.01	5.2	5.79	17.5	Volume distribution
123	0.0	102	100	5.79	3.8	4.79	13.7	Beam length = 2.2
102	0.0	83.9	100	4.79	2.8	3.95	11.0	Obscuration = 0.2204
83.9	0.0	69.3	100	3.95	2.1	3.27	8.9	Volume Conc. = 0.0247 %
69.3	0.1	57.3	99.8	3.27	1.6	2.70	7.3	Residual =0.393%
57.3	0.4	47.3	99.4	2.70	1.2	2.23	6.1	Model indp
47.3	1.1	39.1	98.4	2.23	0.9	1.84	5.2	
39.1	2.3	32.3	96.1	1.84	0.7	1.52	4.6	D(v,0.5) = 12.40 µm
32.3	4.2	26.7	91.9	1.52	0.6	1.26	4.0	D(v,0.9) = 25.45 µm
26.7	7.0	22.0	84.9	1.26	0.6	1.04	3.3	D(v,0.1) = 3.62 µm
22.0	10.0	18.2	74.9	1.04	0.7	0.86	2.7	D(4,3) = 13.46 µm
18.2	12.4	15.1	62.5	0.86	0.6	0.71	2.0	D(3,2) = 7.56 µm
15.1	12.6	12.4	50.0	0.71	0.6	0.59	1.5	Span = 1.8
12.4	11.3	10.3	38.7	0.59	0.7	0.48	0.8	Spec. surf. area 1.0432 sq.m./cc.

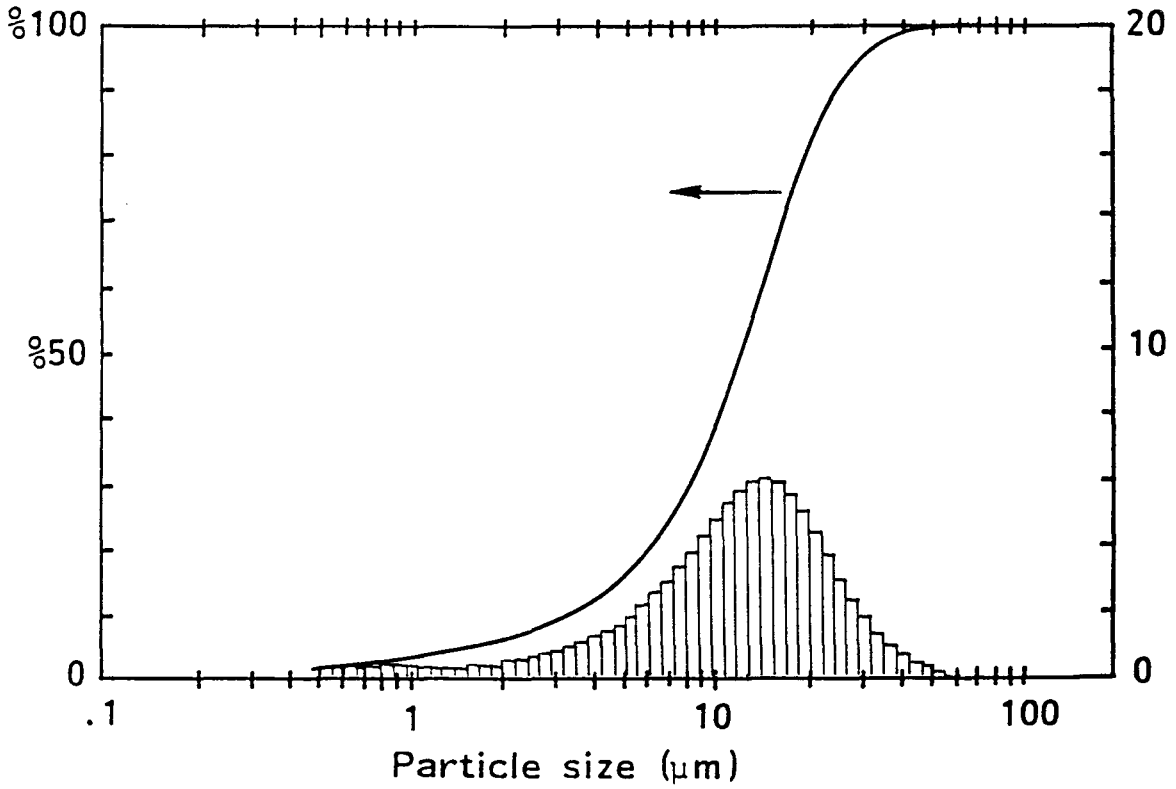

Fig. 3.7b The grain size distribution for $\phi = 0.00$ (pure BN). The average grain size is 12.4μm.

Upper Size	% in	Lower Size	% under	Upper Size	% in	Lower Size	% under	Result source = Sample Sample: $\phi = 0.153$
		180	100	10.3	6.6	8.48	23.2	Focal length = 100
180	0.1	149	99.9	8.48	5.2	7.01	18.0	Presentation=stand
149	0.1	123	99.8	7.01	4.0	5.79	14.0	Volume distribution
123	0.2	102	99.6	5.79	3.0	4.79	11.0	Beam length = 2.2
102	0.5	83.9	99.1	4.79	2.2	3.95	8.8	Obscuration = 0.1972
83.9	1.0	69.3	98.1	3.95	1.7	3.27	7.1	Volume Conc. = 0.0266 %
69.3	1.9	57.3	96.1	3.27	1.3	2.70	5.9	Residual =0.319%
57.3	3.3	47.3	92.8	2.70	1.0	2.23	4.8	Model indp
47.3	4.7	39.1	88.1	2.23	0.8	1.84	4.1	
39.1	6.2	32.3	81.9	1.84	0.6	1.52	3.4	D(v,0.5) = 15.98 µm
32.3	7.4	26.7	74.6	1.52	0.6	1.26	2.9	D(v,0.9) = 42.27 µm
26.7	8.6	22.0	66.0	1.26	0.5	1.04	2.3	D(v,0.1) = 4.37 µm
22.0	9.4	18.2	56.6	1.04	0.5	0.86	1.8	D(4,3) = 19.54 µm
18.2	9.7	15.1	46.9	0.86	0.5	0.71	1.3	D(3,2) = 9.78 µm
15.1	9.1	12.4	37.8	0.71	0.4	0.59	0.9	Span = 2.4
12.4	8.0	10.3	29.8	0.59	0.4	0.48	0.5	Spec. surf. area 0.8178 sq.m./cc.

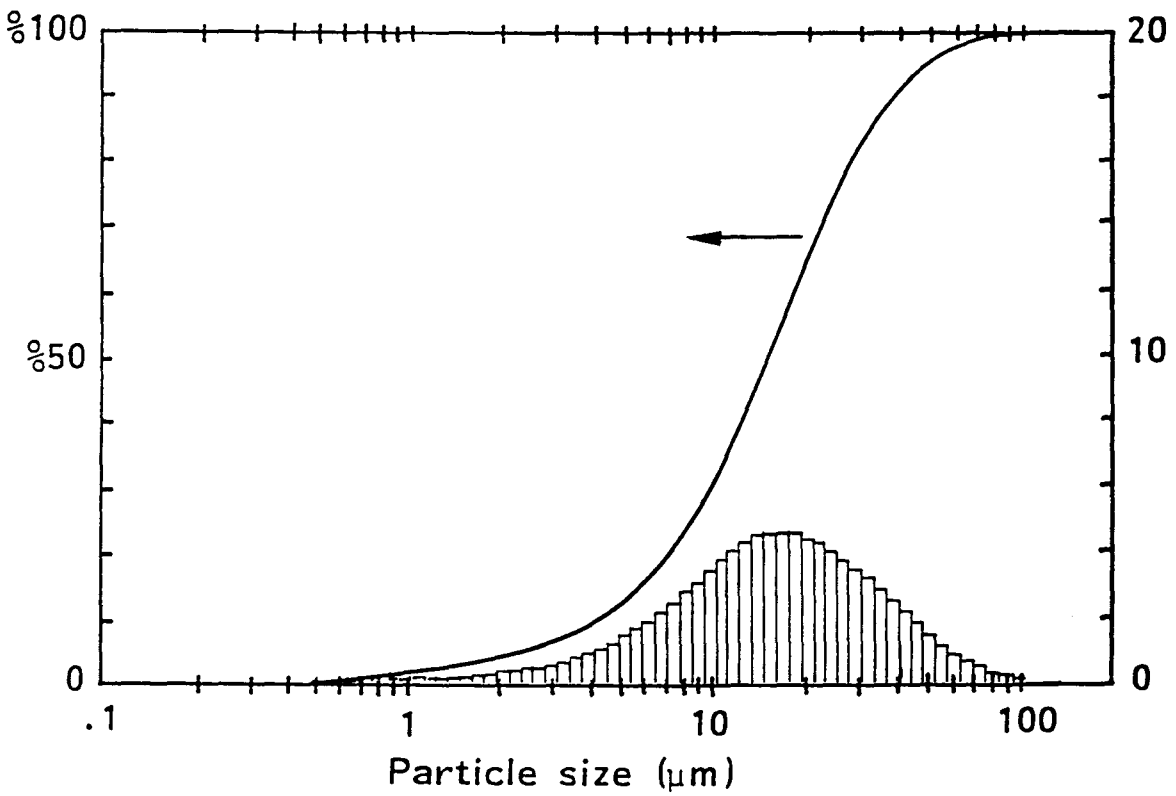

Fig. 3.7c The grain size distribution for $\phi = 0.153$. The average grain size is 16.0μm.

Upper Size	% in	Lower Size	% under	Upper Size	% in	Lower Size	% under	Result source = Sample Sample: $\phi = 0.164$
		180	100	10.3	8.6	8.48	30.2	Focal length = 100
180	0.0	149	100	8.48	6.9	7.01	23.4	Presentation=stand
149	0.0	123	100	7.01	5.3	5.79	18.1	Volume distribution
123	0.0	102	100	5.79	4.0	4.79	14.1	Beam length = 2.2
102	0.1	83.9	99.9	4.79	3.0	3.95	11.1	Obscuration = 0.2562
83.9	0.2	69.3	99.7	3.95	2.3	3.27	8.8	Volume Conc. = 0.0301 %
69.3	0.5	57.3	99.2	3.27	1.7	2.70	7.1	Residual =0.298%
57.3	1.1	47.3	98.2	2.70	1.4	2.23	5.7	Model indp
47.3	2.0	39.1	96.2	2.23	1.0	1.84	4.7	
39.1	3.3	32.3	92.9	1.84	0.8	1.52	4.0	D(v,0.5) = 12.57 µm
32.3	4.9	26.7	88.0	1.52	0.7	1.26	3.3	D(v,0.9) = 28.96 µm
26.7	7.1	22.0	80.9	1.26	0.6	1.04	2.7	D(v,0.1) = 3.60 µm
22.0	9.3	18.2	71.6	1.04	0.6	0.86	2.1	D(4,3) = 14.38 µm
18.2	11.1	15.1	60.5	0.86	0.5	0.71	1.5	D(3,2) = 7.93 µm
15.1	11.3	12.4	49.2	0.71	0.5	0.59	1.1	Span = 2.0
12.4	10.4	10.3	38.9	0.59	0.5	0.48	0.6	Spec. surf. area 0.9732 sq.m./cc.

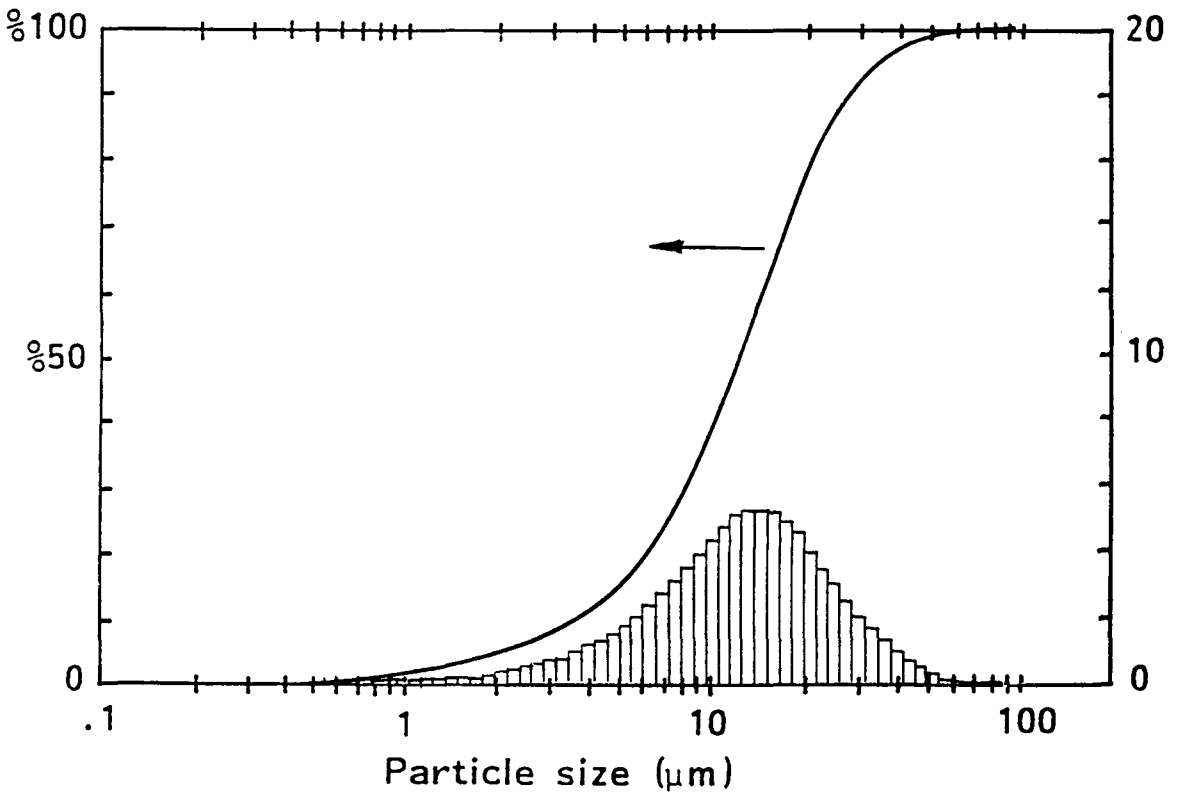

Fig. 3.7d The grain size distribution for $\phi = 0.164$. The average grain size is 12.6μm.

(a)

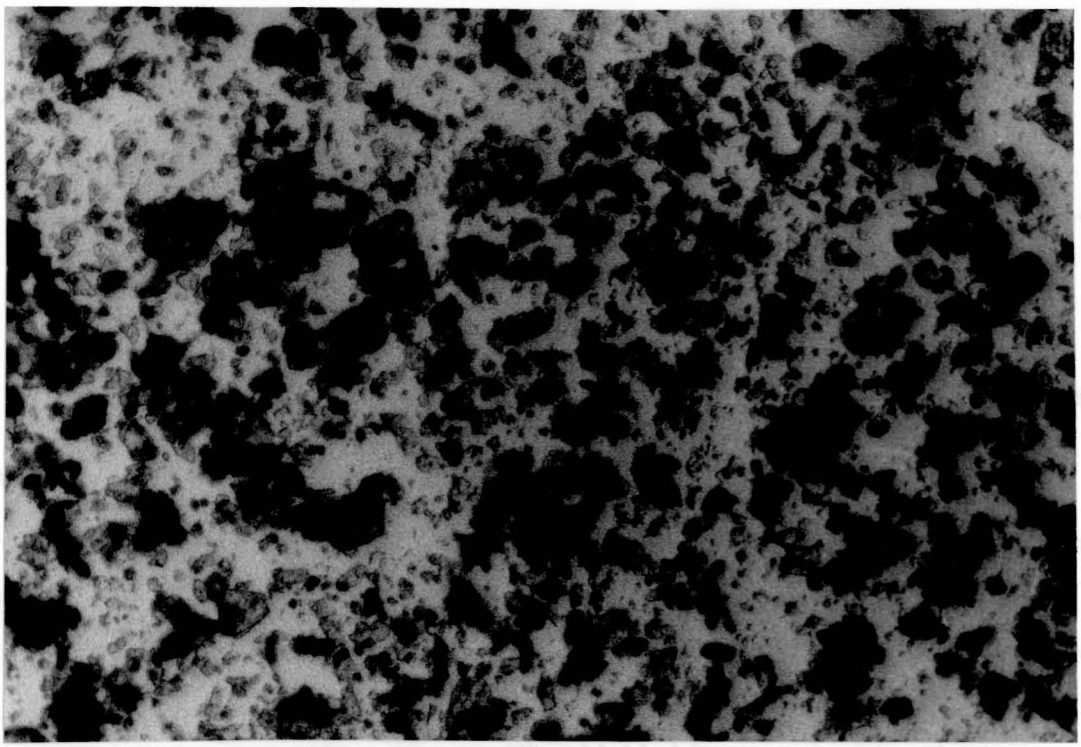

Scale: 22.05 um

(b)

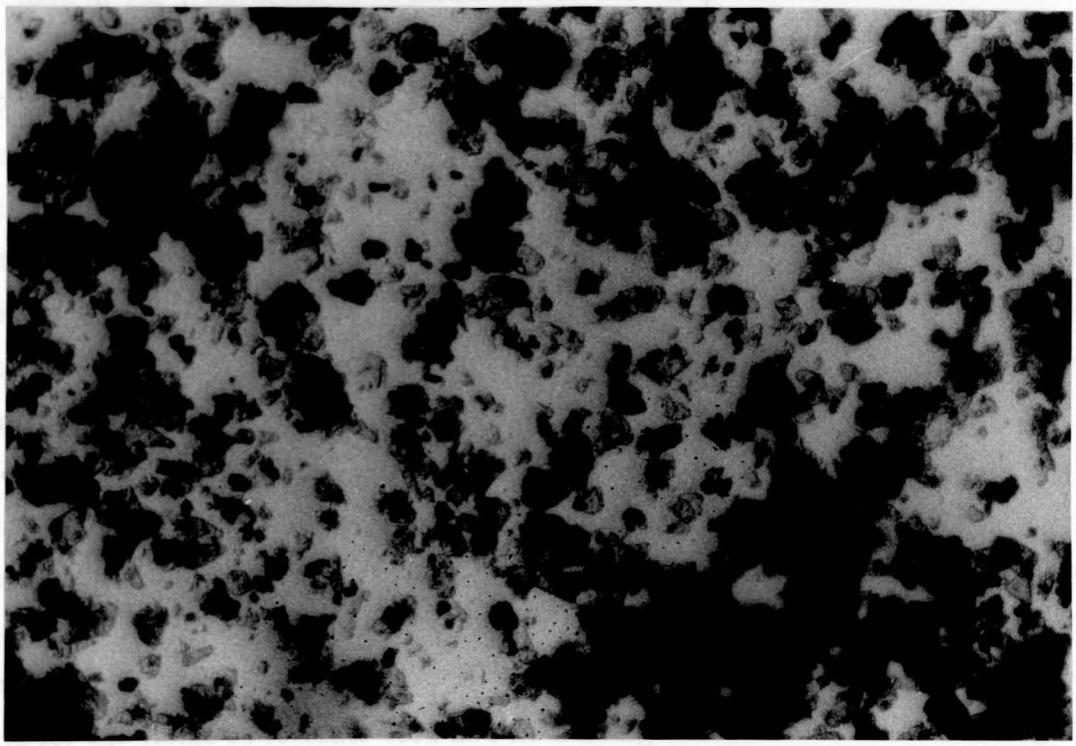

Scale: 22.05 um

Fig. 3.8 Optical micrographs of the grain in a powder with: (a) $\phi = 0.158$; (b) $\phi = 0.41$.

3.3 Measurements of the Conductivity and Dielectric Constant

3.3.1 Measurements on the Disc and Parallelepiped Samples

Axial Conductivity and Dielectric Constant Measurements

The DC resistances of the disc samples for $\phi < \phi_c$ were all measured using a Keithley 617 electrometer in V/I mode (two probe configuration) operated at $100V$. Because in this case the sample resistances can be as high as $5\text{x}10^{14}\Omega$ and the measurement current can go down to $0.2pA$, an electrical shield around both the sample and current lead is absolutely necessary. The shielded box required for this purpose was made in the laboratory. The insulation of the sample holder from current lead to ground was examined by measuring the resistance of an open circuit, i.e. with no sample between current and voltage leads. This measurement shows that the insulation resistance is higher than $2\text{x}10^{16}\Omega$, which is at least 40 times larger than the maximum resistance of the insulating discs measured. Therefore, this procedure made resistance measurements on insulating discs reliable. A $100V$ DC signal was always applied for 30minutes to allow the sample to reach equilibrium, before the reading of the resistance was taken. For $\phi > \phi_c$, the two-probe method was also employed, using the Keithley 617 electrometer operating in an Ohm-meter (constant current) mode for resistances larger than 100Ω. When the resistance was below 100Ω, separate voltage and current leads embedded in each of the electrodes had to be used. In these measurements, the DC current, which was controlled by a combination of the voltage source and buffer resistors, is in the range of 0.05 — $5mA$. The voltage and current were measured simultaneously using two digital volmeters. Good linearity was obtained for the range of currents used and no heating effects were observed during the experiments.

The AC resistance and capacitance of the disc samples were measured in an R—C parallel circuit mode at room temperature in the frequency range $30Hz$ to $100\text{M}Hz$ and with two equidistant points per decade on a log-scale. An ESI 2150 Video Bridge was employed in the frequency range $30Hz$ to $100\text{k}Hz$. The bridge was always set up to auto-average over twenty (the maximum) consecutive measurements, and was calibrated prior to use by making open and short circuit corrections, in order to get rid of the effects of lead resistances and stray capacitances. The bridge was operated in either the constant voltage or constant current mode depending on the resistance of the sample measured. For the samples with a DC resistance larger than 1000Ω, a constant voltage method was used together with the standard oscillator level of $1V$rms, in order to get good signal-to-noise ratio. A constant current, with a rms value of $1mA$, was used to measure the samples of a DC resistance less than 1000Ω. In the high-frequency regime, $300\text{k}Hz$ — $100\text{M}Hz$, a Hewlett-Packard (HP) 4592A network/spectrum analyzer, with a HP45925A impedance test kit, was used. The analyzer was operated in the impedance mode and routinely calibrated using three standard terminations: short, open and a 50Ω load. The data was averaged over 300-500 readings to reject random noise. In both the low- and high-frequency regimes, care was taken to ensure that the levels of signal used did not cause heating. The conductivity and dielectric constant were derived from the equivalent parallel resistance and capacitance readings given out by the instruments.

Transverse DC Conductivity Measurements

The measurements of DC conductivity of the conducting parallelepiped samples ($\phi > \phi_c$ only) were carried out using a conventional four-lead geometry. The voltage across the two voltage leads and current flowing through the sample were measured directly and simultaneously using two digital volmeters.

Because of an unsuitable geometry (i.e. a small cross-section area (8x2mm) rela-

tive to a larger length (24mm)), measurements of the AC resistance and capacitance for insulating parallelepiped samples were not feasible or unreliable, and consequently are not included in this work.

3.3.2 Measurements on the Powder Samples

It was probably the equal densities of graphite and hexagonal boron-nitride that made the powder experiments possible since there is no relative precipitation between the graphite and boron-nitride powders during powder pouring and while they are being compressed. Any humidity inside the powder can lead to a large spurious conductivity, as the BN component has a very high resistivity. Therefore all the powder experiments, including the pouring and the electrical measurements, had to be performed in an air-conditioned room with a relative humidity of less than 12% at room temperature. To check for inconsistencies, each powder experiment was repeated three times.

Measurements in the Axial Direction

The axial DC conductivities of 50%G-50%BN and 55%G-45%BN powders were measured in a polyethylene cylindrical vessel of 42mm internal diameter with a smooth brass bottom, which together with a close fitting non-rotating brass plunger formed the electrodes. The vessel and the plastic framework, which supported the plunger, were mounted on a plastic base. The plunger could be moved downwards using a 0.5mm pitch precision thread mechanism, which was calibrated before performing the experiments. This measurement system is very similar to that used to measure the axial AC conductivity and dielectric constant (see Fig. 3.9). The resistance of the empty vessel is above $2x10^{16}\Omega$, which is over 50 times larger than the maximum resistance of any powder measured.

To have a very low and constant initial apparent powder density in the vessel, special pouring methods had to be used. The plunger, together with the plastic

framework supporting it, was first removed. The powder was first poured into a cylinder with a sieve bottom, which was placed over and covering the orifice of the sample vessel. A solid bar, of the same length as the internal diameter of the cylindrical sieve and resting on the sieve bottom, was slowly rotated around a central pivot to agitate the powder, causing it to fall slowly through the sieve into the vessel. After this procedure, the plunger and the plastic framework were put back in the position, as illustrated in Fig. 3.9, and the whole system was then placed in an electrically shielded metal box. The voltage and shielded current leads from the electrometer were connected to the electrodes of the powder cell. To increase the volume fraction of graphite, the plunger was moved down gradually, and the corresponding volume fraction was calculated from the weight and density of the graphite in the powder and the total volume between the bottom plate and the plunger, whose position relative to the bottom plate is accurately known at all times from the micrometer or calibrated thread position. Near the percolation threshold the volume fraction increments were very small, 0.001 (0.1%). The following formula was used in the graphite volume fraction calculations for a cylindrical vessel in the powder experiments:

$$\phi = \frac{M \cdot wp \cdot \frac{1}{\rho}}{h \cdot \pi r^2}$$

$$= 4.955 \times \frac{wp}{hr^2}. \tag{3.3}$$

Here

M= the mass of powder mixture, 35.00±0.01grams;
wp= 0.50 for the 50%G-50%BN powder and 0.55 for the 55%G-45%BN powder;
ρ= the density of the graphite or boron-nitride, $2.25 g/cm^3$;
h= the separation between the bottom plate and plunger, cm;
r= the internal radius of the cylindrical vessel, cm.

At the beginning of an experiment the apparent density was about $0.36 g/cm^3$ which corresponds to a packing fraction for the G—BN powder of about 0.16. The

downward motion of the plunger was limited by the torque that could safely be applied to the calibrated thread. The resulting maximum apparent density was about $0.63g/cm^3$ and packing fraction of about 0.28. This packing fractions mean that there were always cavities in these powders during the measurements.

The DC resistance was measured using the Keithley 617 electrometer in the V/I mode. A voltage of $100V$ was used for resistances larger than $200G\Omega$ and the voltage was lowered to $10V$ and then down to $0.5V$, as the powder became more conductive with increasing graphite volume fraction while the plunger was moved down. The minimum resistance of powder in these experiments was larger than 100Ω due to the limitation of maximum torque which can be safely applied to the plastic framework and the thread. After the resistance had been read for a particular volume fraction, the Keithley electrometer was set to the zero check state, and then the plunger was slowly advanced to the next volume fraction position. After a pause of 5minutes to let the grains settle down, the zero check state was removed and the resistance recorded, after the reading had become stable. This usually took 15mins on insulating side and less than 1min on conducting side. Resistances between $200G\Omega$ and $20G\Omega$, where $\phi \approx \phi_c$, were too unstable to be measured.

Because the powder experiments gave extraordinary high values of the exponent t, a second pouring method had to be developed to check if the pouring procedure played a role. For this second method, a close fitting perspex piston, with a 1cm slot in the middle, was placed in the cylindrical cells. The slot was then filled and kept full of powder as the piston was moved upwards, with a rotating action, using a 1mm pitch threaded rod, and the powder was stroked into position with a "twist" motion.

Fig. 3.9 shows the system used to measure the axial AC conductivity and dielectric constant. In this case the cylindrical capacitive vessel consisted of a glass wall of 70mm internal diameter, a close fitting non-rotating plunger and the bottom plate. The plunger and the bottom plate, which were made from circuit boards backed by polyethylene plates, formed the two capacitor plates. The plunger was moved down

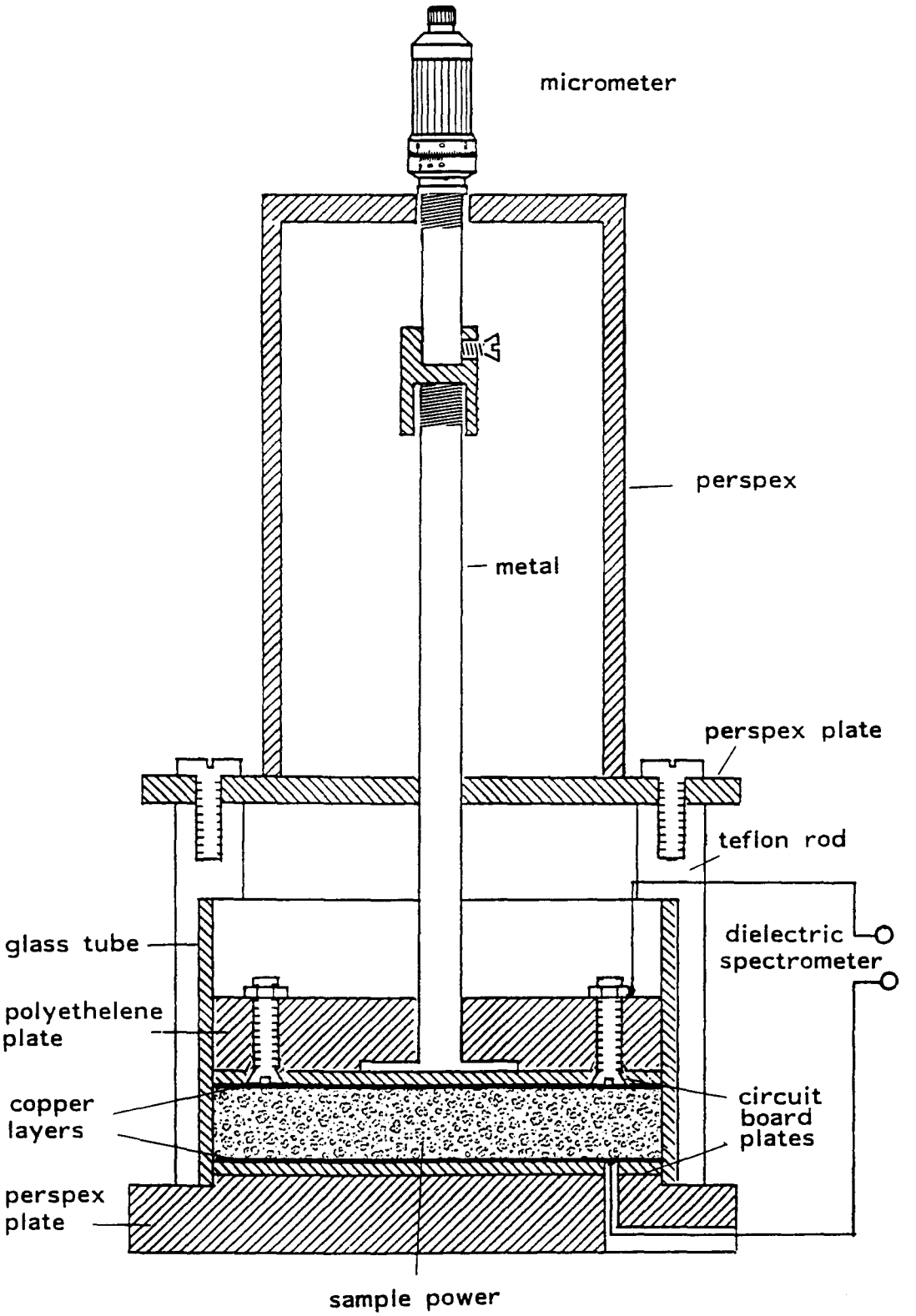

Fig. 3.9 Schematic diagram of the system used to measure the axial AC electrical conductivity and dielectric constant for powders.

using a 25mm micrometer head. The methods of pouring the powder into the vessel were the same as described above and the similar sieves with the appropriate diameters were used. An ESI 2150 bridge ($30Hz$ — $100\text{k}Hz$) and a HP4592A network/spectrum analyzer with HP45925A impedance test kit ($300\text{k}Hz$ — $10\text{M}Hz$) were used to measure the AC resistance and capacitance in the parallel circuit mode at room temperature. The calibration and set up of these two instruments are exactly the same as those for measuring the discs described in the previous subsection. Whenever the volume fraction was changed, the leads of either the ESI bridge or the impedance test kit were first disconnected from the sample vessel. Then the plunger and the bottom plate were electrically shorted out and the plunger was moved to a new volume fraction position. After a few minutes pause, the short circuit was removed and the four leads of the ESI bridge were reconnected to the vessel for low frequency measurements. The leads of the ESI were then replaced by two leads of HP45925A for the high frequency measurements. In this experiment, the leads were kept as short as possible, and great care was taken to ensure that the leads of the instruments were always in the same configuration when performing the measurement as they had been during the calibration procedure.

Measurements in the Transverse Direction

The apparatus and methods used to measure the transverse resistances and capacitances of the powders are very similar to those used for axial direction measurements. Therefore only the major differences in the design of the sample cells are described below.

The DC Measurements

To keep the stress distribution within the powder as close to that in the axial measurements as possible, the "powder cell " of the measurement system for the transverse DC conductivity was designed to be nearly the same as that used for axial measurements. The principal differences are that the walls of the cylindrical vessel

now consist of two 90° brass sectors separated by two 90° polyethylene sectors, and the plunger and bottom of the vessel are both polyethylene. In this case, the geometric factor, which is used to derive the conductivity from the resistance data, could not be calculated in a straightforward manner, and was therefore determined experimentally by painting 90° silver electrodes on the sides of 42mm diameter graphite cylinders of known resistivity and different lengths.

The AC Measurements

In this case the sample cell had to have a parallelepiped shape, with fixed thickness and variable cross-sectional area. Two 170x115mm copper/fibre glass circuit boards, with 150x115mm copper sheet in the middle, formed the two capacitance plates. These two circuit boards, backed by polyethylene sheet, were separated by two 10x10x115mm polyethylene spacers, and screwed to a polyethylene base. The plunger was a close fitting polyethylene section with a cross-section of 10x150mm, and was driven downwards by the same 0.5mm pitch precision screw as used in the axial DC measurements. The capacitance of the empty cell was calibrated against plunger height, so that the capacitance between the area of the capacitor plates covered by the plunger could be corrected for. A slot shaped sieve was used to pour the powders and a soft brush was moved backwards and forwards in the sieve to get the powder to flow through the mesh and into the cell.

3.4 Measurements of the Magnetoresistance and Hall Coefficient

The magnetoresistances of the conducting G-BN parallelepipeds near the percolation threshold were measured at room temperature in magnetic fields up to 1.5T. Fig. 3.10 shows a block diagram of the electric circuits and instruments used for automated measurements of the magnetoresistance and Hall coefficient. The data acquisition program is an analogue to the so-called DIP system, which is used to

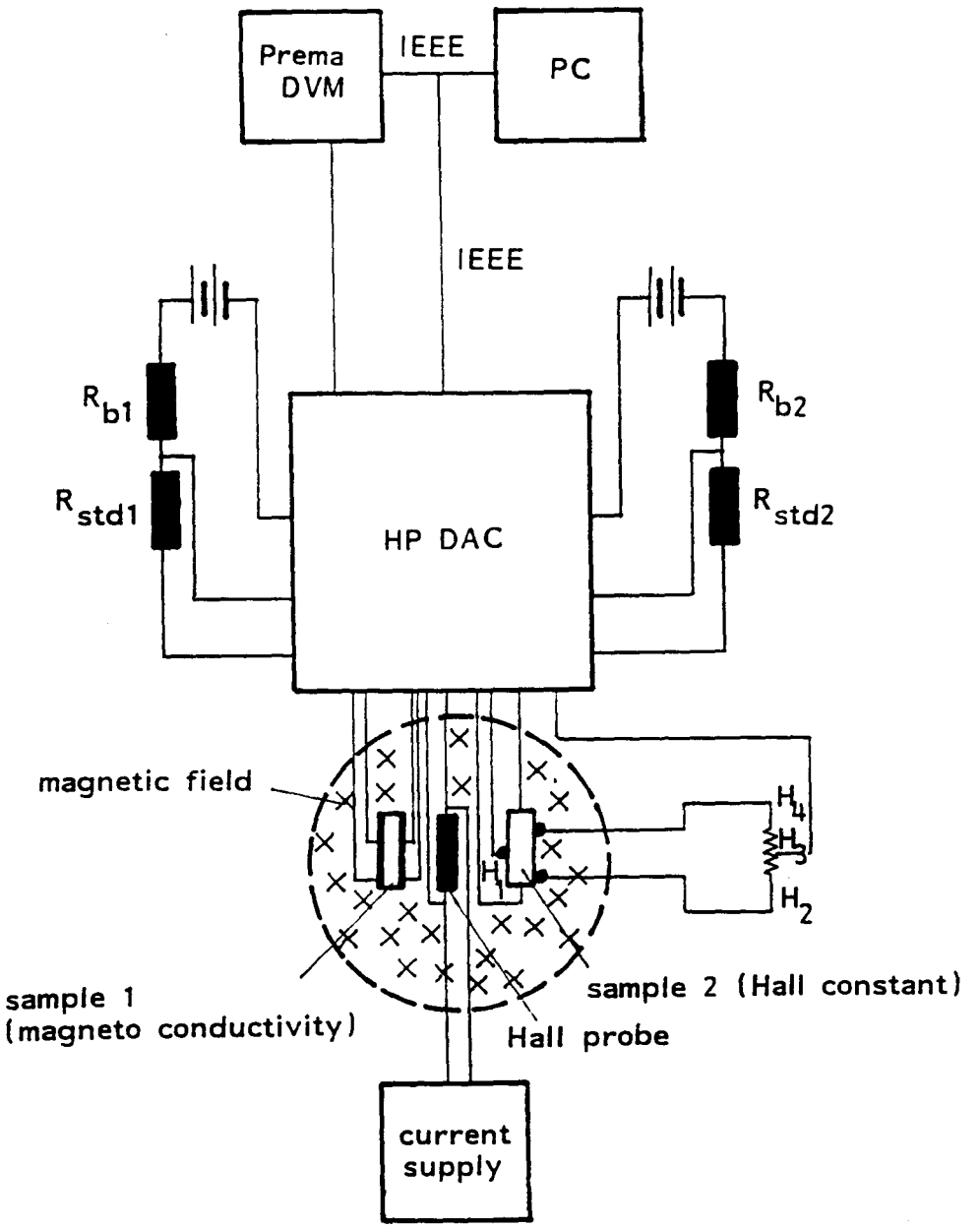

Fig. 3.10 Schematic diagram of the system used to measure the magnetoresistance and Hall coefficient for the G-BN conducting parallelepipeds.

measure the temperature dependence of various resistances in a range 1.8 — 300K, and was fully described by Albers (1994). The one major difference is that the Hall probe reading replaced the thermometer reading and the magnetic field replaced the temperature.

The desired currents through each sample were obtained by choosing appropriate values of the buffer resistors R_{b1} and R_{b2} (see Fig. 3.10). The polarity and magnitude of the magnetic field was controlled manually by reversing and varying the DC current in the windings of the magnet. A relay in the HP DAC (a HP3497A Data Acquisition/Control Unit) was used to reverse the direction of the sample current at every data point. The resistance of the sample was determined from the voltages across the sample and across the standard resistor. In order to cancel the spurious voltage due to misalignment and thermomagnetic effects, the average was taken for four readings: two by reversing the directions of the current and a further two by changing the polarity of the magnetic field. The HP DAC connected in turn the Hall probe leads and the many other voltage leads to the Prema 5000 Digital Voltmeter (DVM). When the circuit, which was being connected to DVM, is stable, the read-out digital signal from DVM is transferred to the PC for data reduction.

Several other salient features of this measurement system are described below.

The sample geometry

The length-to-width ratio of a rectangular parallelepiped sample influences the measured magnetoresistance and Hall coefficient in opposite ways [Putley 1960, Chapter 2]. Here the length is defined along the edge of sample with the same direction of the current, while the width is along the edge perpendicular to both the directions of the current and magnetic field. For the Hall coefficient, if the Hall voltage is measured on a short wide sample, with large area current electrodes at each end, then the voltage measured would be less than that expected from the simple theoretical expression. The reason for this is that the current electrodes at the ends tend to short out the Hall field. Quantitative calculations have shown that to eliminate this

shorting effect the length-to-width ratio must be greater than 3 or 4. On the other hand, the Hall electric field tends to prevent the curvature of the mean free path in the presence of a magnetic field, which is responsible for the increase in resistance. Therefore if the Hall field is shorted out, the measurement of the resistance change due to magnetic field will be more accurate. Therefore, while a large length-to-width ratio (≥ 3) is recommended for Hall effect measurements, a much smaller ratio is better for measuring the magnetoresistance.

Because of this, two different sample geometries were used to measure the magnetoresistance and Hall constant in the present study. For the magnetoresistance, the parallelepiped samples with a length-to-width ratio of $1/6$ were chosen in order to get a larger differential voltage signal due to an external magnetic field. Since the length of the sample is now too short to allow two voltage leads to be connected on its edge, a quasi-four probe method has to be employed to measure the magnetoresistance.

For the Hall coefficient, parallelepipeds with length-to-width ratio of 3, which were also used to measure the transverse conductivity, $1/f$ noise and thermoelectric power, were selected. As shown in Fig. 3.10, one Hall contact H_1 was applied at the geometrical middle point on one side of sample along the direction of the current, and on the another side a $1M\Omega$ (low noise) metal film potential divider $H_2H_3H_4$ was connected. With the magnet off, the position of the wiper (H_3) was adjusted to give zero potential difference between H_1 and H_3. With this circuit, when the magnet is switched on, the Hall voltage should appear between H_1 and H_3.

The Hall probe

A Siemens SBV538 Hall probe, driven by a $30mA$ DC current, was used to measure the magnetic field. It was calibrated at room temperature against the NMR (Nuclear Magnetic Resonance) Gaussmeter in the EPR laboratory of the physics department. The Hall voltage from the probe was measured during the experiment and converted to the magnetic field magnitude using the calibration data.

The magnet

A commercial electric-magnet (Newport Instruments), with conical pole pieces of 145mm initial and 70mm final pole diameters, was used to generate the magnetic field which ranged from 0T to 1.5T. Tapwater flowed though the cooling tubes in the coils. Two HP6528A DC power sources were connected in a master-slave mode to supply the current to the magnet. The direction of the magnetic field was reversed by changing the direction of the coil current, at nearly zero current, using a reversing switch.

The sample and Hall probe holder (not shown in Fig. 3.10)

The two samples to be measured were mounted on a flat polyethylene base, while the Hall probe was mounted on the underside of the base. The polyethylene base was supported by a wooden frame on the side of the magnet and adjusted to be parallel to the pole surfaces. Since the samples were held flat on the surface of the polyethylene base, the magnetic field and the direction of sample current were always vertical to each other during the measurements.

Because no Hall voltage signal could be detected at room temperature using the measurement system described above, measurements were also made at liquid nitrogen temperature, as the Hall coefficient for pure graphite increases rapidly with decreasing temperature. In the low temperature experiment, the sample was mounted on a teflon bar inserted in a stainless steel tube. This tube was then placed in a glass dewar of 17mm inter diameter, filling with liquid nitrogen, and the dewar was clasped vertically in magnetic field. At liquid nitrogen temperature, in addition to the DC method shown in Fig. 3.9 and discussed above, an AC method using a lock-in amplifier, operated at a low frequency, was also used to try to detect the Hall voltages. Unfortunately no Hall voltage was detected at liquid nitrogen temperature, using either the DC or the AC method. Because of the time limitations for this project,

further improvements of the Hall measurement system could not be carried out.

3.5 $1/f$ Noise Measurements

The $1/f$ noise experiments were carried out on conducting discs and parallelepipeds, near the percolation threshold. The measurements can be classified into two types according to their final objective: first, to measure the power-law for the normalized noise power against the sample resistances; second, to measure the sample size dependence of the normalized noise power for the samples near the critical volume fraction, where the fractal structure of the infinite cluster could dominate the physical properties of the sample.

The $1/f$ noise measurements were all made at room temperature over the frequency range $1Hz$ — $1000Hz$. A number of fresh $9V$ alkaline batteries connected in series formed the DC voltage source. A wire wound buffer resistor, or buffer resistors in series, with at least ten times the sample DC resistance, was connected in series with the sample to be measured. The voltage drop across the sample was amplified by a Stanford Applied Research SR560 Preamplifier, with the bandpass filter set at $0.3Hz$ and $3\mathrm{k}Hz$ in the low noise mode and running on its internal rechargeable batteries. The alkaline batteries, sample, buffer resistor(s), and preamplifier were all placed inside a grounded steel box. The output of the preamplifier was transmitted to a HP3562A signal/spectrum analyzer, which performs the analogue Fast-Fourier Transform (FFT) to give a noise power spectrum. A PC computer, connected to HP3562A through the IEEE bus line, recorded and plotted the spectrum. The DC current through the sample was varied by changing either the number of batteries in series or the resistance of the wire wound buffer resistor(s). The background noise from the batteries and preamplifier was examined by measuring the noise generated by a wire wound resistor, which replaced the sample in the circuit and had approximately the same resistance. This measured background noise is about four orders of magnitude smaller than the smallest $1/f$ noise level measured for the samples. The

contribution of the noise from the contacts between the sample and the electrical leads to the measured $1/f$ noise was also found to be negligible in these experiments. This conclusion was made because when one doubled the resistance of the buffer resistor and the voltage of the DC source (therefore the current through the sample is the same but the ratio of buffer resistance to sample resistance was doubled), no change in the slope and the magnitude of the noise power spectrum was observed [Leeman et al. 1980].

The $1/f$ noise spectrum between $1Hz$ and $1000Hz$ was taken for each sample and averaged for between 300 to 1000 sweeps by the signal analyzer. The background or thermal noise (i.e. zero current noise), which superposed on the $1/f$ noise spectrum generated by the current, was recorded first and later subtracted from the $1/f$ noise spectrum. In order to verify the I^2 or V^2–dependence of the $1/f$ noise spectrum, six or seven selected DC currents were used for each sample. The DC resistance of sample was also measured with the same electrical lead configuration, and using the same six or seven DC currents as that for the $1/f$ noise measurements. The results of these resistance measurements showed that the noise measurements were all taken within the Ohmic regime of the samples, and no heating effect was taking place.

The experiment to investigate the sample size dependence of the normalized $1/f$ noise power was performed in the following way. Disc shaped samples with a graphite volume fraction ϕ in the range 0.154 — 0.175 were made and selected. These discs were first cut into the largest rectangular shape possible and the $1/f$ noise was measured, in the transverse direction. Several DC currents were used to check the I^2— dependence of the noise power and the linearity of the resistance. Next, while keeping the sample thickness constant, the length and width were cut down so as to keep an approximately constant length-to-width ratio. The noise and resistance were measured in the same way as before, and then the size of the sample was reduced again. The series of sizes for two typical samples are given below:

$\phi = 0.1537$:
(1) 2.78x15.9x16.4mm,
(2) 2.78x12.8x13.9mm,
(3) 2.78x9.90x11.1mm,
(4) 2.78x7.70x8.60mm,
(5) 2.78x3.50x3.90mm.

$\phi = 0.1785$:
(1) 2.20x18.1x18.1mm,
(2) 2.20x16.3x16.3mm,
(3) 2.20x14.6x14.6mm,
(4) 2.20x12.3x12.3mm,
(5) 2.20x10.2x10.2mm,
(6) 2.20x8.40x8.40mm,
(7) 2.20x6.20x6.20mm.

3.6 Measurements of the Thermoelectric Power

The thermoelectric power measurements were made on conducting parallelepiped samples with graphite volume fractions from 0.154 to 0.82. The temperatures of the hot and cold ends of the sample to be measured were controlled so as to be $5\pm0.2°C$ and $45\pm0.2°C$ respectively. The apparatus, which was placed in an evaporation plant, is shown in Fig. 3.11. Two 50x60x10mm copper blocks formed the heat sink (cold block) and heat source (hot block) respectively. A heater coil was wound onto the hot block, which was thermally and electrically insulated from the copper base plate by four nylon screws. The heat sink is thermally and electrically connected to the copper base plate through two copper screws. The base plate was thermally coupled (welded) to the copper tube, through which the chilled cooling water passed. Two calibrated PT100 thermometers were embedded in each copper block to measure the temperatures. A standard four-probe method was employed to measure the resistances of these two thermometers. A constant current of $1mA$ from two Lakeshore 123 current sources passed through each thermometer. The voltage drops across the two thermometers were monitored continuously by two digital voltmeters. The voltage drop across the PT100 in the hot copper block and the $1mA$ current signal were simultaneously fed to the temperature sensor of a homemade PTC (positive temperature coefficient) temperature controller. The output of the temperature controller was fed to the heater coil on the hot block, which provided the power necessary to control the temperature of the hot block.

Silver paste was painted on the two 8x2mm ends of parallelepiped sample. The

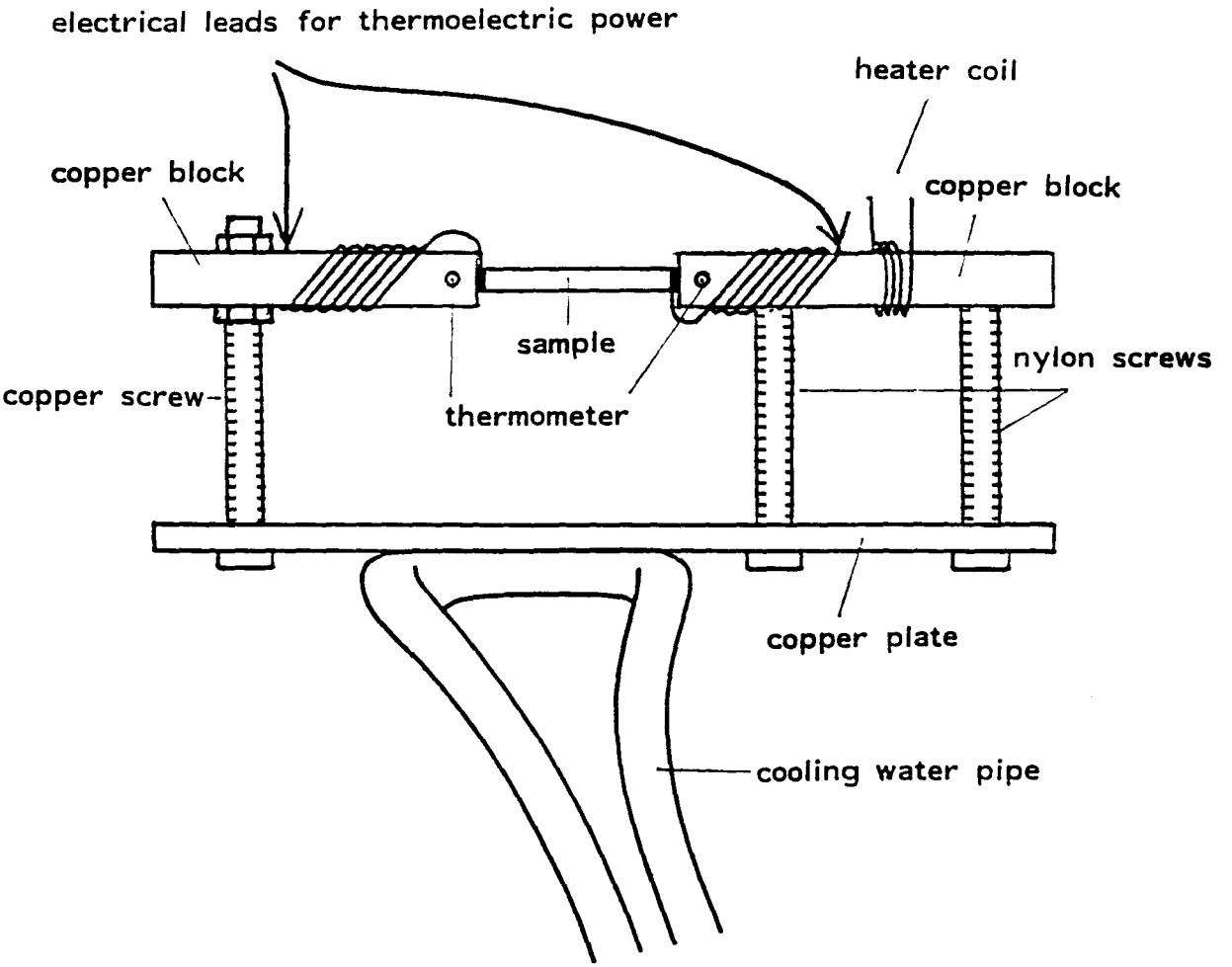

Fig. 3.11 Apparatus used to measure the thermoelectric power. The whole system shown is in a vacuum plant.

sample was then mounted, with the silver paint still wet, between the two copper blocks, after two electrical leads (copper wires) had been embedded in silver paint.. These leads, between the sample and each copper block, were used to measure the electrical potential difference. In order to avoid unwanted heat gradients, all the electrical leads, including all the leads for the two thermometers, were heat sunk by winding several turns of each wire around the corresponding copper blocks. A Prema 5000 $6\frac{1}{2}$ digital voltmeter with resolution of $0.1\mu V$ was used to measure the voltage between the cold and hot ends of sample. During the experiment, iced water was pumped through the cooling tube which cooled the heat sink (cold block) down to $5\pm0.2°C$, while the hot copper block was warmed up to $45\pm0.2°C$ by the temperature controller and heater. Inside the belljar the pressure was less than $1.0\text{x}10^{-5}$Torr. The potential difference between the two ends of the sample being measured was read from the DVM, when the temperatures of two PT100 thermometers had been stable for about half an hour. It should be noted that in the temperature range from $5°C$ to $45°C$ there is no thermodynamic phase transition in the G-BN samples, so that a constant thermoelectric power is a reasonably good approximation for these samples. This was later confirmed in the experiments since approximately the same thermoelectric power data was obtained when the temperature of the hot end of sample was set-up in the range $10° - 45°C$, but a larger temperature difference was preferred as it gave more accurate voltage readings on the DVM.

Before performing the measurements on the samples, the entire system was calibrated by soldering a constantan wire between the two copper wires wound onto both the cold and the hot copper blocks, and making measurements under the same conditions as the sample experienced during the experiment. The thermoelectric power of copper-constantan thermocouple measured in this system was $38.4\mu V/\text{K}$, reasonably close to the generally accepted value $40.2\mu V/\text{K}$.

3.7 Data Fitting Technique

The least squares fitting program of a commercial software package "Microscientist" was used to fit the relevant percolation equations to the experimental data obtained for the G-BN samples. A statistical program in the package gave the standard deviation with 95% confidence for each estimated parameter. For a parameter, which was obtained from fitting the experimental data from different runs, a weighted average was taken over all the estimated values in the following way

$$\overline{a} = \frac{\sum_j \overline{a}_j \cdot \frac{1}{\delta_j^2}}{\sum_j \frac{1}{\delta_j^2}}, \tag{3.4}$$

where $\overline{a}$ is the best final estimation of parameter a, $\overline{a}_j$ is a least squares fitting of the data obtained from the j-th run, and δ_j is the corresponding standard deviation. δ^*, the standard deviation given for $\overline{a}$, is obtained from

$$\delta^* = \frac{1}{\sqrt{\sum_j \frac{1}{\delta_j^2}}}. \tag{3.5}$$

The critical volume fraction ϕ_c is the most fundamental parameter used to describe a particular percolation system, as it explicitly appears in all the expressions involving various critical exponents. The following method was used for fitting the data to obtain the best values for ϕ_c and the critical exponents.

First, ϕ_c and conductivity exponents t and $\overline{s}$ were obtained by simultaneously fitting the two percolation equations for DC conductivity on each side of the percolation transition to the DC conductivity data. In this step, ϕ_c, the two pre-factors and the two exponents t and $\overline{s}$, were treated as free parameters and were determined as the values for which a minimum residual was obtained.

Secondly, the ϕ_c value obtained in step one was fixed, the pre-factor and the exponent in the relevant percolation equations, other than those for the DC conductivity, were allowed to vary. An estimation of the pre-factor and the exponent and their

standard deviations were obtained through the fitting program.

Thirdly, some small perturbations were given to ϕ_c, and the fitting program was re-started, using the pre-factor and the exponent obtained in the previous step as initial values, to check if the new value of ϕ_c results in a better fit of the pre-factor and the exponent. The change in the ϕ_c value by this method was always found to be insignificant. These procedures provided very reliable values for the fitting parameters.

Chapter 4

THE ELECTRICAL CONDUCTIVITY, DIELECTRIC CONSTANT AND MAGNETORESISTANCE

4.1 Introduction

As previously stated, the electrical conductivity and dielectric constant of random metal-insulator mixtures are the most widely investigated physical properties in percolation studies. Like other second order phase transitions, metal-insulator transitions are observed by a steep change of electrical conductivity in a narrow range of metal volume fractions. As already discussed in Chapter two, scaling theory predicts that, near the percolation threshold ϕ_c, the DC conductivity follows the power-laws (2.19) and (2.20) and that the low frequency dielectric constant follows another power-law (2.23). It also predicts that the AC conductivity and dielectric constant scale with frequency as described by (2.29), (2.30) and (2.31). Two physical models, namely intercluster polarization and anomalous diffusion, have been suggested to explain the AC scaling behaviour. They give rise to different expressions for the exponents x and y in (2.27) and (2.28), and (2.36) and (2.37) respectively.

The experimental data for the DC conductivity and the real part of the low frequency dielectric constant obtained from the disc samples, and the 50%G-50%BN and 55%G-45%BN powders are presented and analyzed in Section 4.2. The experimental results for the complex AC conductivity measurements are given and discussed in Section 4.3. The measured relative magnetoresistivity and magnetoconductivity are presented in Section 4.4. The chapter ends with a summary of the finding and discussions in Section 4.5.

In this chapter, the vacuum permittivity ε_o is left out in both $\varepsilon(\phi,0)$ and $\varepsilon(\phi,\omega)$, i.e. they are relative dielectric constant, in contrast to that used in Chapter 2.

4.2 The DC Conductivity and Low Frequency Dielectric Constant

The axial DC conductivity was measured for two sets of disc samples below and above the percolation thresholds, while the transverse DC conductivity was measured only on parallelepipeds cut from the second set of disc samples on the conducting side. Except where otherwise stated hereafter, the disc and parallelepiped samples referred to are the second set. For the 50%G-50BN and 55%G-45%BN powders, the measurements of the axial and transverse DC conductivities were made, using different cells, as described in Subsection 3.3.2. All the low frequency dielectric constants were measured at $100Hz$ and $1000Hz$.

In this section, the experimental results on the DC conductivity and the real part of the low frequency dielectric constant for G-BN disc samples and powders are presented. The discussion and comparison with other previously published experimental results are given, usually by a comparison of the critical volume fraction ϕ_c and the critical exponents t, $\bar{s}$ and s.

4.2.1 Results

Fig. 4.1 shows the logarithm of the room-temperature axial DC conductivities $\sigma(\phi, 0)$ as a function of the volume fractions for the second set of disc samples and a typical run on 55%G-45%BN powder. Both the conductivities vary by more than 14 orders of magnitude over the range of $0 \leq \phi \leq 0.23$, with a relatively small scatter of the data near the critical volume fraction. The crossover or critical region, defined by $(\sigma_i/\sigma_c)^{\frac{1}{t+\bar{s}}} \sim (10^{-16}/10^2)^{\frac{1}{t+\bar{s}}}$, is too small to observe. Similar results have been obtained for the first set of disc samples and other runs on the 55%G-45%BN and 50%G-50%BN powders. The two percolation equations, (2.19) and (2.20) with a common ϕ_c, are fitted simultaneously to the axial DC conductivity data for the discs. This fit gives a small uncertainty in and equally good statistical properties of the estimated parameters on both sides of the percolation threshold. The data and best fit results are shown in Figs. 4.2a and b, where both fits use the same value of $\phi_c(0.150)$. The transverse DC conductivity data, obtained from the parallelepiped samples cut from the disc samples with $\phi > \phi_c$, together with its best fit line ($\phi_c = 0.150$), are also given in Fig. 4.2a. Fig. 4.2c shows axial dielectric constant data for the discs, where the solid line is a least squares fit of the power-law relationship of (2.23) to both the $100Hz$ and $1000Hz$ data. In this fit ϕ_c was fixed at the value of 0.150, obtained from the best fit of the disc DC conductivity data plotted in Figs. 4.2a and b. The parameters ϕ_c, t, $\bar{s}$ and s for the disc samples are summarized in Table 4.1. Transverse DC conductivity and dielectric measurements on the parallelepiped samples on the insulating side were not possible due to unsuitable geometric factor. The capacitive measurements on the samples well above ϕ_c could not be made because of the high conductances of the samples and the limitation of the instruments used.

The conductivity data for all the discs from $\phi = 0$ to ϕ=0.82 is plotted as a function of volume fraction on a semi-log scale in Fig. 4.3. The theoretical curve in this case is a best fit to the GEM equation and the parameters are ϕ_c=0.150±0.002, $\log \sigma_i$=-15.86±0.04, $\log \sigma_c$=1.89±0.02, $\bar{s}$=1.05±0.18 and t=3.03±0.07. These parameters are very close to those (Table 4.1) obtained using a simultaneous fit to the two percola-

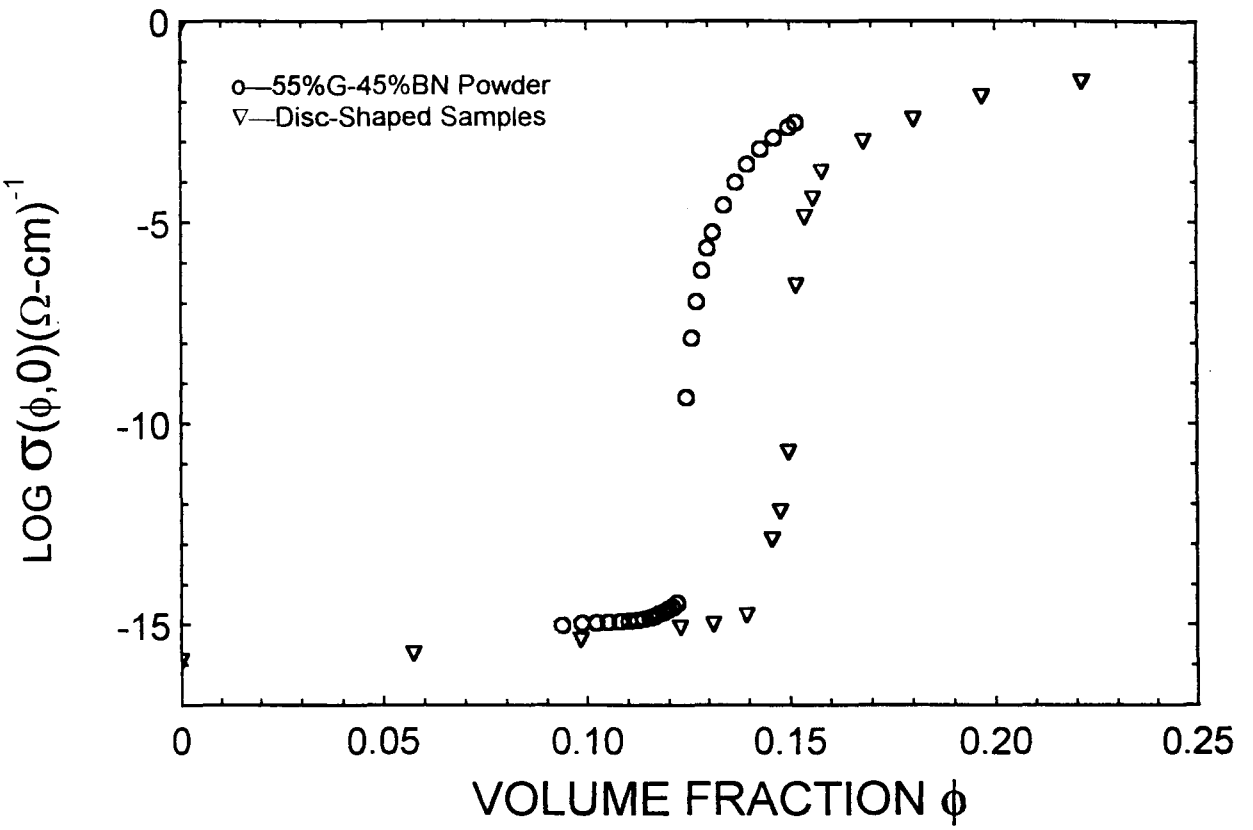

Fig. 4.1 The axial DC conductivity $\sigma(\phi, 0)$ versus the volume fractions on semi-log scale for disc shaped samples and a typical run on 55%G-45%BN powder.

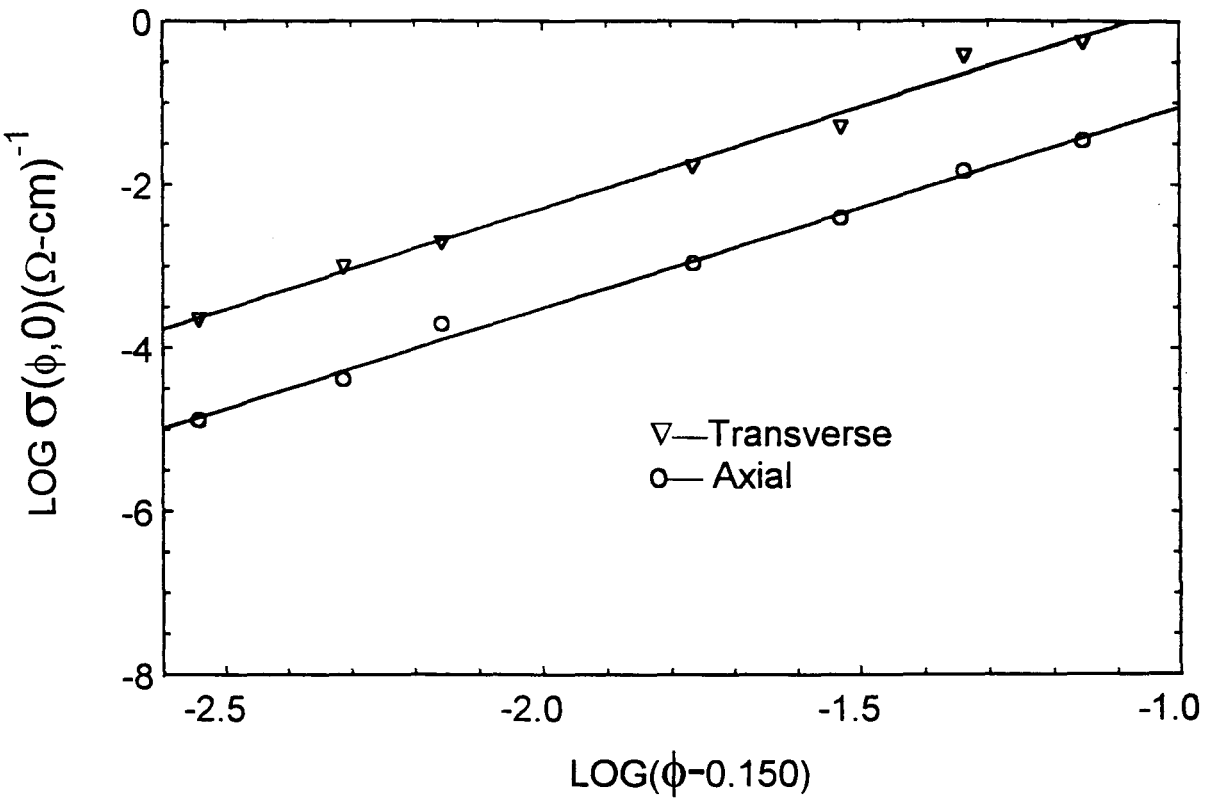

Fig. 4.2a The axial and transverse DC conductivities against $(\phi - \phi_c)$ for $\phi > \phi_c$. The critical volume fraction is found to be ϕ_c=0.150 ±0.001, and the values of t exponent are t = 2.63±0.07 and 2.68±0.13 in the axial and transverse directions respectively.

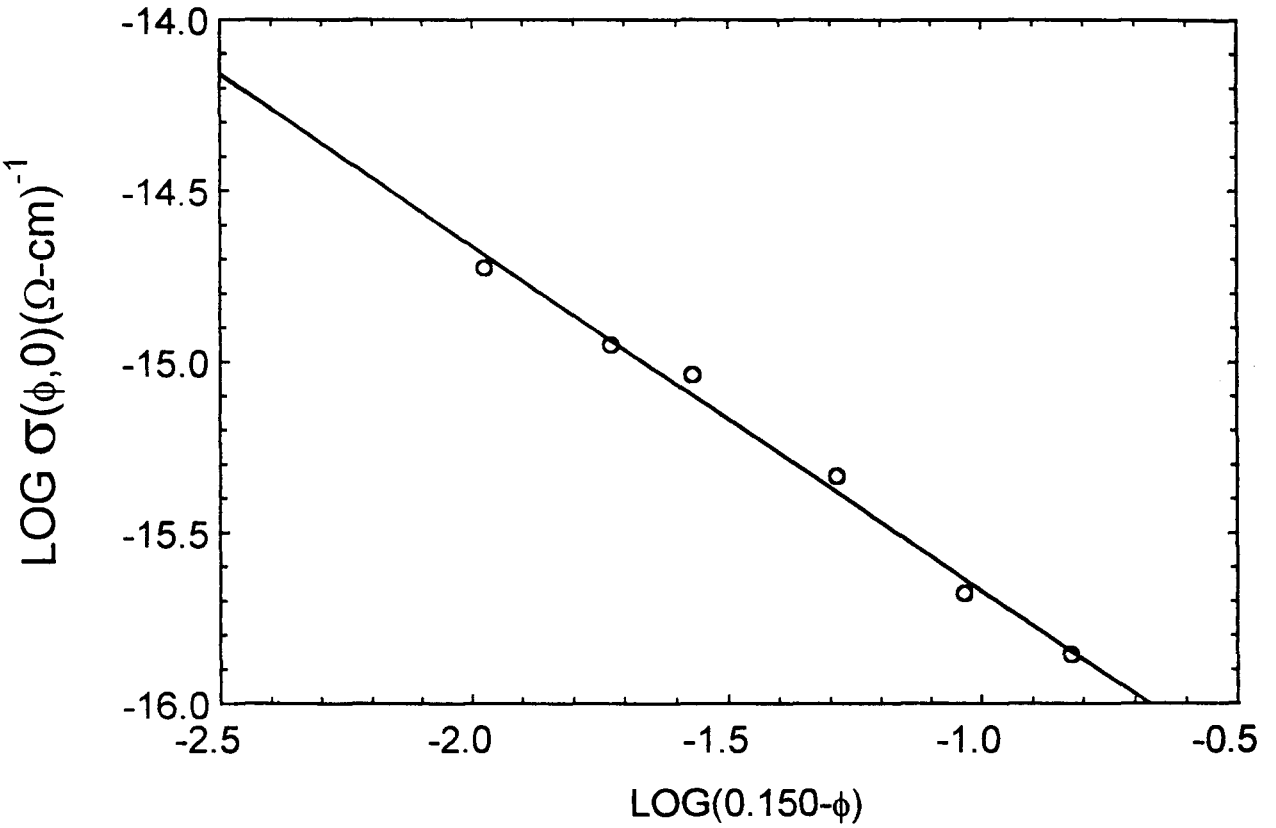

Fig. 4.2b The axial DC conductivity against $(\phi_c - \phi)$ for $\phi < \phi_c$, where ϕ_c =0.150. The value of $\bar{s}$ is found to be 1.01±0.05.

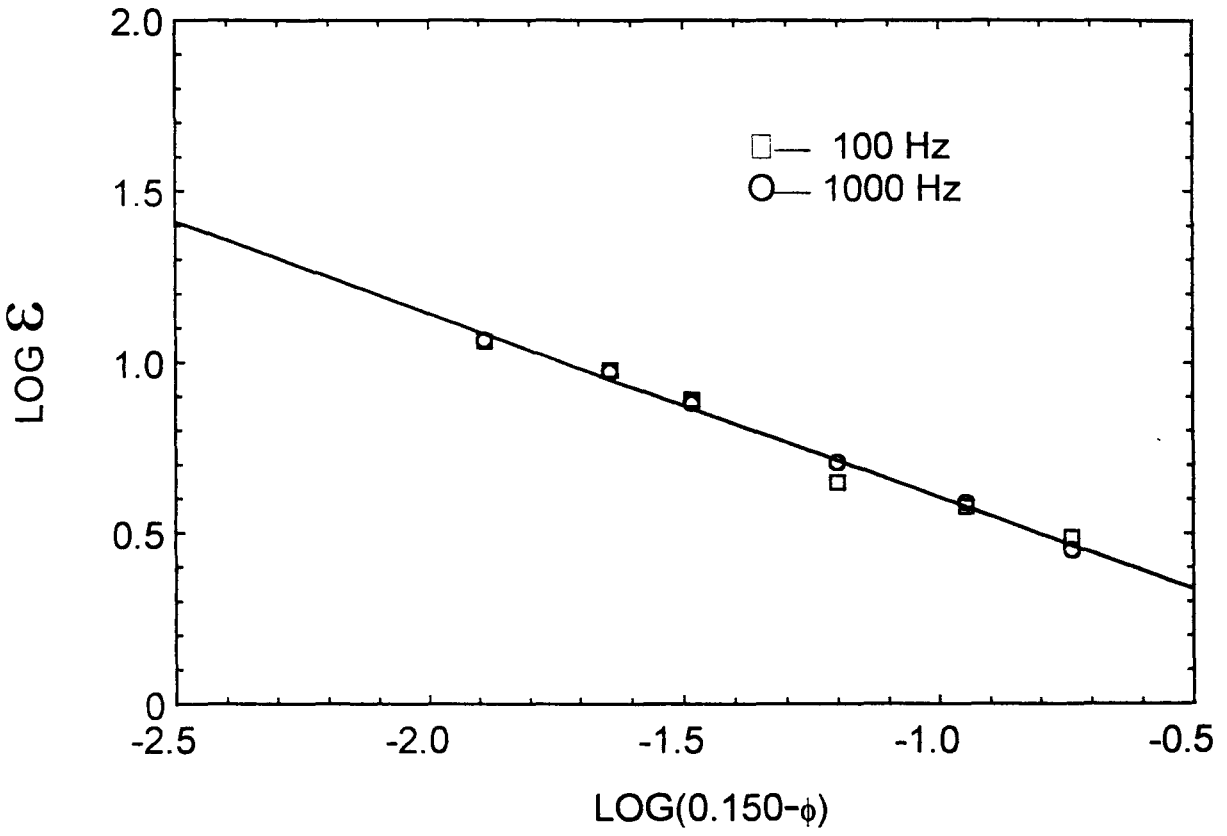

Fig. 4.2c The axial dielectric constant against $(\phi_c - \phi)$ for $\phi < \phi_c$. The exponent s is determined by least squares fitting using $\phi_c = 0.150$, and the fitting result is s =0.53±0.07.

Table 4.1 The observed critical volume fraction ϕ_c and exponents $\bar{s}$, s and t.

SAMPLE	ϕ_c	$\bar{s}$	s	t
Discs				
Axial AC	0.150 ± 0.001		0.53 ± 0.07	
Axial DC	0.150 ± 0.001	1.01 ± 0.05		2.63 ± 0.07
Transverse DC	0.150 ± 0.001			2.68 ± 0.13
Axial AC	0.153 ± 0.001		0.40 ± 0.02	
Axial DC	0.153 ± 0.001	1.06 ± 0.04		2.90 ± 0.20
'Poured Powder'				
50%G				
Axial AC	0.114 ± 0.001		0.60 ± 0.01	
Axial DC	0.120 ± 0.001	0.42 ± 0.01		4.85 ± 0.46
Transverse AC	0.108 ± 0.002		0.91 ± 0.02	
Transverse DC	0.116 ± 0.003	0.26 ± 0.05		6.10 ± 0.16
55%G				
Axial AC	0.124 ± 0.001		0.72 ± 0.01	
Axial DC	0.123 ± 0.001	0.47 ± 0.01		4.80 ± 0.14
Transverse AC	0.109 ± 0.001		0.83 ± 0.06	
Transverse DC	0.124 ± 0.001	0.46 ± 0.01		6.06 ± 0.13
'Twist' Powder				
50%G				
Axial AC	0.127 ± 0.001		0.53 ± 0.01	
Axial DC	0.123 ± 0.001	0.93 ± 0.13		4.64 ± 0.04

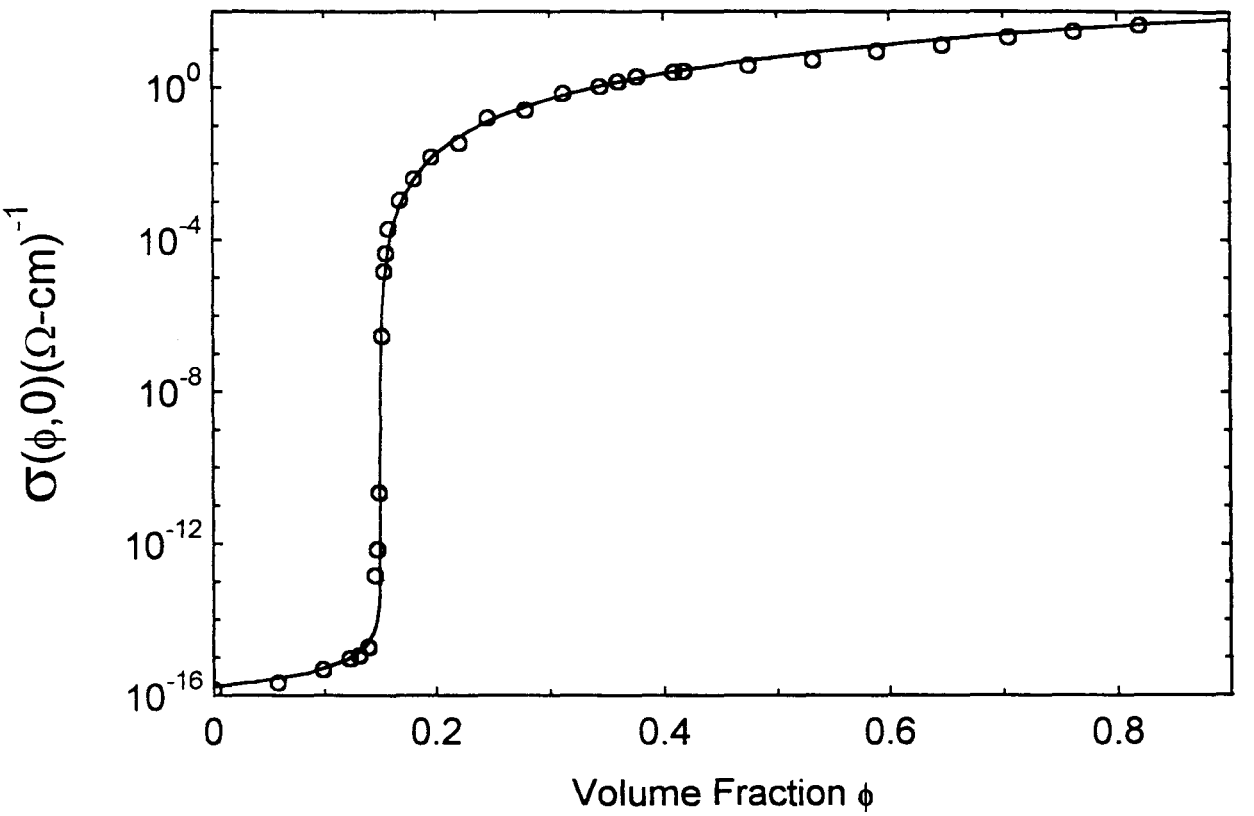

Fig. 4.3 The axial DC conductivity against ϕ for the disc samples over the full accessible range of ϕ. The solid line is a best fit to the GEM equation. The fitted parameters are given in the text.

tion equations, to the data in the volume fraction range from $\phi = 0$ to $\phi = 0.24$. In the range $0 < \phi < 0.24$ the GEM equation gives ϕ_c=0.150±0.002, $\log \sigma_i$=15.86±0.01, $\log \sigma_c$=1.50±0.13, $\overline{s}$=1.05±0.04 and t=2.7±0.24 in excellent agreement with the values given in Table 4.1.

Using $\phi_c = 0.150$, Equation (2.19) is also fitted to the axial disc conductivity data in the range $0.150 < \phi < 0.82$, as shown in Fig. 4.4. In this case, the conductivity exponent t is found to be 2.74, consistent with the value obtained from the data over the narrower volume fraction range $0.150 \sim 0.240$. Similar observations, that the percolation equations can, in some cases, fit the DC conductivity data over a wide range of volume fractions, were also noted by many authors [McLachlan 1986 and Kolek and Kusy 1991, and references therein].

The parameters ϕ_c, t and $\overline{s}$ for the axial and transverse DC powder conductivity data, on both sides of the metal-insulator transition, were also obtained using simultaneous fits of the data to Equations (2.19) and (2.20). Again due to the limitation of the instruments, the axial and transverse dielectric constant data at $100Hz$ and $1000Hz$ could be obtained for $\phi \leq \phi_c$ only. Therefore in this case both ϕ_c and s had to be treated as fitting parameters. Figs. 4.5a, b, and c show the data and fitted results for a typical run of powder experiments. The parameters ϕ_c, t, $\overline{s}$ and s obtained by fitting the experimental data were averaged over three runs of the powder experiments, and the results are summarized in Table 4.1. It is seen from the table that the values of ϕ_c for the transverse capacitive measurements are somewhat lower than those for the axial. This is attributed to the very different geometry of the two capacitive cells used. The dielectric exponent s, found at $100Hz$ and $1000Hz$, are virtually equal.

4.2.2 Discussion

The critical volume fractions

The observed critical volume fractions for the two sets of discs of 0.150±0.001

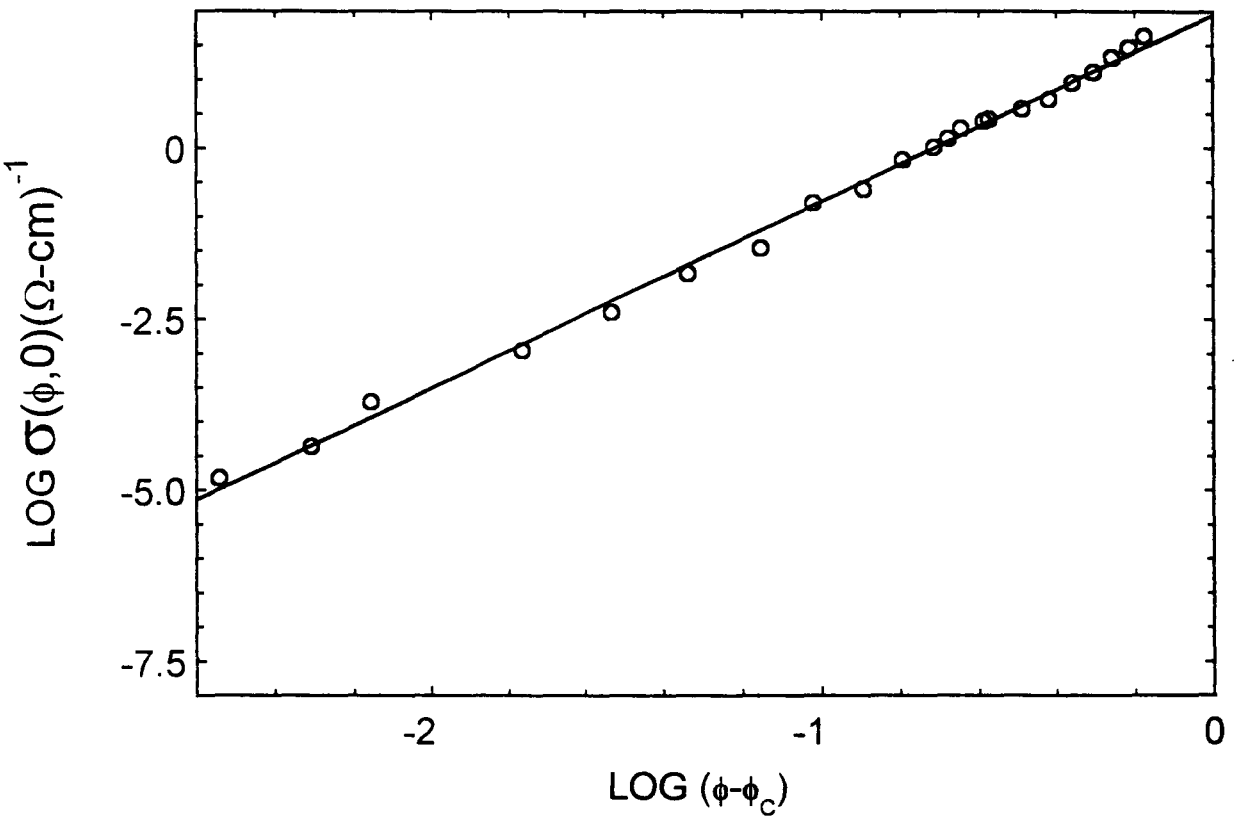

Fig. 4.4 The axial DC conductivity for the conducting disc samples against $(\phi - \phi_c)$ over the full accessible range of ϕ, where ϕ_c= 0.150. The solid line is a least squares fit to the data, which yields t=2.74.

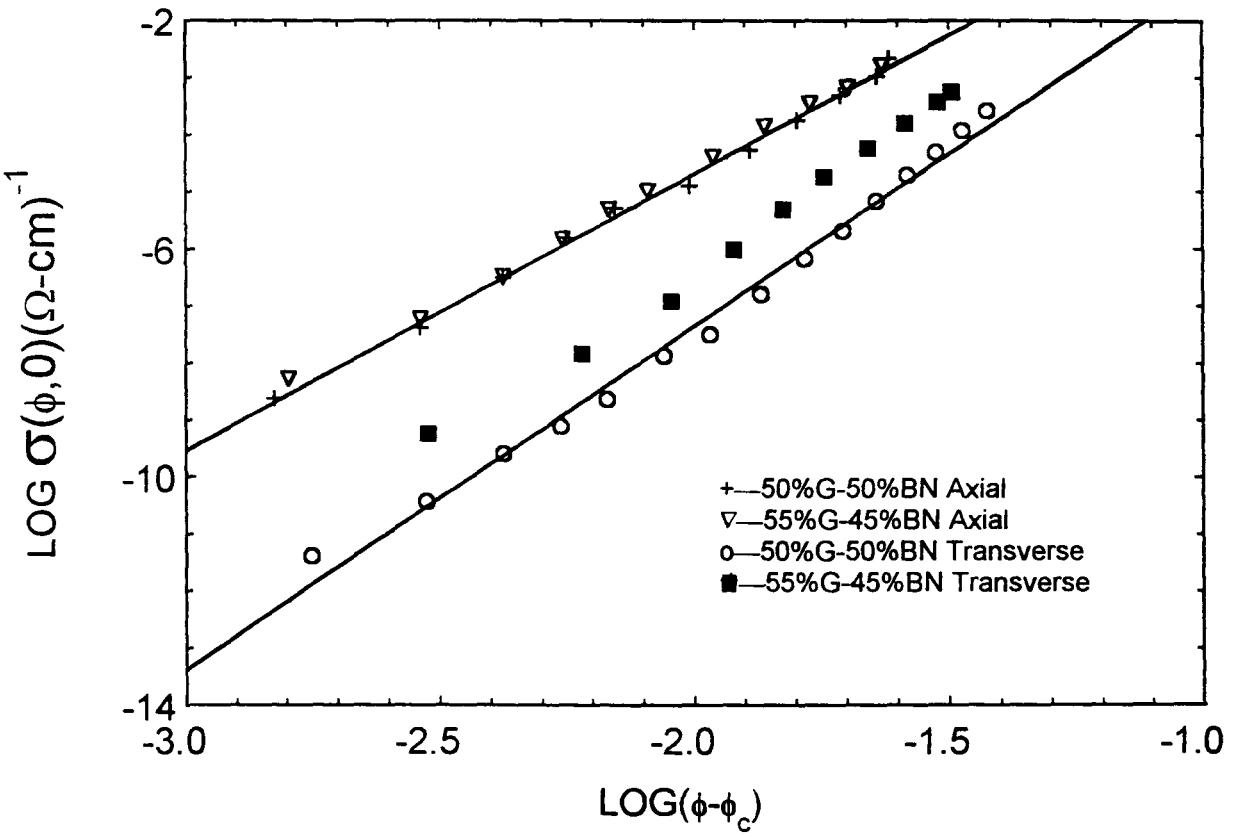

Fig. 4.5a The axial and transverse DC conductivities against $(\phi_c - \phi)$ for $\phi > \phi_c$ for powders undergoing compression on log-log scale. The solid lines show least squares fit to the data (o and +). The fitted parameters ϕ_c, t, $\bar{s}$ and s are summarized in Table 4.1.

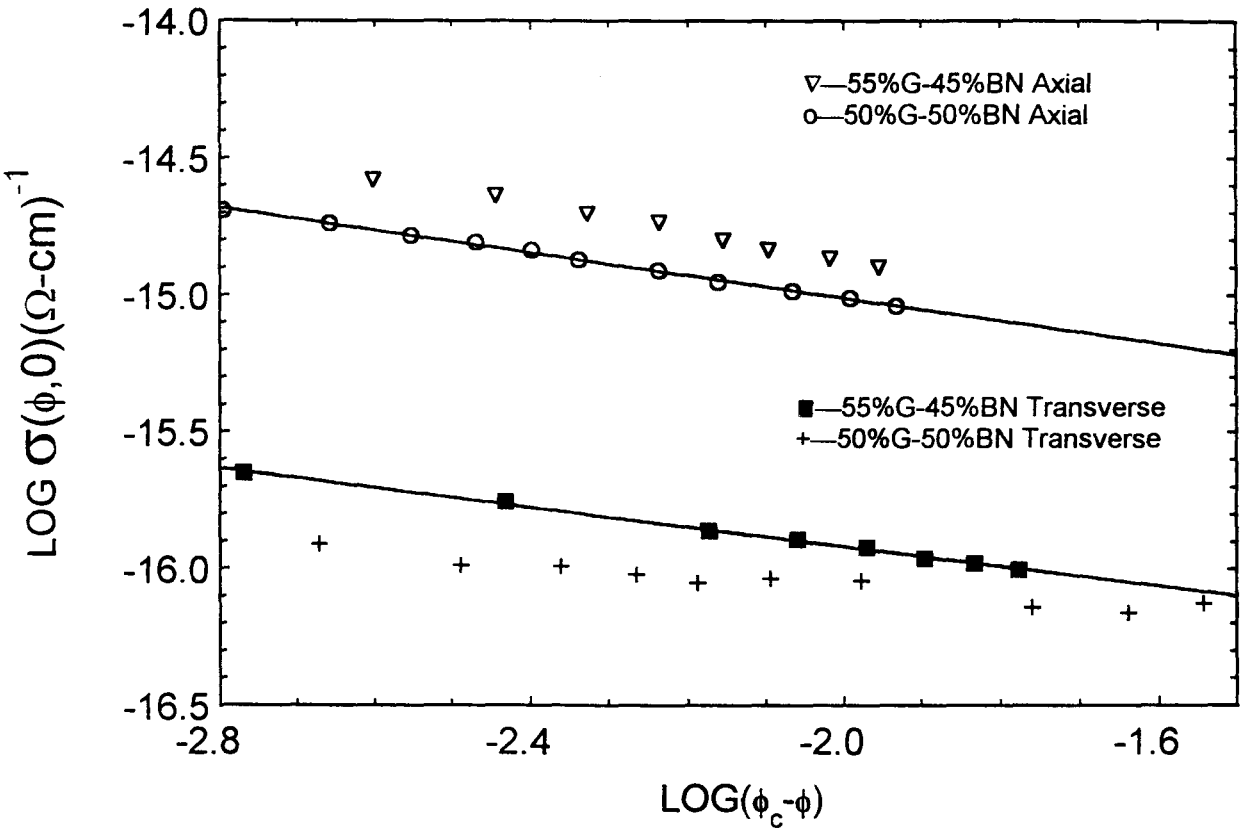

Fig. 4.5b The axial and transverse DC conductivities against $(\phi_c - \phi)$ for $\phi < \phi_c$. The ϕ_c values used are the same as those used in Fig. 4.5a.

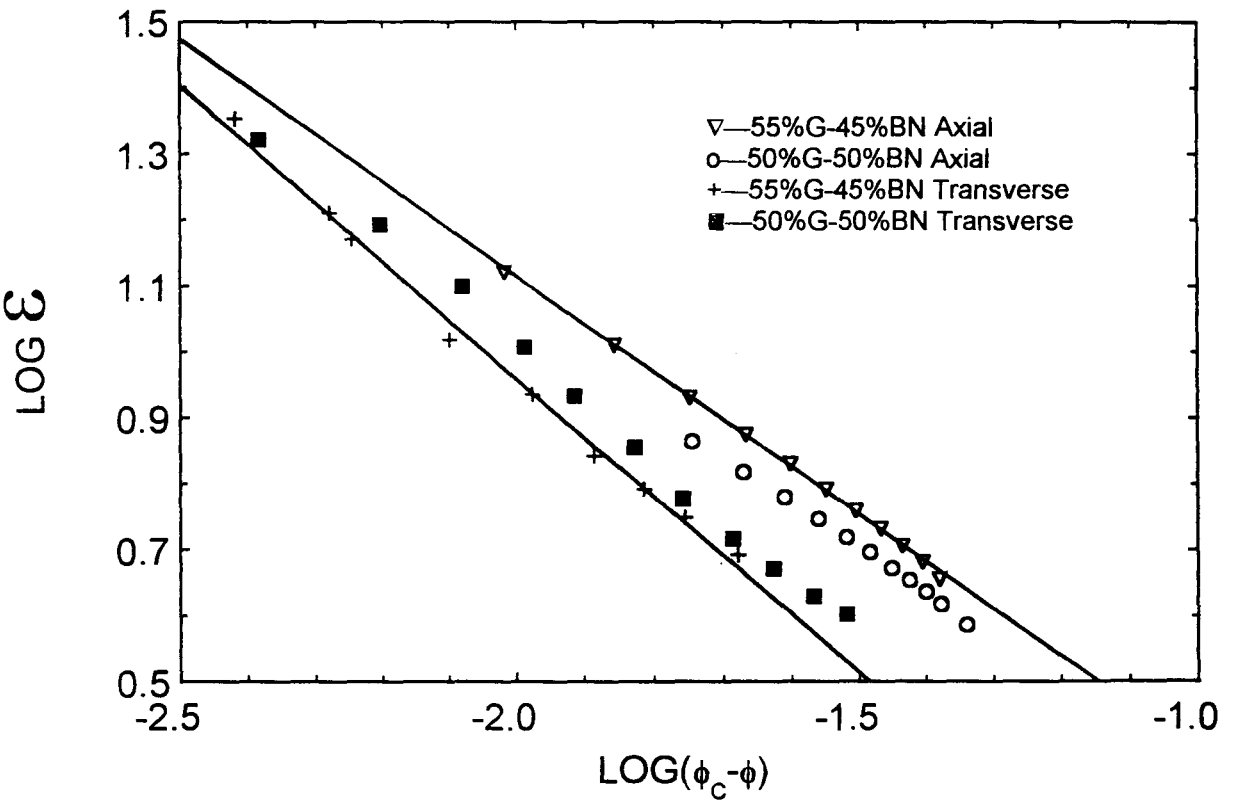

Fig. 4.5c The axial and transverse dielectric constants against $(\phi_c - \phi)$ for $\phi < \phi_c$. The ϕ_c values used are the same as those used in Fig. 4.5a.

and 0.153±0.001 are within the bounds ($\phi_c = 0.16 \pm 0.02$) for hard or impermeable spheres of a single size, such that the nearest neighbours just touch, placed randomly on a three dimensional lattice [Scher and Zallen 1970], and random close packed structures [Fitzpatrick et al. 1974]. This observation can be explained by the concept of the excluded volume, introduced into percolation studies of continuum media by Balberg and his collaborators (1984, 1987b). Normally it is the excluded volume or the geometry of the grains that determines the critical volume fraction ϕ_c. The excluded volume can be much larger than the actual volume for extended shapes, such as rods and discs, and results in a ϕ_c lower than 0.16. For spheres the actual and excluded volumes are the same. Therefore the measured critical volume fractions ϕ_c=0.150 and 0.153 agree with the approximate spherical shape of the grains in the G-BN disc samples, shown in the photographs presented in Fig. 3.8. Unlike in the experiments of Kirkpatrick (1979), the grains of both the G and BN used in this study are not single sized, which could influence the critical volume fraction. As previously discussed the size distributions of the G-BN grains are thought to be very similar. Because only the grain shape determines the excluded volume, the critical volume fraction ϕ_c is not expected to vary much from 0.16 due to the range of grain sizes [Balberg et al. 1984]. The conclusion is therefore that there is no reason why the two G-BN disc systems should not have the typical or random value of $\phi_c = 0.16$ [Scher and Zallen 1970, Balberg 1987b]. This also means that one cannot attribute abnormal values of exponent s, $\bar{s}$ and t obtained for the discs to an extreme value of ϕ_c.

From Table 4.1 for the powders the values of ϕ_c lie between 0.11 and 0.125, which are obviously different from 0.16±0.02. This is believed to be due to large cavities(air pores) in the powders, which could not be got rid of by pressure during the powder experiments since the starting packing fraction of both powders was typically 0.16 and the finishing (maximum) packing fraction is about 0.3, as was described in Subsection 3.3.2. In this case the G and BN grains tend to form a thick coating surrounding insulating cavities. This type of structure was originally considered by Malliaris and Turner (1971), but improved upon by Kusy (1977). Kusy argues that if the conducting particles have a much smaller radius than the insulating ones, the conducting powder

will tend to coat the insulating particles. Then, if the two or three dimensional two phase powder coating the voids is beyond the percolation limit, the resulting composite will be conducting but with a low value of ϕ_c. The practical minimum ϕ_c for this model is about 0.03. For $\phi_c \simeq 0.1$, according to Kusy's curve shown in Fig. 2.2, the ratio of the radii is about 7. Therefore, if the average size of cavities is of about 7 times the typical size of graphite grains, this could leads to a ϕ_c of about 0.10.

The conductivity exponent t

From the stress-strain experimental results, given in Subection 3.2.3, the structure of the G-BN disc system belongs to the inverted Swiss-cheese model, which predicted universal values of 1.7~2.0 for the conductivity exponent. The observed conductivity exponents, t = 2.6 ~2.9 for the disc and parallelepiped systems, are very different from the universal value. Within the inverted Swiss-cheese model, Balberg (1987a) suggested that barrier tunnelling of the charge carriers between the conducting grains in the backbones can give rise to a larger t exponent. As there is no oxide or polymer coating between the conducting G grains or clusters, tunnelling on the backbones of the G-BN percolation systems can be ignored. In Fig. 4.4, it is seen that one can fit the conductivity data in the range of $0.15 < \phi < 0.82$, with a single conductivity exponent and nearly equally good statistical probability near and far away from ϕ_c. Furthermore, Fig. 4.5a shows that the powder conductivity data, in the axial and transverse directions, can be fitted to the percolation equation on the conducting side over a range of about seven orders of magnitude in the conductivity, including points very near the critical volume fraction. This is strong evidence that a single metal conduction mechanism controls the conduction process on the conducting side.

A further consideration is the influence of the "hollow" cavities. As previously discussed in this subsection the powders should be visualized as a conductor-insulator mixture of two components, which coats the air filled cavities. As a powder system approaches and goes through the percolation threshold, the powder "coating" density increases and the cavities shrink (some may even vanish). Although the axial and

transverse DC conductivities give the same ϕ_c for the powders, the different exponents show that the axial and transverse directions are not equivalent in a percolation sense. As shown in Figs. 4.5a and b, the axial conductivities are higher than the transverse ones on both sides of ϕ_c, which could be due to the intergrain pressure being higher in the axial (compression and gravity) direction than in the transverse one. A large range of intergrain conductance could contribute to the enhancement of t [Kogut and Straley 1979]. This could be the one of the reasons why the transverse direction, probably with smaller intergrain contact pressures and hence a larger range of intergrain conductance, has a larger t.

Although the presence of very different microvoid structures could lead to the observed variation of the exponent t in G-BN systems, further experiments or computer simulations are needed. Unfortunately, these ideas have not yet been incorporated into any lattice simulations or model experimental systems, and probably occur in other continuum percolating composites. Further evidence for this cavity model is the experiments on thick film of glass-RuO_2 [Pike 1978], which also show very high t values (3 $\sim$5). In this system, the percolating filaments of RuO_2, obtained from a powder whose radius is much smaller than that of the glass beads, encapsulate a matrix of sintered glass beads. The ϕ_c for this system is very low ($\phi_c \leq 0.021$) in accord with the results of Kusy (1977), but this structure and the resultant ϕ_c can also be understood in terms of grain consolidation model [McLachlan 1991]. Carmona et al. (1984) also noted the analogies of their fibre-polymer geometry (with t values up to 3.5) to that of the thick film resistors. These results would suggest that the ratio of the radius of conducting grains to the radius of insulating one not only determines the critical volume fraction, according to Kusy (1977), but noticeably influence the exponent t as well. However, for the G-BN powders, as the size of the cavities is about 7 times that of the graphite grains, this could be the cause of their very large values of the conductivity exponent t. More theoretical and experimental work is necessary to determine how the grain size and presence of cavities affect the critical exponents.

Deprez and McLachlan (1988) made powder compression experiments which were

analogous to the present ones, except that the measurements were made using four different pure graphite powders and therefore for $\phi_c < \phi < 1$. They obtained $t(\phi_c)$ values, for the axial and the transverse directions respectively, of 1.94(0.295) & 2.8(0.27), 2.7(0.315) & 2.7(0.33), 1.52(0.27) & 2.1(0.25), and 1.5(0.38) & 2.4(0.37). These results show that both an anisotropic conductivity and different shapes of particles can give rise to different t and ϕ_c values, in single powder compression experiments. In the present case, the abnormally large t value in the powders is attributed to the number and nature of the cavities and voids as well as a larger range of intergrain conductances.

Another possible explanation for the large t values that must be considered is the anisotropy of the conductivity. To date this phenomenon has only been extensively investigated experimentally and numerically in two dimensional systems[Nan 1993 and references therein]. It has been found that while the t value in one direction increases with anisotropy, in other direction it decreases. This could be, but is probably not, a feature of two dimensional systems only. Therefore as t is larger than the universal value in both systems and approximately equal in both directions for the compressed discs, this "mechanism" can probably be ruled out.

The differences in the ϕ_c and t values measured for the "fully" compressed discs and powders undergoing compression, show that they belong to different classes of conductivity experiments. The conclusion of the above arguments is that the porosities, including large cavities, in continuum samples give rise to changes in the critical volume fraction ϕ_c and possibly in the conductivity exponent t.

The exponents $\bar{s}$ and s

The expected value for the exponent s from computer simulations is in a range of 0.87 ~0.89 [Stauffer and Aharony 1994]. From Table 4.1 it can be seen that a large range of s and $\bar{s}$ values have been observed in the present experiments. For the compressed discs, the s values, obtained from the real part of the dielectric constant, is clearly smaller than $\bar{s}$, obtained from DC conductivity data on the insulating side,

while for the poured powders undergoing compression the reverse is usually the case. Unfortunately, for powders poured by rotation, this is again reversed. An examination of the powder results show that the ϕ_c values observed from different pouring methods are closer to each other than either the s or $\bar{s}$ values. This shows that the exponent s and $\bar{s}$ are probably more sensitive to the microstructures of the discs and powders than is ϕ_c. However, this does not appear to be the case for the exponent t. As previously argued for the exponent t, the DC axial $\bar{s}$ value, which is greater than the universal value of s, cannot be accounted for using the inverted Swiss-cheese structure of the G-BN discs.

The values of $\bar{s}$ in this thesis appear to be the first obtained by ultra high resistivity measurements. It should be noted that the $\bar{s}$ values observed from the resistivity measurements are generally in disagreement with the s value obtained from dielectric measurements. In case of the two sets of disc samples, the s values from dielectric measurements is about half that from resistivity measurements. This would imply that the exponent $\bar{s}$ obtained from resistivity measurements could belong to another class of critical exponents. However, it could be due to the anisotropic conductivity of the graphite or some other specific feature of the G-BN systems. Further progress in this direction could not be made in this thesis.

An examination of previous values obtained for s from experimental dielectric measurements gives $s = 0.73$ for silver particles embedded in KCl matrix [Grannan et al. 1981], $s = 0.68$ for amorphous carbon in teflon [Song et al. 1986], and $s = 0.55$ and $s = 0.62$ for filamentary and nodular nickel in polypropylene respectively [Chen and Johnson 1991]. These values are higher than those obtained from disc dielectric measurements for both sets of the G-BN disc samples. However, a pattern is emerging that the values of s for comparable three dimensional continuum systems tend to be lower than the ("theoretical" or "universal") values obtained from computer simulations.

4.3 The Complex AC Conductivity

All the measurements of frequency-dependences of AC conductivity and dielectric constant were made in axial direction at room temperature in a frequency range from $30Hz$ to $100\mathrm{M}Hz$ for the disc samples and from $30Hz$ to $10\mathrm{M}Hz$ for the powders undergoing compression. The relevant experimental details for these experiments have been described in Section 3.3.

The experimental results for AC conductivity $\sigma(\phi,\omega)$ and dielectric constant $\varepsilon(\phi,\omega)$, obtained from G-BN disc samples, 50%G-50%BN and 55%G-45%BN powders, will be presented and discussed in terms of the intercluster polarization model, as discussed in Subsection 2.3.2.

4.3.1 The Exponents x and y

Figs. 4.6a, b and c show the AC conductivities versus the applied frequency on a log-log scale, for the selected samples, with graphite volume fractions near the percolation threshold. For $\phi < \phi_c$, the AC conductivities increase linearly with the signal frequency. Above ϕ_c, the samples show no dispersion in the low frequency range, as the conductivity is seen to be essentially constant. A DC-AC crossover frequency ω_c exists, beyond which the conductivity starts to increase with frequency, and eventually, in some cases very close to ϕ_c, shows a linear behavior on a log-log plot, i.e. a power-law behavior. The crossover frequency ω_c increases continuously as $(\phi-\phi_c)$, or the DC conductivity, increases. It should be noted that, at high frequencies, there is no difference in the dispersion of the insulating and conducting samples close to the critical volume fraction, as the slopes have approximately the same value. In contrast, the lack of dispersion in the low-frequency range distinguishes the conducting samples from insulating ones, which allows an estimate of the critical volume fraction ϕ_c to be made. For example, it can be seen from Fig. 4.6a that there is a flat response for

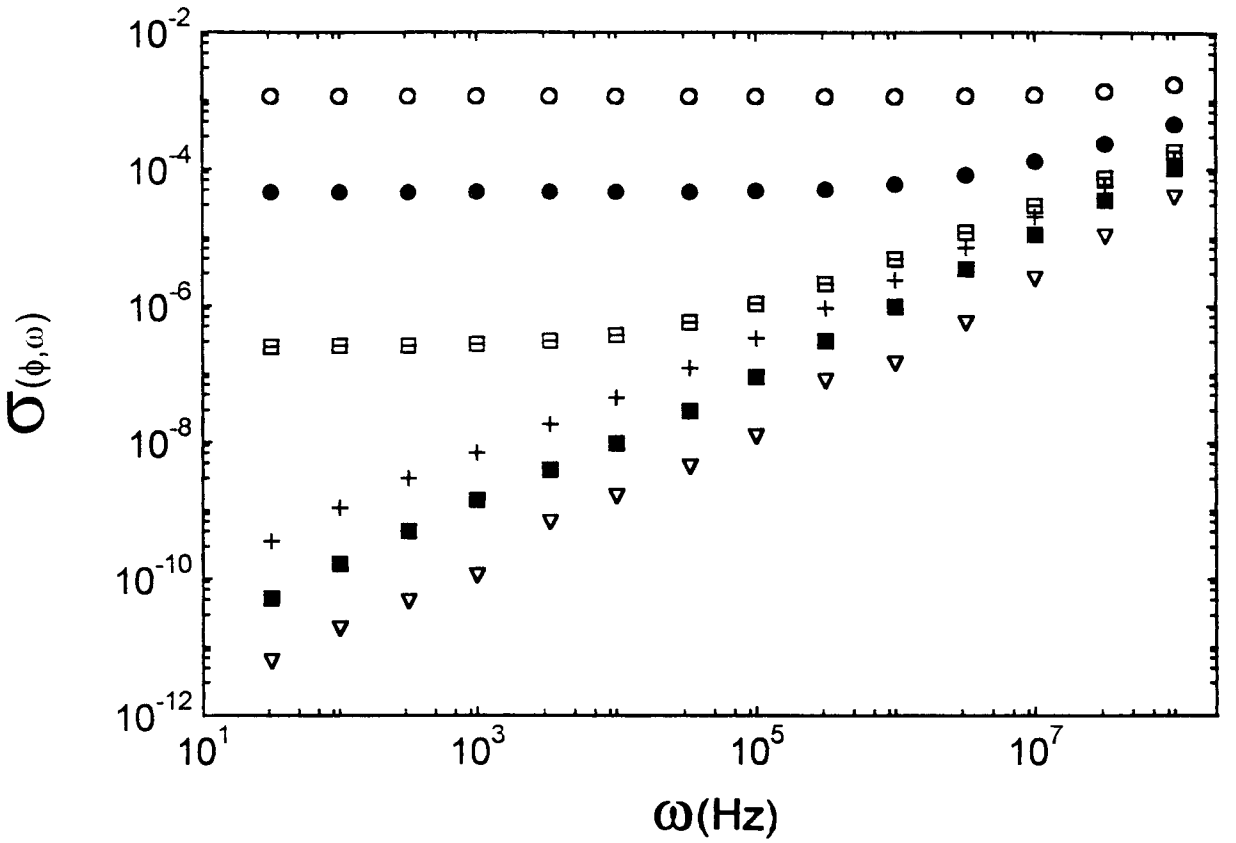

Fig. 4.6a The axial AC conductivities against frequency for the disc samples. ϕ =0.168(○), 0.158(•), 0.152(⊟), 0.150(+), 0.148(■),0.139(▽). The ϕ_c obtained from the DC conductivity data is 0.150±0.001.

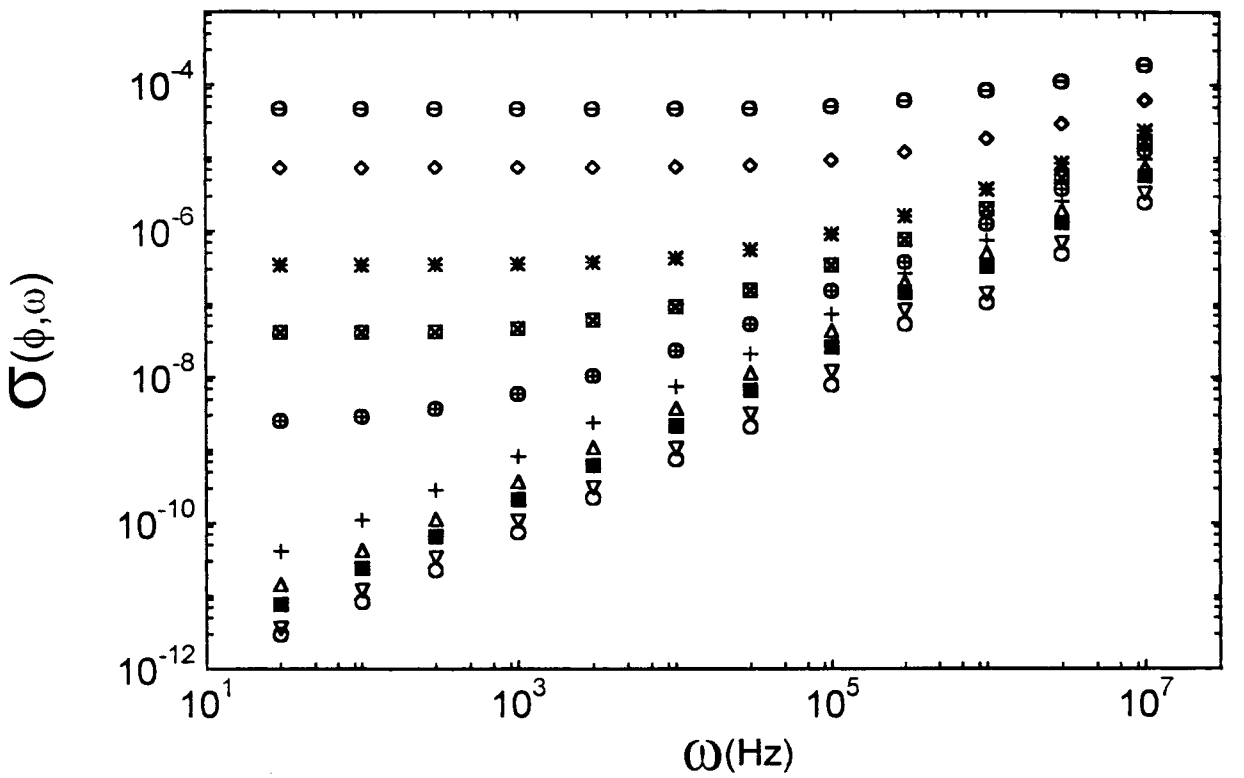

Fig. 4.6b The axial AC conductivities against frequency for the 50%G-50%BN powder. Here ϕ_c= 0.114±0.001. ϕ = 0.130(⊖), 0.124(◇), 0.118(✳), 0.116(⊠), 0.115(⊕), 0.113(+), 0.111(△), 0.109(■), 0.107(▽), 0.101(○).

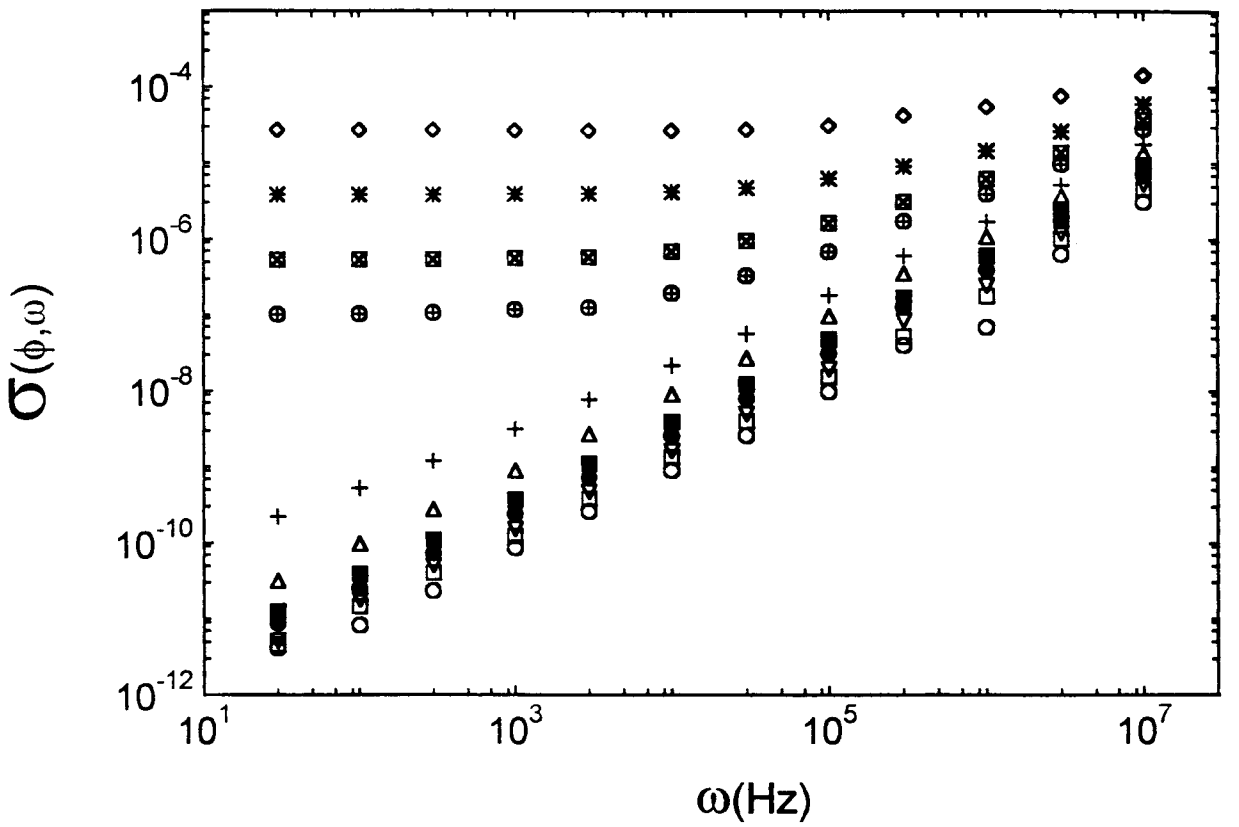

Fig. 4.6c The AC axial conductivities against frequency for the 55%G-45%BN powder. Here ϕ_c= 0.124±0.001. ϕ=0.133(◇), 0.129(✳), 0.127(⊠), 0.125(⊕), 0.123(+), 0.121(△), 0.120(■), 0.118(•), 0.116(▽), 0.115(□), 0.112(○).

frequencies lower than 10kHz for ϕ=0.152 sample, while the frequency response is linearly increasing over the whole frequency range for the ϕ=0.150 sample. There is no sample with a volume fraction ϕ between 0.152 and 0.150. Therefore the value of the critical volume fraction ϕ_c for the disc system can be estimated to be in the range of 0.150$\sim$ 0.152, which is in agreement with ϕ_c=0.150$\pm$0.001 obtained by fitting the two percolation equations simultaneously to the DC conductivity data.

The observed frequency dependence of the conductivity can be explained qualitatively in terms of the intercluster polarization, as was done by Song et al. (1986), and Chen and Johnson (1991). For $\phi > \phi_c$ and in the low frequency range, the current through a sample is almost entirely carried by the backbone, which consists of interconnected metal (graphite, in this case) clusters, because the capacitive "junctions", between neighboring finite clusters, form very high-impedance paths at the low frequencies. Consequently, the AC conductivity at these low frequencies differs only slightly from its DC value. As the frequency increases, the impedance of the intercluster capacitive junctions decreases and as a result the current can also flow along these low reactive impedance paths, which do not always incorporate into the backbone. Therefore the observed AC conductivity near ϕ_c results from two mechanisms: the capacitive impedance paths shunted by the backbone. At higher frequencies, the capacitive paths offer lower impedances as they have become more conducting and can finally short circuit most of the conducting path along the backbone, which results in the power-law behavior in ω for the insulating samples. Near the critical volume fraction ϕ_c ($\phi \geq \phi_c$), there exist only a few filamentary percolating paths consisting of very small clusters and this makes the impedance of the capacitive paths comparable to that of the resistive ones at low frequencies. Thus ω_c will become lower than that of samples well above ϕ_c. For $\phi < \phi_c$, the impedances of the capacitive junctions will be predominant over whole frequency range, as there is no DC percolating path through the sample.

According to the scaling law discussed in Subsection 2.3.2, the scaling function g_+ depends only on ω/ω_c. Figs. 4.7a, b, and c show the reduced AC conductivity

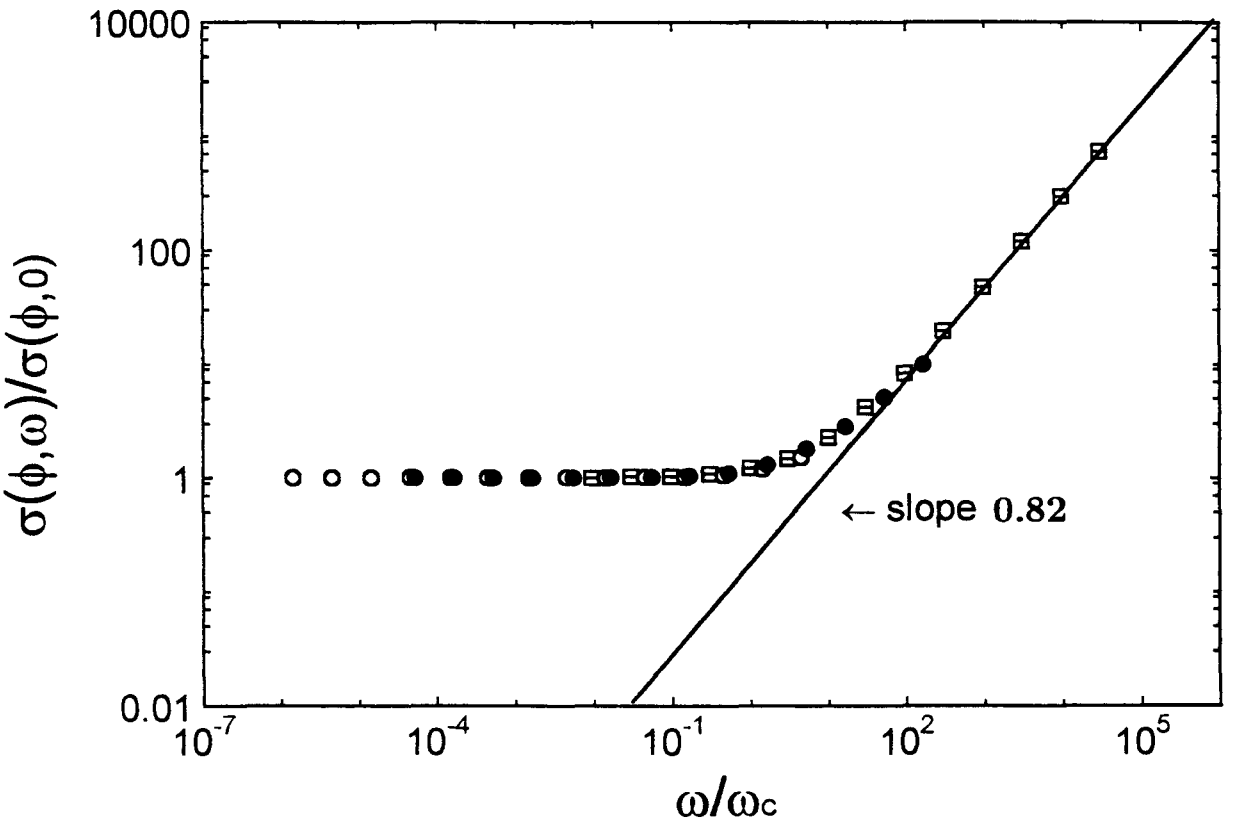

Fig. 4.7a The scaled axial AC conductivity $\sigma(\phi,\omega)/\sigma(\phi,0)$ against the scaled frequency ω/ω_c for the disc samples. The straight line is a power-law fit to the scaled data in the high-frequency regime. The slope is $x = 0.82 \pm 0.02$. ϕ =0.168(◯), 0.158(•), 0.152(⊟).

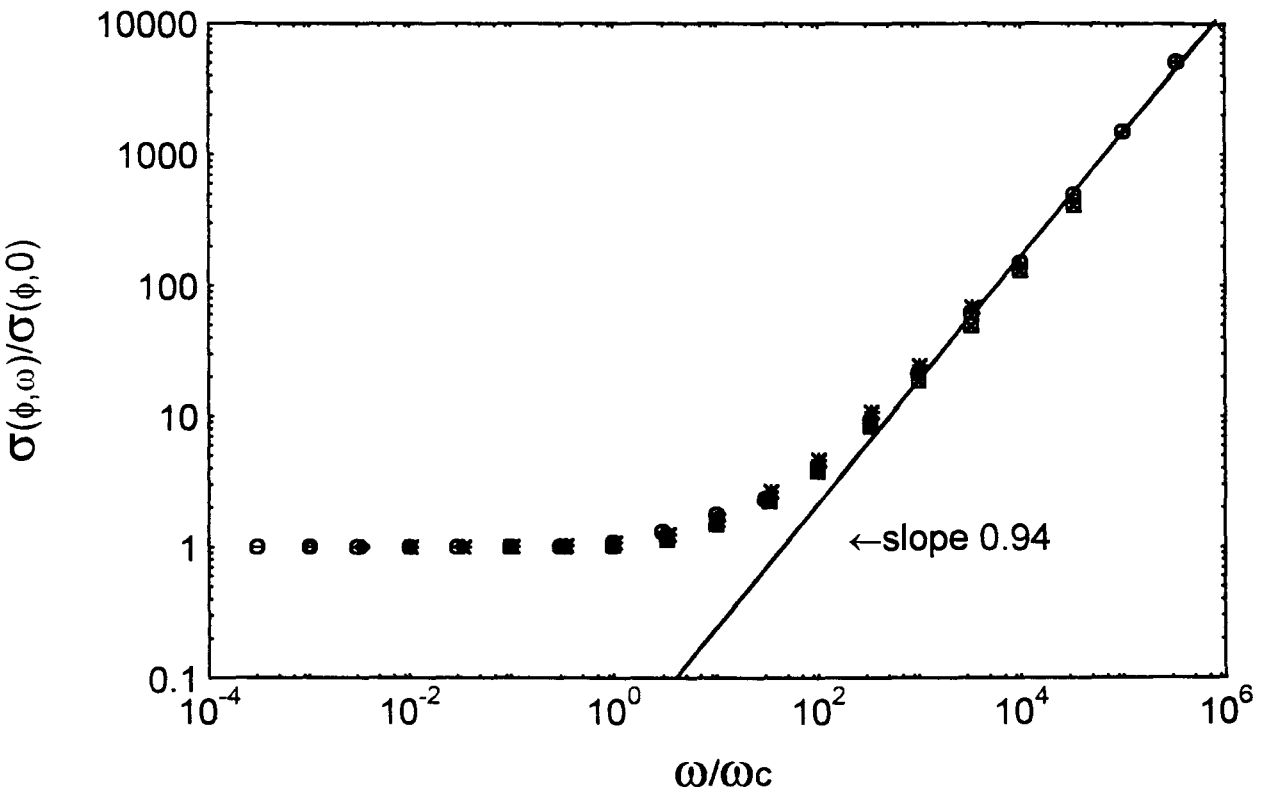

Fig. 4.7b The scaled axial AC conductivity $\sigma(\phi,\omega)/\sigma(\phi,0)$ against the scaled frequency ω/ω_c for the 50%G-50%BN powder. The slope is x =0.94±0.02. ϕ=0.130(⊖), 0.124(◇), 0.118(∗), 0.116(⊠), 0.115(⊕).

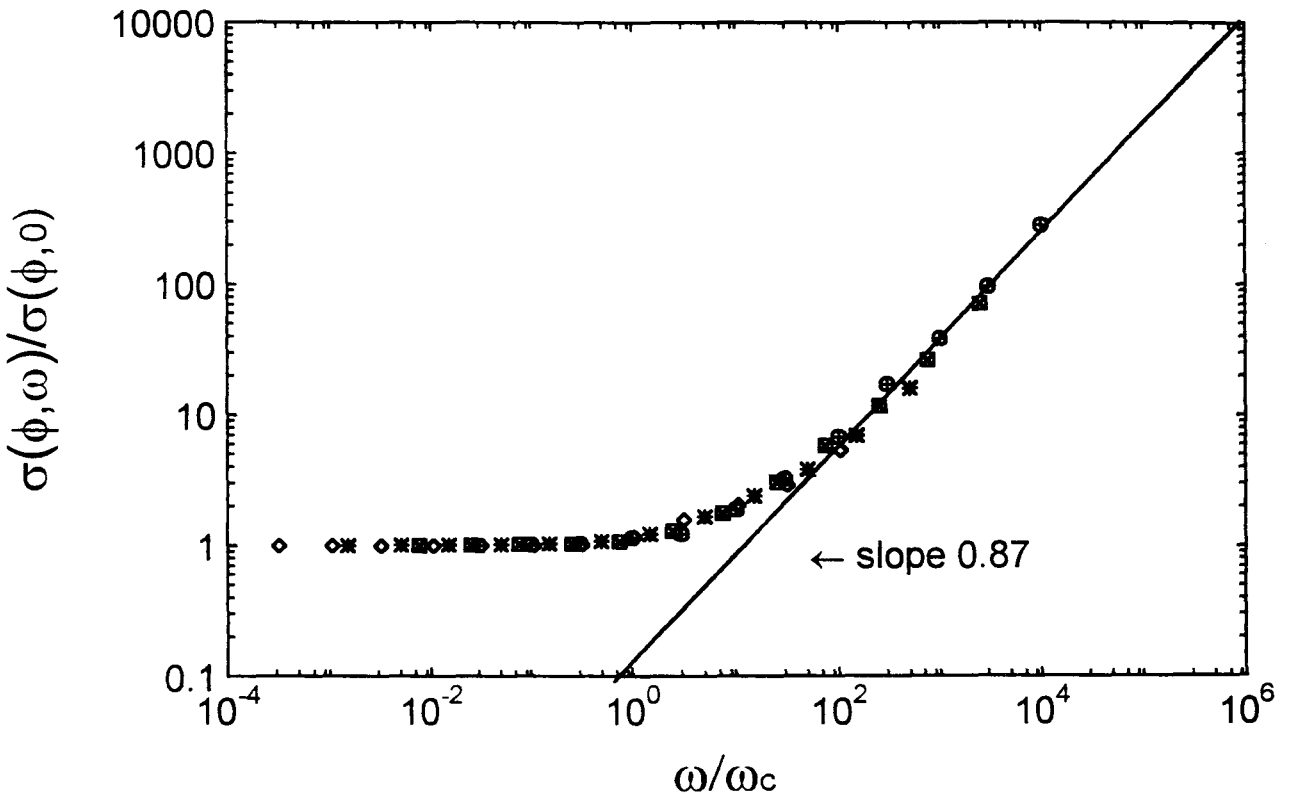

Fig. 4.7c The scaled axial AC conductivity $\sigma(\phi,\omega)/\sigma(\phi,0)$ against the scaled frequency ω/ω_c for the 55%G-45%BN powder. The slope is $x = 0.87 \pm 0.02$. ϕ=0.133($\diamond$), 0.129($*$), 0.127($\boxtimes$), 0.125($\oplus$).

$\sigma(\phi,\omega)/\sigma(\phi,0)$ for the conducting samples versus the reduced frequency ω/ω_c. To obtain the scaled plot, ω_c was treated as a fitting parameter for each sample and selected to give the best fit to the universal curve. Using this approach it was found that the data belonging to different samples could indeed be made to collapse into a single or universal curve. In the region $\omega/\omega_c > 1$, $\sigma(\phi,\omega)/\sigma(\phi,0)$ obeyed the power-law $\sigma(\phi,\omega)/\sigma(\phi,0) \propto (\omega/\omega_c)^x$, which yields x=0.82±0.02, 0.94±0.02, and 0.87±0.01 for disc samples, 50%G-50%BN and 55%G-45%BN powders, respectively.

The variations of AC axial dielectric constant as a function of frequency for the samples on insulating side of ϕ_c are shown in Figs. 4.8a, b, and c, respectively. The dielectric constant increases with decreasing $(\phi_c - \phi)$. Similar to the response of the AC conductivity $\sigma(\phi,\omega)$ on the conducting side, the dielectric constant of samples with ϕ somewhat below the critical volume fraction remain constant at low frequencies. Figs. 4.9a, b and c show the imaginary part of complex AC conductivity (see Subsection 2.3.2), $\omega \cdot \varepsilon(\phi,\omega)$, against the frequency on log-log scale. The general trend is that nearly parallel straight line plots over whole frequency range are observed, as shown in the figures. The exponent y can be obtained by fitting the relation $\omega \cdot \varepsilon(\phi,\omega) \propto \omega^{1-y}$ to the high frequency ($\geq$ 100kHz) data of the samples near the percolation threshold. Using these plots, the values of the exponent y were found to be y=0.14±0.02, 0.07 ± 0.01, and 0.10±0.01 for disc samples, 50%G-50%BN and 55%G-45%BN powders, respectively.

The observed critical exponents of x and y can be interpreted by the model of intercluster polarization, where the conducting component is considered to be a pure conductor, and the dielectric component is taken to have no loss. As discussed in Chapter 2, the theoretical predictions based on this model give $x = t/(t+s)$ and $y = s/(t+s)$ in the frequency range $\omega_c < \omega < \omega_o$, where t and s are the DC conductivity and dielectric exponent respectively, $\omega_o = \sigma_c/2\pi\varepsilon_i$ and $\omega_c = \omega_o \left|\phi - \phi_c\right|^{t+s}$. The upper bound frequency ω_o is calculated using $\sigma_c = 8.3 \times 10^2 \Omega - m$, and $\varepsilon_i = 2.8\varepsilon_o$, which were given in Section 3.1, where $\varepsilon_o = 8.85 \times 10^{-12} C^2/N \cdot m^2$, and the result is $\omega_o \sim 5.4 \times 10^{12} Hz$. The lower bound frequency ω_c depends explicitly on the volume

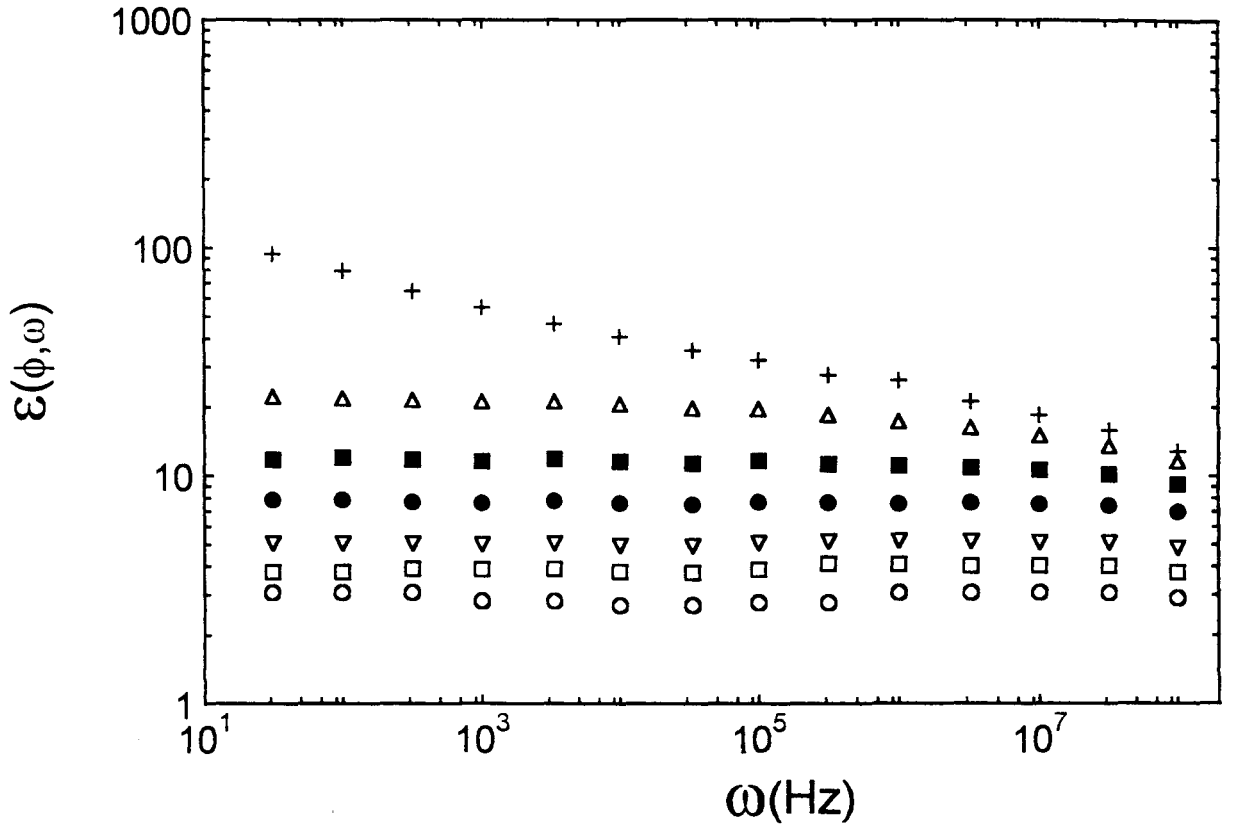

Fig. 4.8a The axial AC dielectric constant $\varepsilon(\phi,\omega)$ ($\phi < \phi_c$) against frequency for the disc samples. $\phi = 0.150(+)$, $0.139(\triangle)$, $0.131(\blacksquare)$, $0.123(\bullet)$, $0.098(\nabla)$, $0.057(\square)$, $0.000(\bigcirc)$.

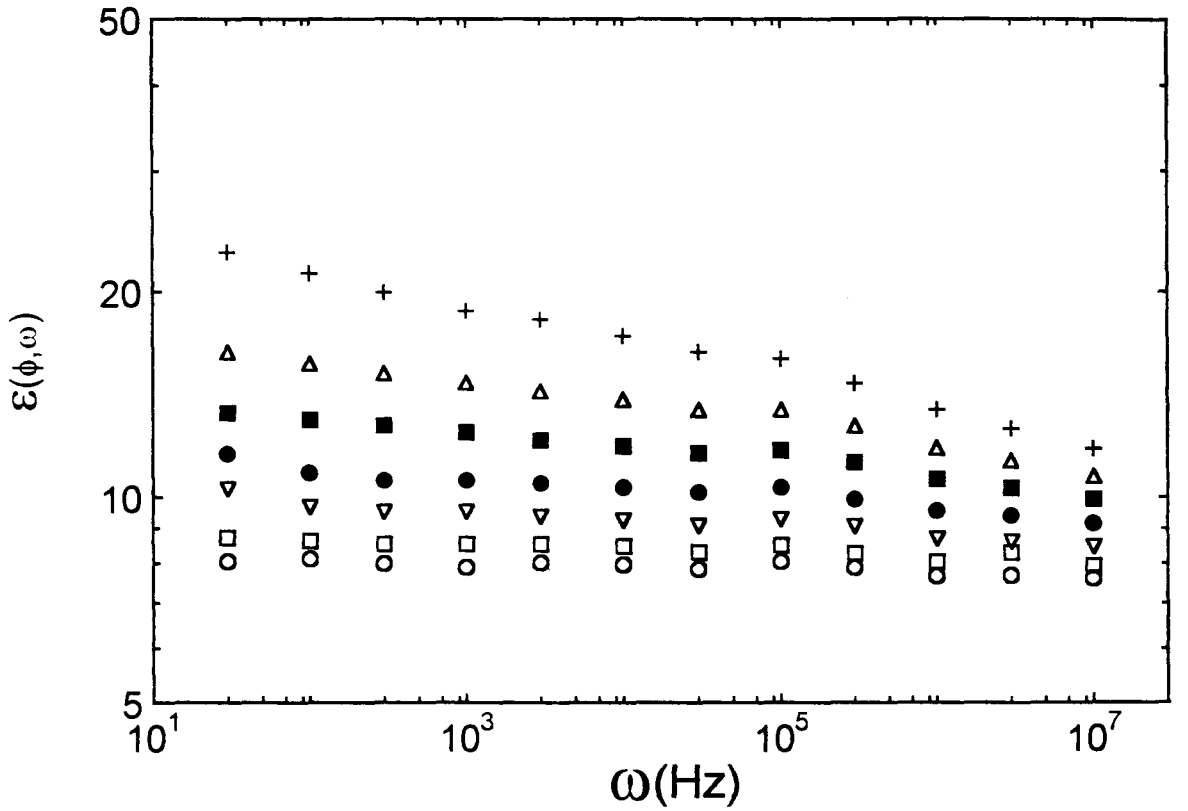

Fig. 4.8b The axial AC dielectric constant $\varepsilon(\phi,\omega)$ ($\phi < \phi_c$) against frequency for the 50%G-50%BN powder. ϕ =0.113(+), 0.111(△), 0.109(■), 0.107(•), 0.105(▽), 0.103(□), 0.101(○).

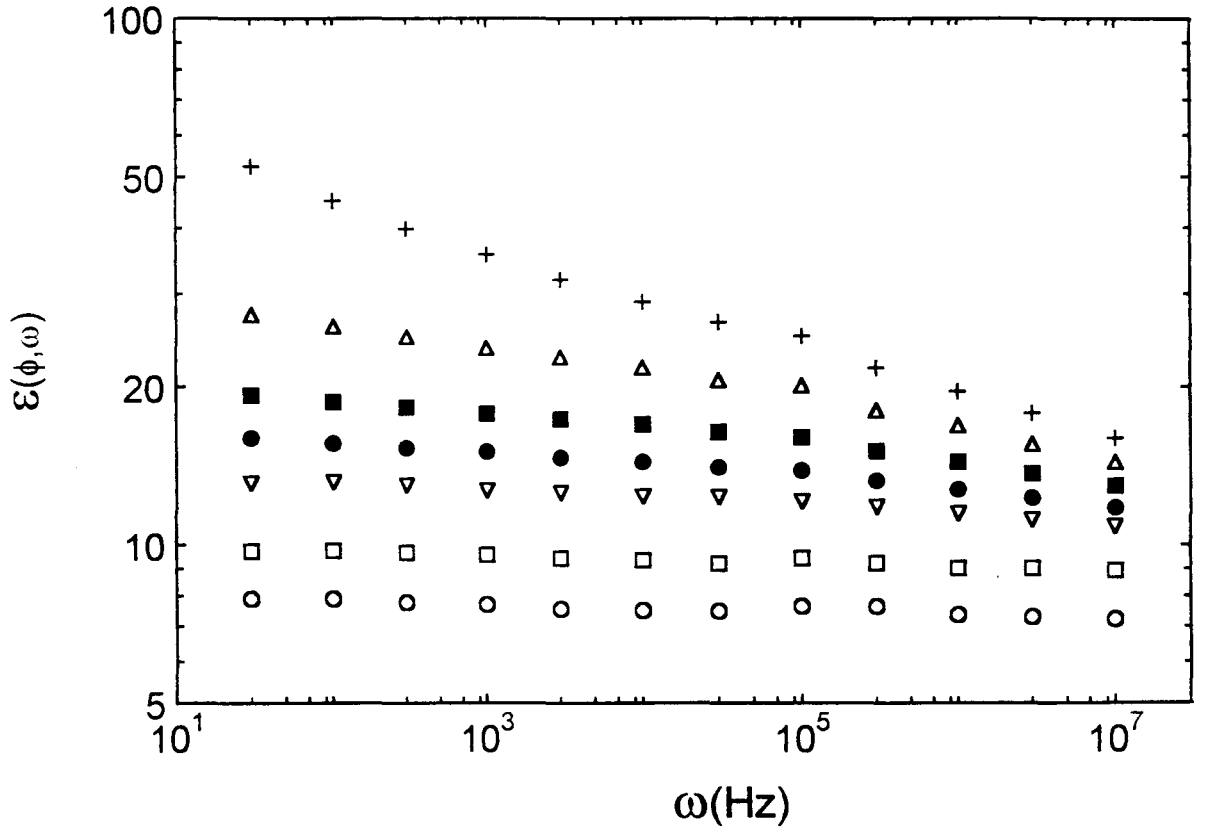

Fig. 4.8c The axial AC dielectric constant $\varepsilon(\phi,\omega)$ ($\phi < \phi_c$) against frequency for 55%G-45%BN powder. ϕ=0.123(+), 0.121(△), 0.120(■), 0.118(•), 0.116(▽), 0.115(□), 0.112(○).

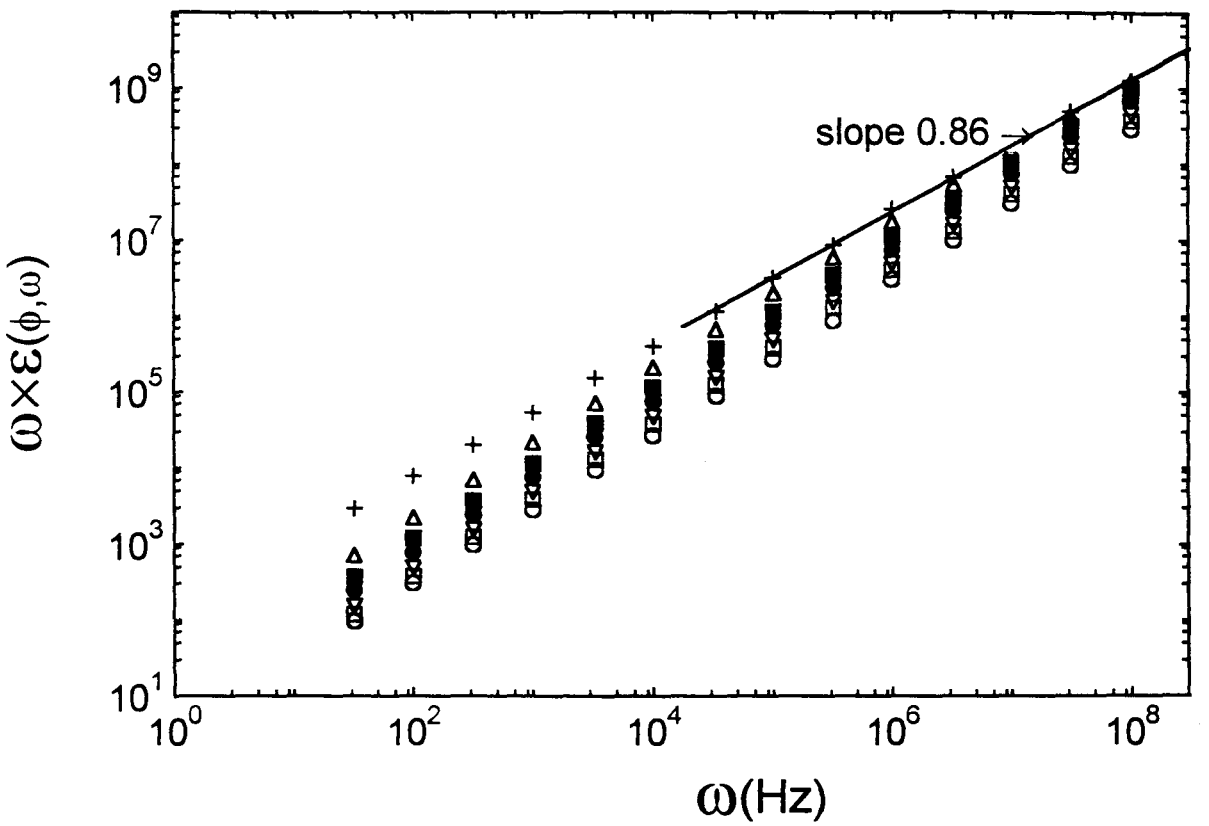

Fig. 4.9a The imaginary part of complex AC conductivity, $\omega \cdot \varepsilon(\phi,\omega)$, against the frequency on log-log scale for the disc samples. The exponent y is found to be 0.14±0.02. ϕ = 0.150(+), 0.139(△), 0.131(■), 0.123(•), 0.098(▽), 0.057(□), 0.000(○).

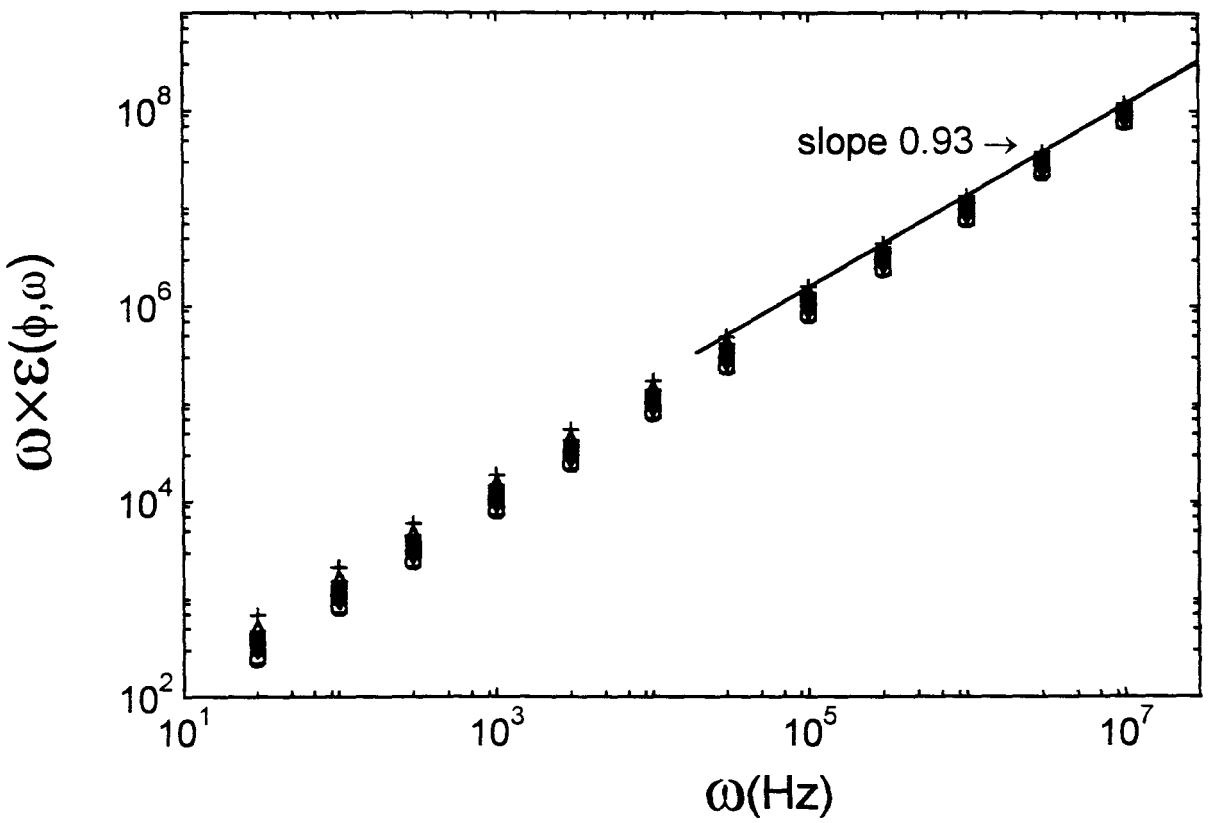

Fig. 4.9b The imaginary part of complex AC conductivity, $\omega \cdot \varepsilon(\phi,\omega)$, against the frequency on log-log scale for the 50%G-50%BN powder. The exponent y is found to be 0.07±0.01. ϕ =0.113(+), 0.111(△), 0.109(■), 0.107(•), 0.105(▽), 0.103(□), 0.101(○).

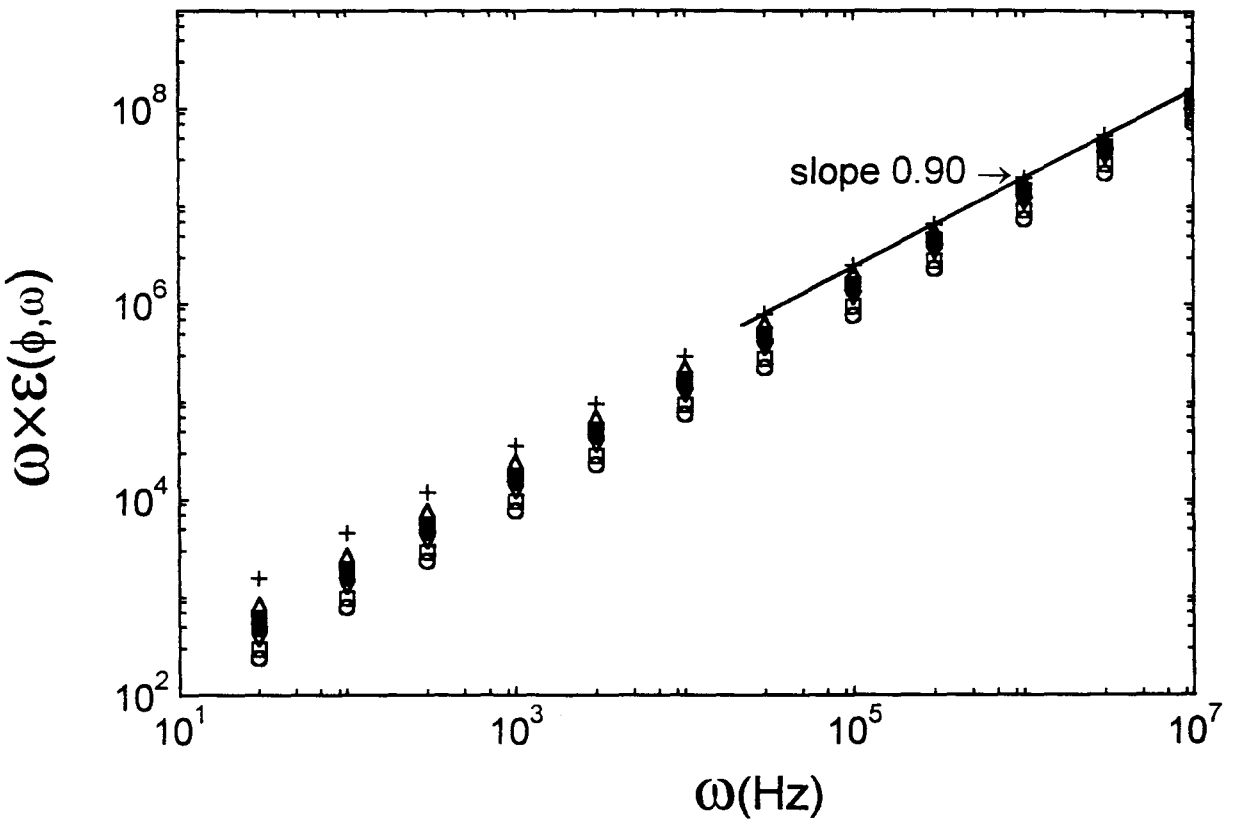

Fig. 4.9c The imaginary part of complex AC conductivity, $\omega \cdot \varepsilon(\phi,\omega)$, against the frequency on log-log scale for the 55%G-45%BN powder. The exponent y is found to be 0.10±0.01. ϕ =0.123(+), 0.121(△), 0.120(■), 0.118(•), 0.116(▽), 0.115(□), 0.112(○).

fraction ϕ. The calculated and observed values of ω_c (see the next subsection) for each sample are given in Tab'e 4.2. These results show that the frequency ranges used to derive the exponents x and y are within the estimated frequency bounds of the scaling law ($\omega_c < \omega < \omega_o$). Using the values of the critical exponents t=2.63 and s=0.53, given in Table 4.1 for disc samples measured in the axial direction, one gets x=0.83 and $y = 0.17$, which are consistent with the observed values based on the AC conductivity and dielectric constant data for the disc samples. For the 50%G-50%BN powder, the values of x and y derived from its DC conductivity exponent $t = 4.85$ and the low frequency dielectric exponent $s = 0.60$ are to be 0.89±0.01 and 0.11±0.01 respectively. These values of the exponents x and y are just outside the experimental error bars of the directly observed values of $x = 0.94 \pm 0.02$ and $y = 0.07 \pm 0.01$. For the 55%G-45%BN powder, the values of $t = 4.80$ and $s = 0.72$ give $x = 0.87$ and $y = 0.13$, which are in excellent agreement with the directly observed values $x = 0.87$ and $y = 0.11$. All measured values of two exponents x and y in the three G-BN systems satisfy the scaling relation $x + y = 1$ (Equation (2.31)), within the experimental uncertainty. Therefore, the finite cluster polarization can probably model the AC electric conductivity and dielectric constant near the percolation threshold for all the three G-BN percolation systems.

In addition to the intercluster polarization effects, the anomalous diffusion of the charge carriers in the percolation clusters could also make a contribution to the electrical conduction of the samples. At higher frequencies, electrons can scan or diffuse only over a distance $L_\omega \sim \omega^{-1/(2+\theta)} < \xi$ on the conducting clusters, if the clusters are self-similar fractals. Since the conductivity is predicted to increase with decreasing L_ω [Gefen et al., 1983], the observed conductivity should also increase with increasing ω. Within the framework of this model, using the Einstein relation between the diffusion and conduction, and averaging over the contributions of charge carriers situated in different clusters, Gefen et al. (1983) showed that $x = t/\nu(2 + \theta)$ and $y = (2\nu - \beta)/\nu(2 + \theta)$, where the critical exponents t, ν, β and θ have been introduced in Section 2.3. Because the exponents ν, β and θ cannot be determined for the samples studied here, one can only use their universal values in three dimensions,

Table 4.2 Comparison of the observed cross-over frequencies ω_c (Hz) on the conducting side of the percolation threshold and the theoretical predictions of the R-C model, using the observed exponents t and s.

Discs			
ϕ	ω_c(th.)	ω_c(exp.)	σ_{dc}(exp.)
0.152	1.6×10^{4}	8.3×10^{3}	2.50×10^{-7}
0.158	5.2×10^{5}	2.0×10^{6}	4.56×10^{-5}
0.168	1.7×10^{7}	5.7×10^{7}	1.10×10^{-3}
50%G			
0.115	2.4×10^{-4}	3.0×10^{1}	2.49×10^{-9}
0.116	1.1×10^{-2}	3.0×10^{2}	4.10×10^{-8}
0.118	4.6×10^{-1}	2.9×10^{3}	3.43×10^{-7}
0.124	6.8×10^{1}	3.0×10^{4}	7.37×10^{-6}
0.130	8.8×10^{2}	1.0×10^{5}	4.69×10^{-5}
55%G			
0.125	8.9×10^{-3}	1.0×10^{3}	1.02×10^{-7}
0.127	3.6×10^{-1}	4.0×10^{3}	5.35×10^{-7}
0.129	3.2×10^{0}	2.0×10^{4}	3.82×10^{-6}
0.133	5.2×10^{1}	9.5×10^{4}	2.71×10^{-5}

which gives $x = 0.58$ and $y = 0.42$. The observed values of the exponents x and y in all three G-BN sample systems are then clearly in disagreement with the prediction of anomalous diffusion model, implying that anomalous electron diffusion in the backbone does not play a role in the electric conduction mechanism of the G-BN sample systems in the frequency range observed. It is believed [Gefen et al. 1983] that anomalous diffusion will only become more important at frequencies higher than those used in the present work.

The critical exponents x and y have been previously studied experimentally on various continuum percolation systems. The AC conductivity and dielectric constant of thin gold films near the percolation threshold were measured by Laibowitz and Gefen (1984). The thickness of the thin Au films used in their experiments were in a range $6 \sim 10$nm and spanned the metal-insulator transition. The frequency range covered was from $100Hz$ to $10\mathrm{M}Hz$. The power-laws, (2.29) and (2.30), were observed. These experimental results gave x=0.95±0.05 and y=0.13±0.05. These values are in agreement with (2.31) within the experimental uncertainty, but are individually different from any of the universal values, which are in two dimensions, $x = y = 0.5$, predicted by the intercluster polarization (R—C) model, and $x = 0.33$ and $y = 0.67$ from anomalous diffusion model, or in three dimensions, $x = 0.72$, $y = 0.28$ from the $R - C$ model and $x = 0.58, y = 0.42$ from the anomalous diffusion model. Nevertheless this experiment was an important step in the characterization of the full AC response of a percolation system. However, several points remain to be investigated, such as the influence of the substrate (Si_3N_4) at higher frequencies and the two-dimensional structure of the metallic clusters [Clerc et al. 1990].

Song et al. (1986) studied the AC electrical properties of three-dimensional amorphous carbon-teflon compacted mixtures, in the frequency range from $10Hz$ to $13\mathrm{M}Hz$. The experimental values of exponents x and y are 0.86 ± 0.06 and 0.12 ± 0.04 respectively. These values of the exponent x and y are similar to those obtained for the G-BN disc samples in the present study, but are also different from the universal values in three dimensions, predicted by either the R—C model or the anomalous

diffusion model. These authors also noted that their exponents were closer to those found by Laibowitz and Gefen (1984), therefore the thin gold films studied by the latter might have some three-dimensional properties.

Chakrabarty et al. (1993) measured the complex AC conductance of carbon-paraffin wax mixtures, as a function of frequency from $7Hz$ to 100kHz near the percolation threshold. The exponents were found to be x =0.72±0.01 and y = 0.23±0.05, which are remarkably close to the three dimensional universal values based on the $R-C$ model as discussed in Chapter 2. In a recent paper, Lee et al. (1993) investigated the AC conductivity and dielectric constant of carbon black-epoxy bulk composites over a very wide frequency range from $100Hz$ to 10GHz. Near the percolation threshold, the AC conductivity scales as Equation (2.29) with an exponent x=0.65±0.05 over the full frequency range while the dielectric constant scales as Equation (2.30) with an exponent y=0.26±0.01, in a limited frequency range of 2kHz ~ 1.5MHz. In these two carbon-polymer systems, the carbon grains were thought to be coated with the polymers during the sample preparation. This microstructure is very different from that of G-BN systems, although the conducting components are similar in their conductivities. Therefore, as in the G-BN case, there is thought to be no intergranular tunneling, the difference of the values of critical exponents x and y between the carbon-polymers and G-BN systems, is not too surprising.

Chen and Johnson (1991) also studied the complex AC impedance of three different random metal-insulator composites near their percolation thresholds. Their three systems include filamentary and nodular shaped nickel particles embedded in the polypropylene matrix, abbreviated as Ni/F-PP and Ni/N-PP respectively, and silver particles in the matrix of potassium chloride (Ag-KCl). The AC conductance, capacitance and dielectric loss tangent of these metal-insulator composites were measured between $5Hz$ and 13MHz. They observed the critical exponents x and y, which are x = 0.88 ± 0.01, 0.81±0.01 and 0.77±0.01, and y = 0.14 ± 0.01, 0.13±0.04, and 0.22±0.01, for Ni/F-PP, Ni/N-PP and Ag-KCI respectively. Using their DC conductivity and dielectric constant exponents $t = 3.1, 2.2$, and s = 0.55, 0.62 for Ni/F-PP

and Ni/N-PP respectively, one can calculate the theoretical values for the exponent x and y, expected from the R-C model, through Equations (2.29) and (2.30), which are x = 0.85, 0.78, and y=0.15, 0.22, respectively. Thus good agreement between theory and experiment has been obtained for Ni/F-PP and Ni/N-PP, but only if the experimental (non-universal) s and t values are used.

Hundley and Zettl (1988) investigated the temperature dependence of the exponents x and y for a thin-gold-film percolation system, at temperatures between 4.2 and 300K and at frequencies between $100Hz$ and $1GHz$. Their gold films were very similar to these of Laibowitz and Gefen (1984). Above 100K, their observed exponents of $x = 0.35 \pm 0.05$ and $y = 0.71 \pm 0.05$ displayed no apparent temperature effects. Between 23 and 100K, both the AC conductivity and the AC dielectric constant still appeared to scale with frequency but became very temperature dependent. With decreasing temperatures in this range, the exponent x decreased from 0.35 down to zero while the y increased from 0.71 up to unity. Below 23K, the AC conductivity showed no frequency-scaling behaviour, like a homogeneous metal, while the dielectric measurements became unreliable. Above 100K, their observed exponent x of 0.35 is less than the observed exponent y of 0.71, which is contrary to that for the G-BN systems as well as the other percolation systems discussed above. This difference has not yet been resolved.

In conclusion, the values of exponents x and y, obtained by Chen and Johson (1991), and the present work, seem to be fairly similar. These results can all be reasonably interpreted by the intercluster polarization model, using the experimentally measured values of exponents t and s. However, it must also be noted that the values of the conductivity exponents t for these systems are noticeably different from one another.

4.3.2 The Crossover Frequency ω_c and Exponent q

Figs. 4.10a, b, and c show the experimental crossover frequency ω_c as a function of sample DC conductivity $\sigma(\phi,0)$ on a log-log scale for the samples on the conducting side. The same results are also presented in Table 4.2 (page 117) for comparison with the theoretical predictions. It is seen from this table that for the G-BN discs the observed values of the crossover frequency ω_c are in fairly good agreement with the predictions of the R-C model, using the measured exponents t and s. One salient feature of this table is that for the powders the calculated ω_c, which explicitly depends on the t value, is several orders of magnitude smaller than the directly observed one, partially due to the extraordinarily large values of t. However, the trend of ω_c as a function of sample DC conductivity agrees with the predictions of scaling theory, as illustrated in Figs. 4.10a, b and c. Using least-squares fitting to the power-law $\omega_c \propto \sigma^q(\phi,0)$, the exponent q is found to be q=1.03±0.01, 0.84±0.01, and 0.82±0.01 for the disc samples, 50%G-50%BN and 55%G-45%BN powders, respectively. These measured values of q are consistent with the result, q=0.82, obtained from the thin gold films at temperatures from 100 to 300K by Hundley and Zettl (1988). Benguigui (1985) obtained q =1.1 from the mixtures of glass and iron balls with a diameter of 1.2 — 1.5mm. More recently, Chakrabarty et al. (1993) measured q=1.1 in carbon-wax mixtures at room temperature.

Scaling theory, based on the intercluster polarization effects, which was discussed in Section 2.3, gives an expression for the exponent q in terms of the conductivity exponent t and dielectric exponent s, which is $q=(t+s)/t$ on the conducting side. This implies that the values of exponent q can never be less than unity. The directly observed exponents q = 1.03, 0.84 and 0.82 in this study are in disagreement with the predicted values of 1.20, 1.15 and 1.06, using the measured values of the DC conductivity exponent t and dielectric constant exponent s. A large discrepancy between the observed exponent (0.82) and the theoretical value (1.66 in that case) was also noted in Hundley and Zettl's paper (1988). Although the value of exponent q=1.1, reported by Benguigui (1985) and Chakrabarty et al. (1993) respectively, are larger

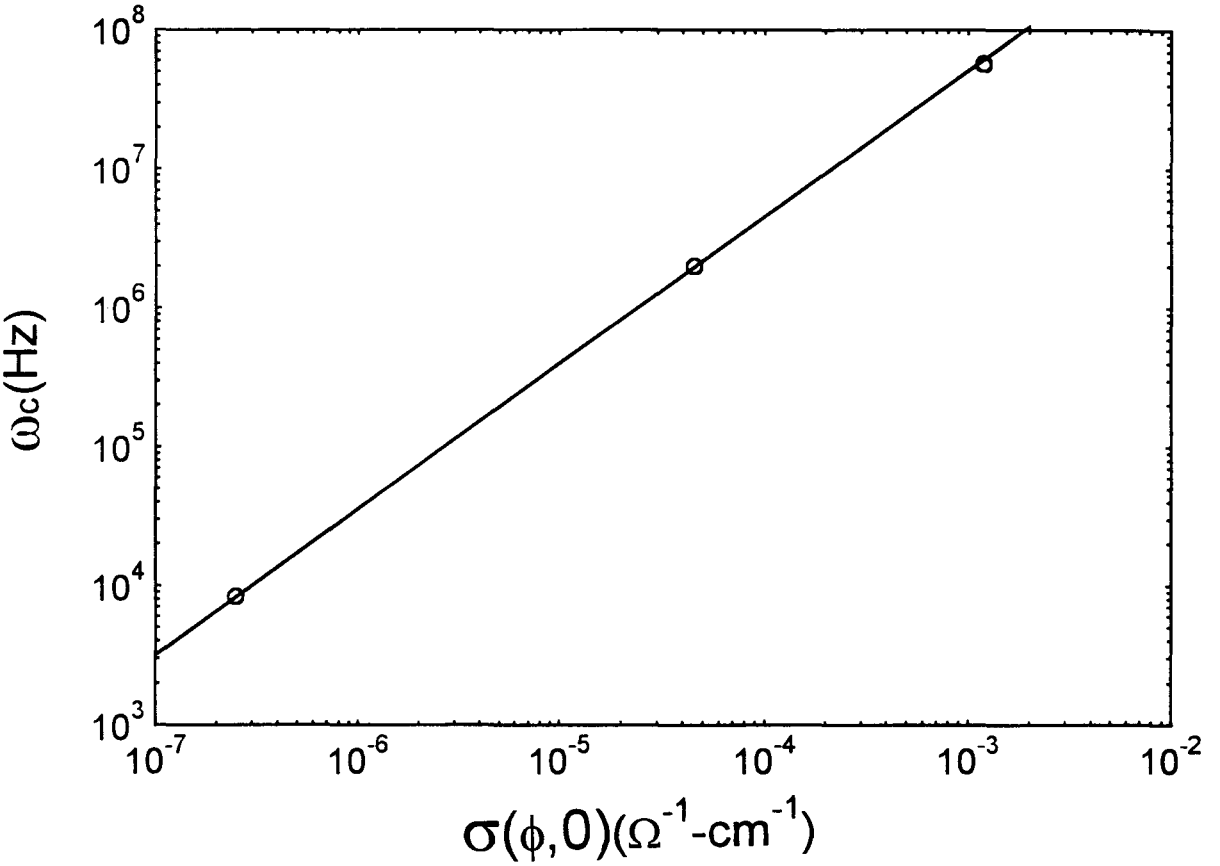

Fig. 4.10a The crossover frequency ω_c against the DC conductivity on a log-log scale for the disc samples. The solid line is a least squares fit to the data and the exponent q is obtained from the slope. q = 1.03±0.01.

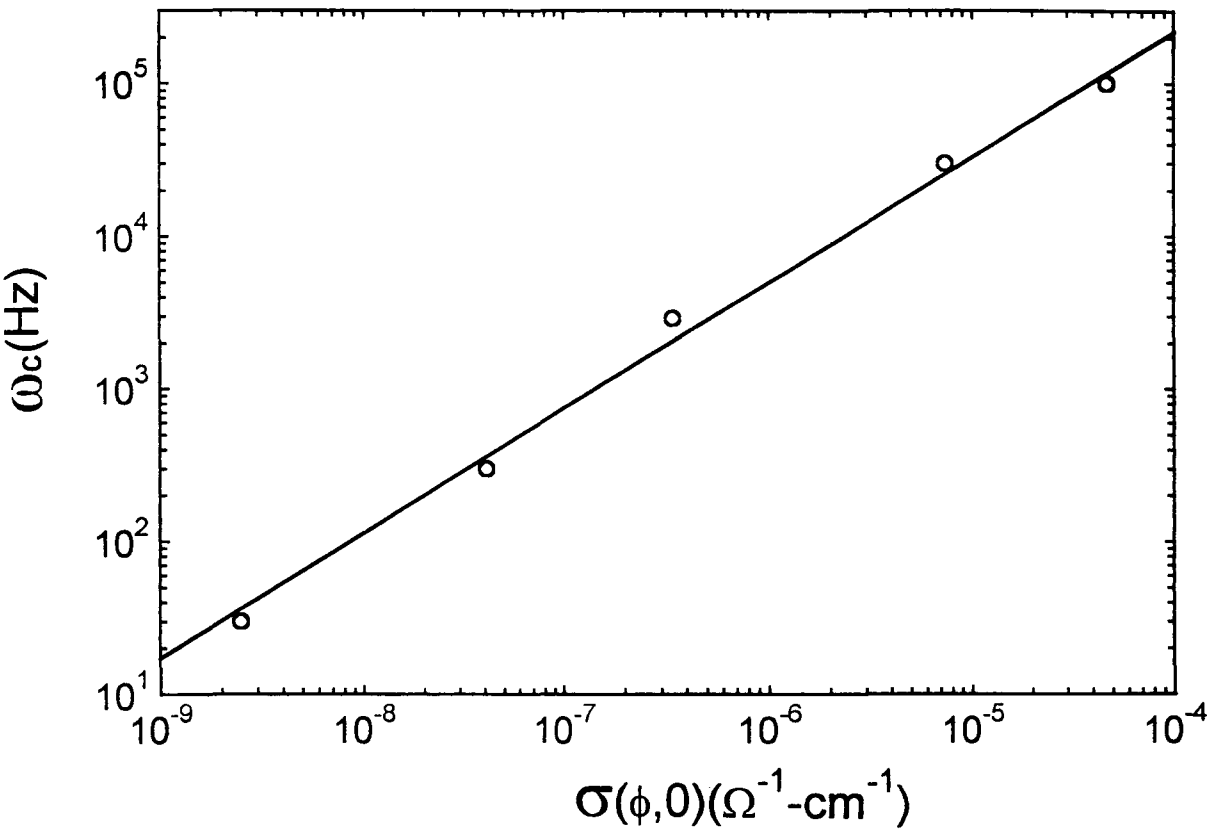

Fig. 4.10b The crossover frequency ω_c against the DC conductivity on a log-log scale for the 50%G-50%BN powder. q =0.84±0.01.

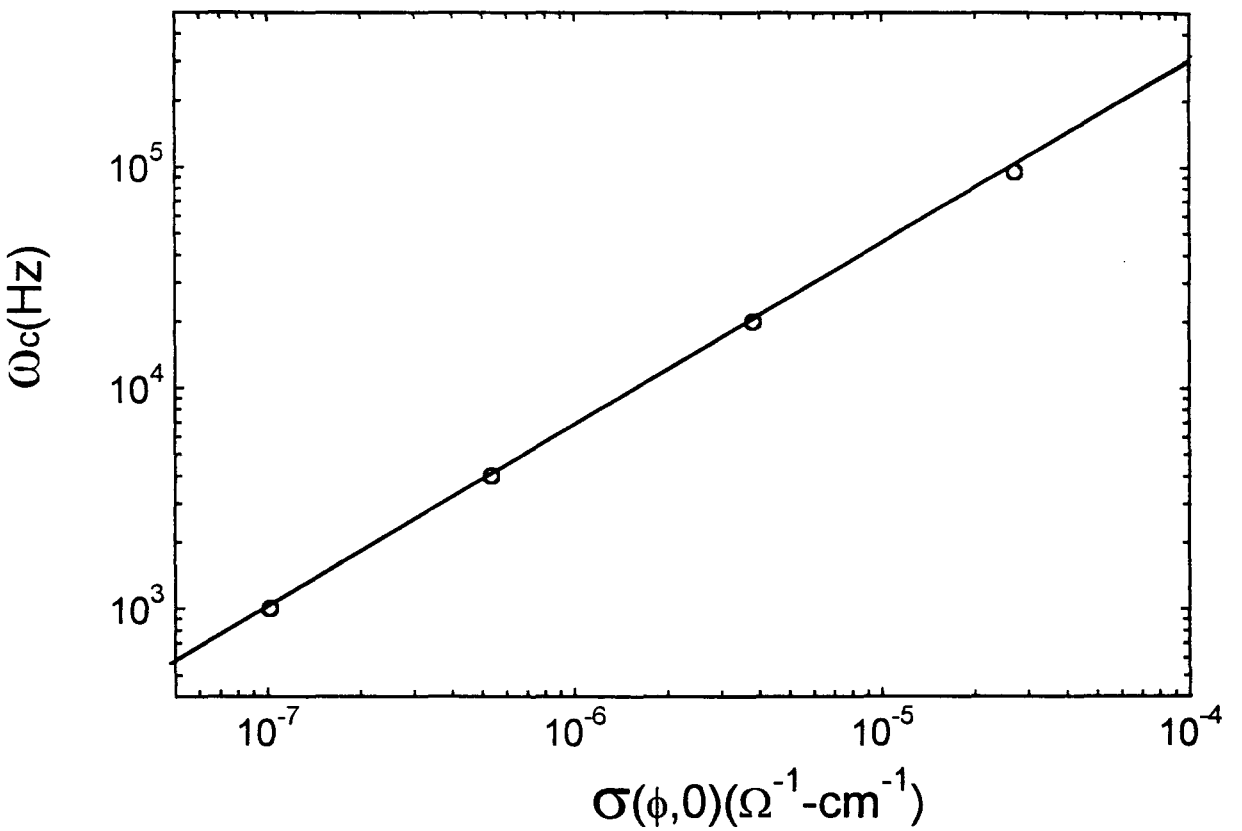

Fig. 4.10c The crossover frequency ω_c against the DC conductivity on a log-log scale for the 55%G-45%BN powder. q =0.82±0.01.

than unity, these values are still about 30% smaller than the predicted exponents of 1.4 in both cases. Chakrabarty et al. claimed that an insufficient range of data, which only span just over one decade in frequency and in the DC conductivity, was responsible for the discrepancy between the observed value and the theoretical prediction for q. This limitation does not apply to the present study, or that of Hundley and Zettl, which spans 7 decades and gives still lower values of q. It is clearly observed in Figs. 4.10a, b and c that both the crossover frequency data and the DC conductivity data cover four or more decades, and obey a power-law with a very small scatter in the data.

From Figs. 4.9a, b and c, when $\omega \cdot \varepsilon(\phi,\omega)$ is scaled (normalized) by the DC conductivity $\sigma(\phi,0)$ for each value of ϕ, one gets the scaled plots shown in Figs. 4.11a, b and c, which correspond to Figs. 4.9a, b and c respectively. Except the data for the $\phi = 0.150$ sample shown in Fig.4.11a, all the curves in each figures almost collapse into a single straight line. Since the disc sample with ϕ=0.150 is just on the percolation threshold, its different behaviour could probably be ignored. Because no frequency scaling is necessary to scale the plots of $\omega \cdot \varepsilon(\phi,\omega)$, Figs. 4.11a, b and c show that the crossover frequency is $\omega_c \sim 1$ for nearly all the G-BN samples on the insulating side. These results also lead to the conclusion that, using the theoretical relation $\omega_c \propto \sigma^q(\phi,0)$ and taking into account the different values of the DC conductivities of the insulating samples, the exponent q is zero below the percolation threshold for the three G-BN systems. This value of q=0 is in disagreement with the predictions made by the R-C model, which gives $q = -(t+s)/\bar{s}$ on the insulating side. Using the observed values of the exponents t, s and $\bar{s}$, the exponents q are found to be -3, -13 and -12 for the G-BN discs, 50%G-50BN and 55%G-45%BN powder systems, respectively. Therefore on the insulating side of percolation, the intercluster polarization model seems not apply to the G-BN systems. No previous experimental result for ω_c on the insulating side of the percolation threshold is, to the author's best knowledge, available for comparison.

It has been shown in Section 3.3 that the porosity of the disc samples is about 0.18 while the 50%G-50%BN and 55%G-45%BN powders undergoing compression are even

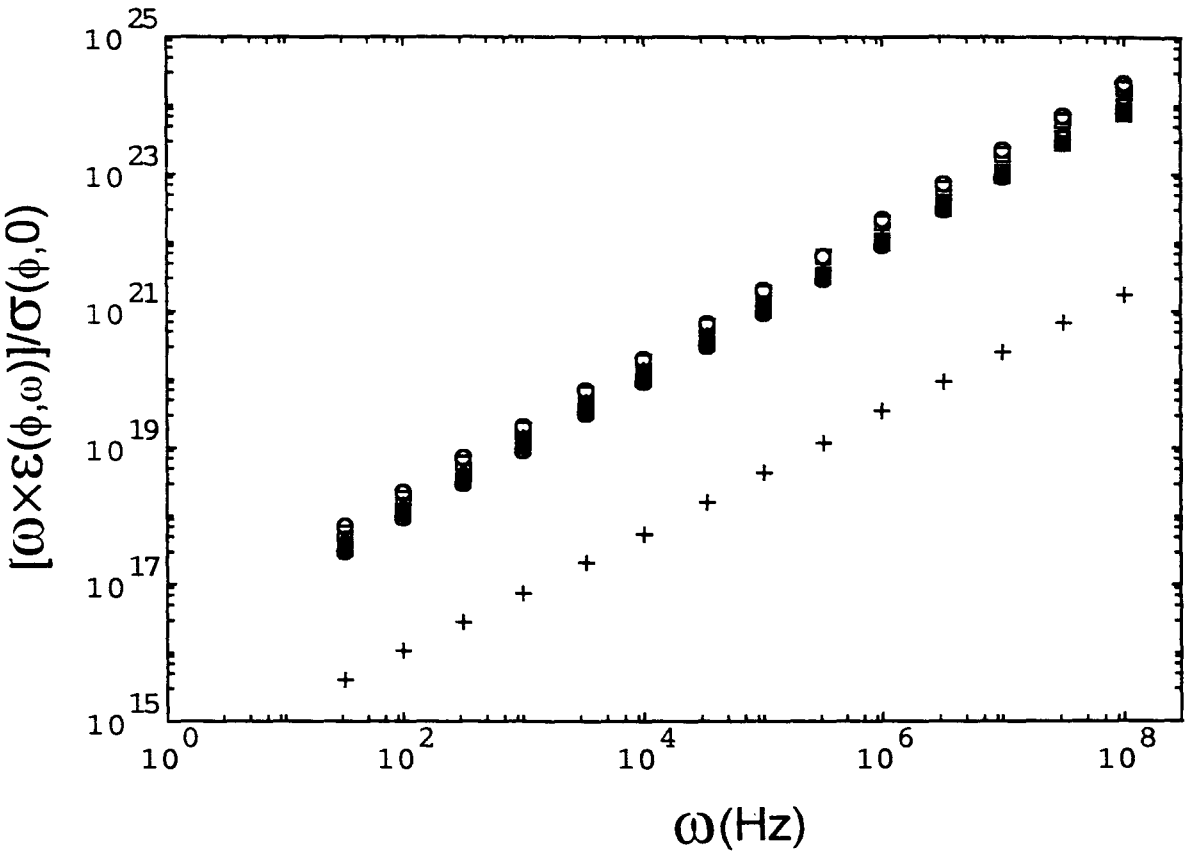

Fig. 4.11a The normalized imaginary part of complex AC conductivity, $\omega \cdot \varepsilon(\phi,\omega)/\sigma(\phi,0)$, against the frequency on a log-log scale for the disc samples. ϕ = 0.150(+), 0.139(△), 0.131(■), 0.123(•), 0.098(▽), 0.057(□), 0.000(○).

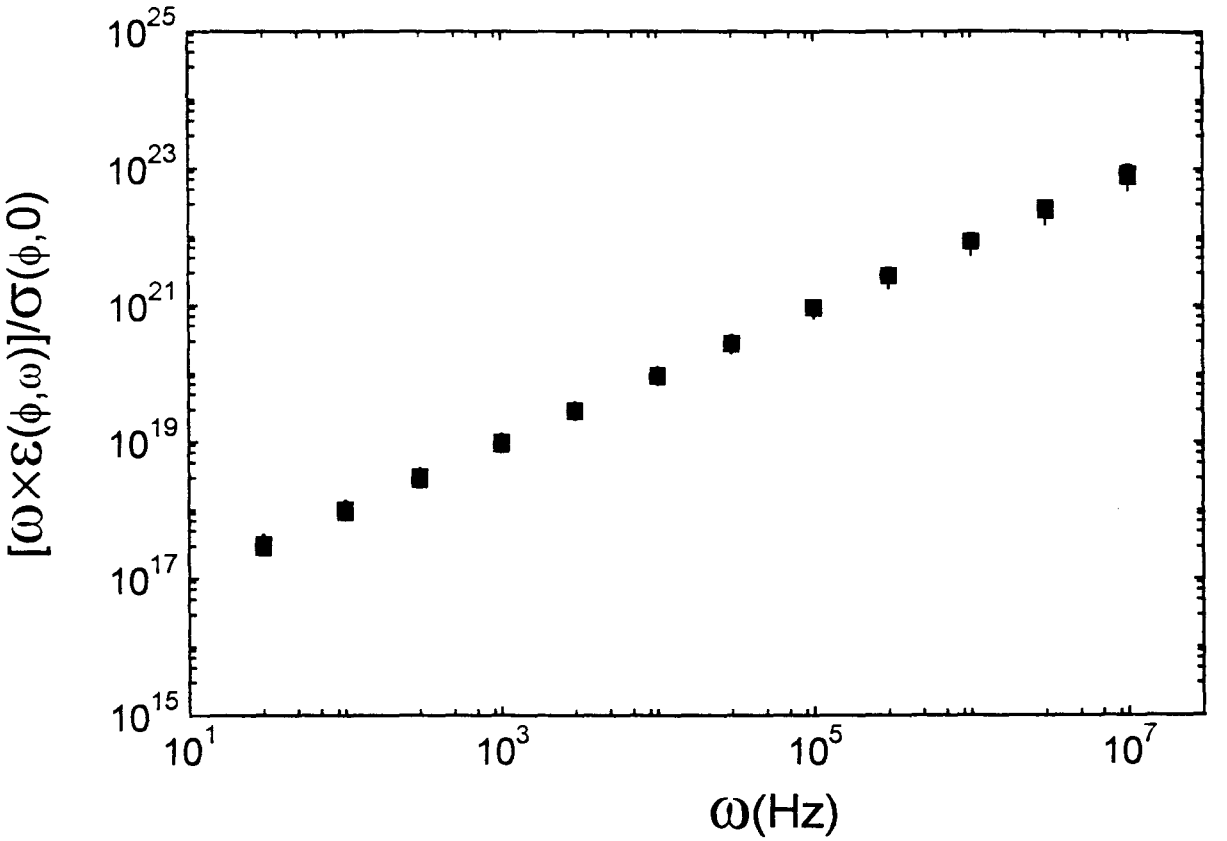

Fig. 4.11b The normalized imaginary part of complex AC conductivity, $\omega \cdot \varepsilon(\phi,\omega)/\sigma(\phi,0)$, against the frequency on a log-log scale for the 50%G-50%BN powder ($\phi < \phi_c$). ϕ=0.113(+), 0.111(△), 0.109(■), 0.107(•), 0.105(▽), 0.103(□), 0.101(○).

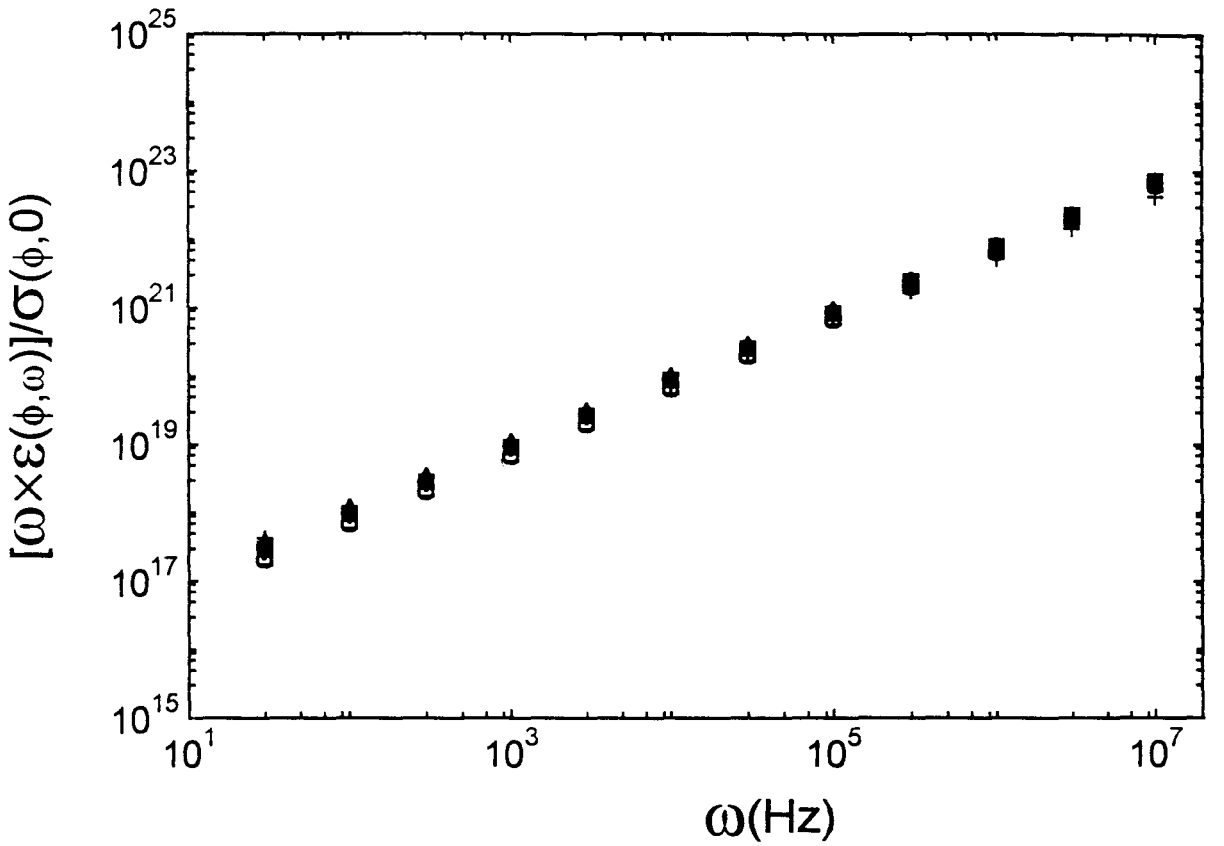

Fig. 4.11c The normalized imaginary part of complex AC conductivity, $\omega \cdot \varepsilon(\phi,\omega)/\sigma(\phi,0)$, against the frequency on a log-log scale for the 55%G-45%BN powder ($\phi < \phi_c$). ϕ =0.123(+), 0.121(△), 0.120(■), 0.118(•), 0.116(▽), 0.115(□), 0.112(○).

more porous, 0.70 or more, as the maximum packing fractions for the powders are about 0.3. It is therefore most surprising that the very different microstructures and porosities of the discs and powders of the two G-BN percolation systems produce the same, or nearly the same, values of the exponent q on the both sides of percolation. This shows, at least in the G-BN systems, that the exponent q is not as sensitive to the microstructure and possibly also to the anisotropy of conducting phase as is t.

It is seen from the above discussions that, up till now, the measured values of exponent q on the conducting side of the percolation threshold for different continuum percolation systems, viz. thin gold films, carbon-wax mixtures, and the G-BN discs and powders, are in all cases lower than the theoretically predicted values. Furthermore, the measured cross-over frequencies in the G-BN powder systems are several orders of magnitude larger than the theoretical predictions. These facts suggest that some important factors have not been incorporated in the intercluster polarization model. Even more alarming is the fact that no model is available to account for $q \simeq 0$ on the insulating side of the percolation threshold for the G-BN systems. As the anomalous diffusion of charge carriers gives q value of 1.4 for $\phi > \phi_c$, even larger than the observed values, it will not be considered further in this thesis. In summary, it is not clear what is responsible for the discrepancy in the q values, on either side of ϕ_c, between theory and experiment.

4.3.3 The Loss Tangent tan δ

Using the same set of measurements as in the previous section, Figs. 4.12a, b, and c show the log-log plots of the loss tangent $\tan\delta$ versus the frequency for volume fractions very close to the percolation threshold ϕ_c. In order to avoid overlap not all curves have been shown for each ϕ value in all of the G-BN sample systems. Comparing $\tan\delta$ for the different G-BN sample systems, the following trends are observed. For $\phi \geq \phi_c$, in the low frequency range, $\tan\delta$ decreases linearly with increasing frequency. As the frequency increases, $\tan\delta$ reaches a minimum value, $\tan\delta_m$ at ω_m, and then bends upward with a much smaller slope. This result agrees qualitatively with numerical simulations on the conducting side of percolation threshold [Clerc et al.

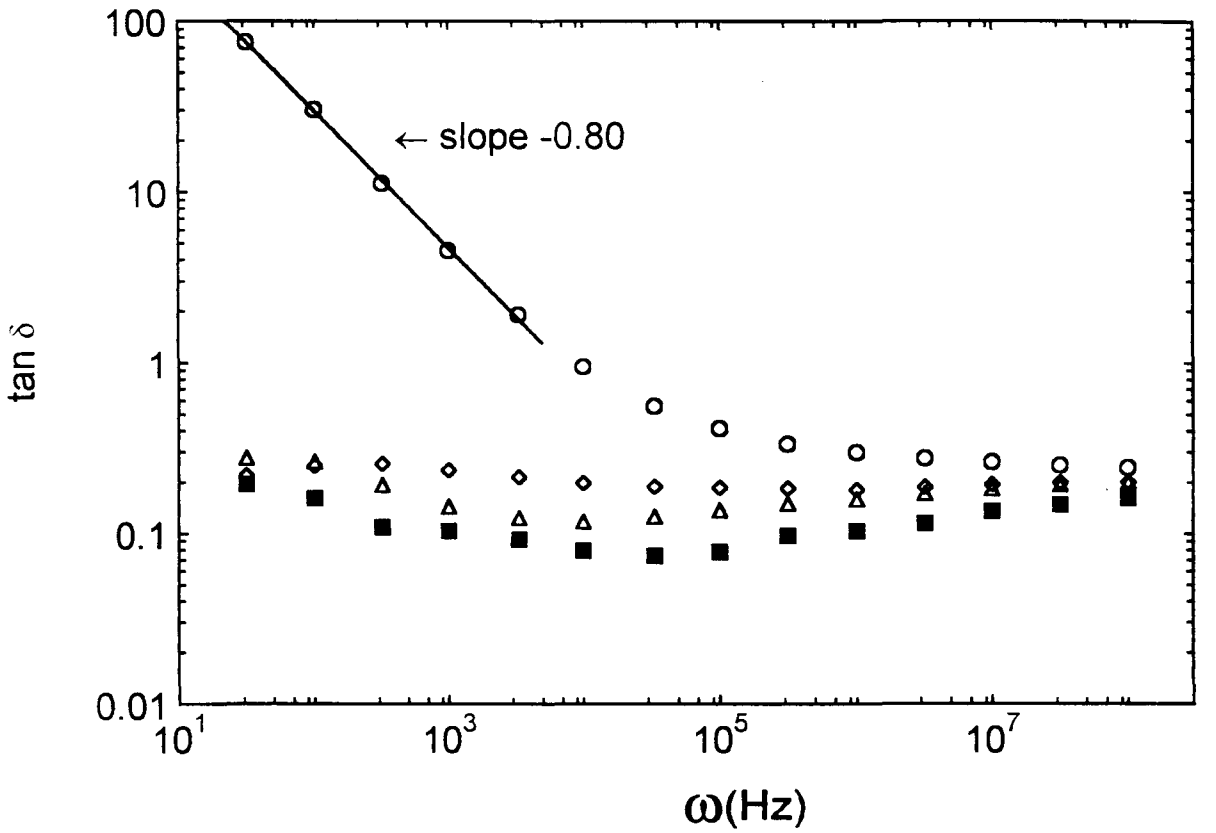

Fig. 4.12a The loss tangent $\tan\delta$ for the samples very close to the percolation threshold against the frequency on a log-log scale for the disc samples. ϕ =0.152(○), 0.150(◇), 0.139(△), 0.131(■).

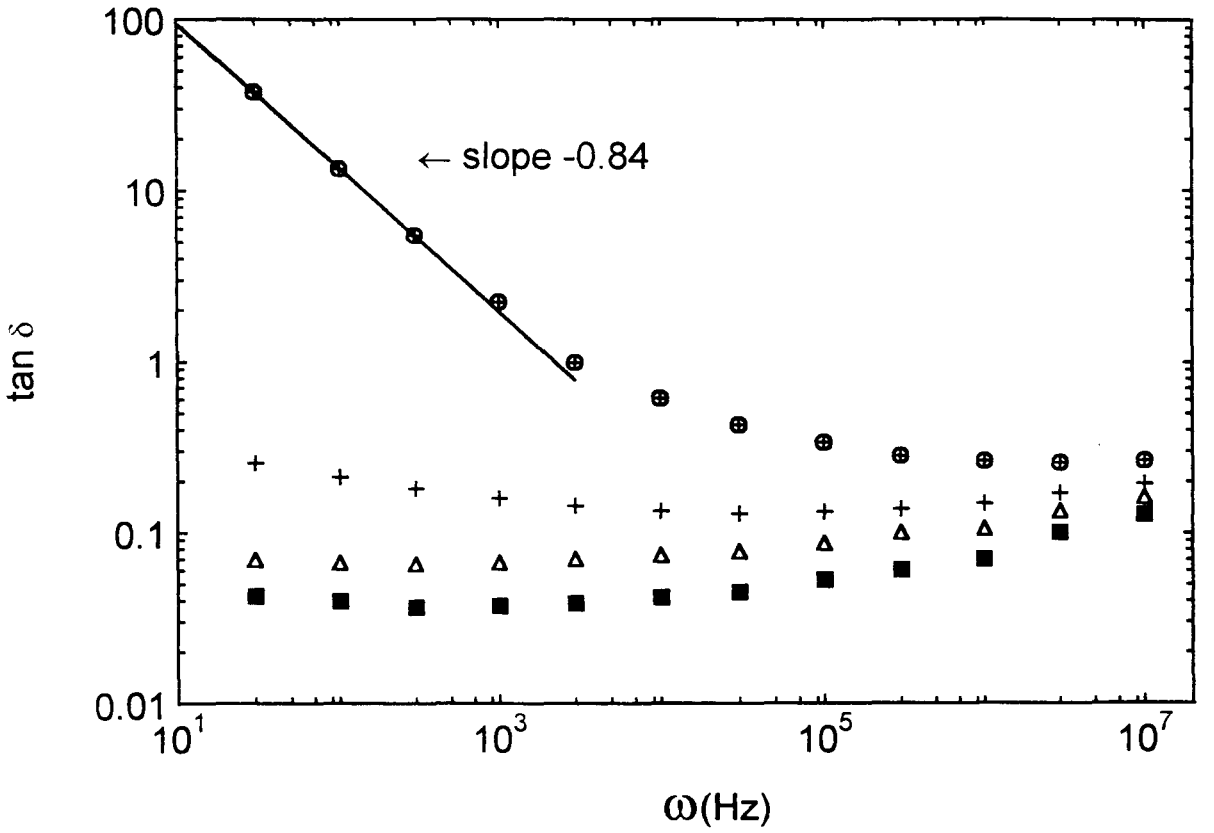

Fig. 4.12b The loss tangent $\tan\delta$ for the samples very close to the percolation threshold against the frequency on a log-log scale for the 50%G-50%BN powder. ϕ =0.115(⊕), 0.113(+), 0.111(△), 0.109(■).

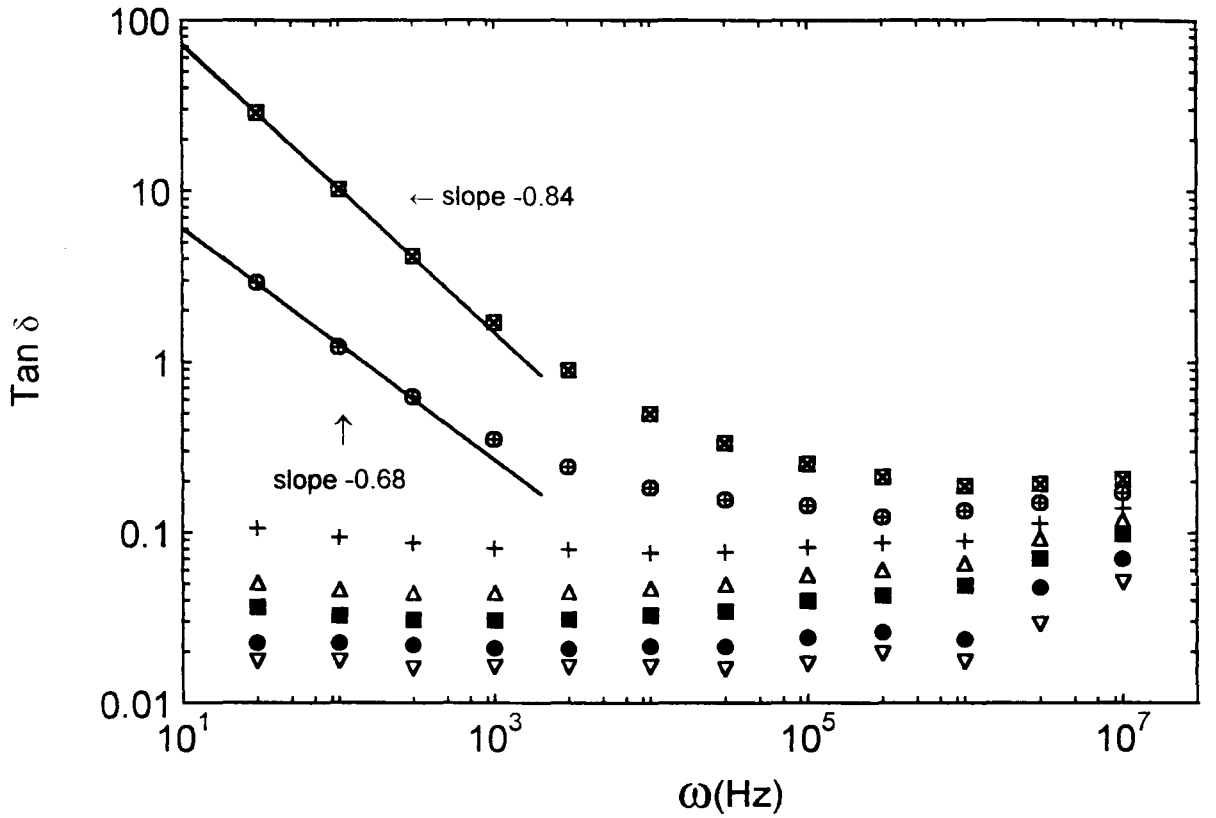

Fig. 4.12c The loss tangent $\tan\delta$ for the samples very close to the percolation threshold against the frequency on a log-log scale for the 55%G-45%BN powder. ϕ =0.127(⊠), 0.125(⊕), 0.123(+), 0.121(△), 0.120(■), 0.118(•), 0.116(▽).

1990]. As Chen and Johnson (1991) argued in their paper, for a sample above ϕ_c, a $1/\omega$ dependence of the loss tangent, $\tan\delta = 1/\omega RC = \sigma_c/\omega\varepsilon_i \propto 1/\omega$, is expected in the low frequency regime $\omega < \omega_c$, where the energy loss in the dielectric is due to the DC conductance along the backbone. The slopes for the samples just above ϕ_c are found to be -0.80 ($\phi = 0.152$), -0.84 ($\phi = 0.115$), and -0.68(ϕ=0.125) for the discs, 50%G-50%BN and 55%G-45%BN powders respectively. These values, somewhat different from -1, may show that the metal-insulator transition of these samples has not yet been completed. For $\phi < \phi_c$, a flat minimum, with a slight dip, in $\tan\delta$ is observed. As ϕ approaches ϕ_c from below, $\tan\delta$ tends to become a constant, or less frequency-dependent, in agreement with the prediction based on the intercluster polarization model. This phenomenon is attributed mostly to the fact that, below ϕ_c, there is no continuous percolating cluster in the samples and the insulating barrier between the larger conducting clusters dominates the electric (now mainly dielectric) behaviour, resulting in a smaller, less frequency-dependent, loss tangent [Chen and Johson 1991].

The observed minimum in the loss tangent $\tan\delta$, as a function of frequency, for G-BN samples below ϕ_c, is qualitatively inconsistent with the results of computer simulations in three dimensions reported by the French group [Clerc et al. 1990, and references therein]. They showed, using the effective-medium approximation (EMA) and the transfer-matrix algorithm of the R—C model, that there is a global maximum of loss tangent at the crossover frequency ω_c (see Subsection 4.3.2) below the percolation threshold. Since the very similar trends in $\tan\delta$ against frequency are observed in both disc and powder G-BN systems, the difference in the porosities and the bad electrical contacts between graphite grains in the powder samples are probably not the cause of the discrepancy between the present experiment and the numerical calculations. Further theoretical and experimental work is required to clarify this "puzzle".

From the minimum of $\tan\delta$ against the frequency just below ϕ_c, the values of $\tan\delta_c$ are estimated from Figs. 4.12a, b and c, and found to be $0.22\pm0.02, 0.13 \pm 0.02$,and 0.09 ± 0.01 for the discs, 50%G-50%BN and 55%G-45%BN powders respectively. Using $\delta_c = y * (\pi/2)$ (see Section 2.3), the critical exponent y can be calculated from

the minima, $\tan\delta_c$, which gives y=0.14±0.01, 0.08±0.02, and 0.06±0.01 respectively. These results are reasonably close to those obtained from the plots of imaginary part of the complex AC conductivity versus the frequency, as shown in Figs. 4.9a, b, and c. Therefore, these two reasonably consistent values of y obtained by different methods of analysis show that there are some consistencies in the R—C model when applied to the G-BN continuum systems.

The loss tangent as a function of frequency for percolation systems has been experimentally studied by many authors. Laugier et al. (1986) performed AC electrical measurements on random mixtures of plain and silver-coated glass microbeads, for $\phi < \phi_c$, in the frequency range from DC to 50MHz. The mean diameter of the beads was roughly 30μm, with a dispersion in size of around 50%. They found the minimum of $\tan\delta(\omega)$ to be 0.55±0.05, in good agreement with the value of 0.47±0.04 expected from the $R-C$ model. They also noted an unexpected increase in the loss tangent on the low-frequency side of the minimum. This was attributed to the non-vanishing DC conductivity of the glass beads, and was confirmed by the computer simulation, using a non-zero DC conductivity for the insulating component [Laugier 1987]. This explanation, however, does not apply to the present case of study as the DC resistivity of BN powder is about 1×10^{16}Ohm-cm and the "dry" air pores in the powders are even more resistive, because the relative humidity in the air pores is less than 12% at room temperature when the measurements were made. Therefore it is not clear what physical information is contained in the slight increase of $\tan\delta$ with decreasing frequency at lower frequencies for $\phi \leq \phi_c$ in the G-BN percolation systems.

The frequency dependence of AC conductivity and dielectric constant of water/AOT/oil microemulsions (AOT being the surface-active agent, or surfactant) has been studied by Van Dijk (1985) and Van Dijk et al. (1986). In this system the water forms droplets, 5 $\sim$ 10nm in diameter, coated by the AOT, which are far more conductive than the continuous oil phase because of the ions dissolved in the water. The AC conductivity was measured in the frequency range from 10kHz to 13MHz. A plot of $\tan\delta$ shows a plateau over nearly two decades of frequency for two or more sam-

ples near ϕ_c, with a value of $\tan\delta_c$=0.67±0.04, which gives y=0.35 from δ_c=y*(π/2). This is consistent with their value of x=0.62±0.02 and hence y=0.38, obtained using the method described in Subsection 3.3.1. Chen and Johnson (1991) observed a frequency-independent loss tangent for Ni/F-PP samples (ϕ=0.06 and 0.05) close to the percolation threshold with $\phi \leq \phi_c$, similar to the G-BN sample systems. They showed that the measured loss tangent, $\tan\delta$, at a given frequency diverges as the metal volume fraction approaches the percolation threshold from below. This divergence obeyed an empirical percolation equation $\tan\delta \propto (\phi_c - \phi)^{-(t-2s)}$, proposed by the same authors. However, the power law for the loss tangent that they reported may be due to an incorrect critical volume fraction ϕ_c=0.08±0.01, which was obtained by fitting the DC conductivity data on the conducting side only. This value of ϕ_c is also inconsistent with the AC conductivity data shown in their Fig. 6, where the samples with ϕ=0.070 and 0.081 show a plateau as a function of frequency at low frequencies, indicating that they are on conducting side of the percolation threshold. Furthermore, as these are the only authors to observe a $\tan\delta \propto (\phi_c - \phi)^{-(t-2s)}$ relationship, one must conclude that this power law may only apply to their (or very similar) system.

4.4 The Magnetoresistance

Measurements of the Hall coefficient were attempted at room temperature and at liquid-nitrogen temperature using the previously described G-BN parallelepiped samples, with a length-to-width ratio of 3 [Putley 1960]. A lock-in amplifier, operating at low frequencies (5$\sim$ 33Hz), and *Prema* 5000 digital voltmeter with a resolution of 0.1μm were both used to try to detect the Hall voltage. Unfortunately, no Hall signal could be detected by the instruments used, using maximum available magnetic field of 1.5Tesla and the largest current, typically about 2mA, which can be safely used without heating the samples. Due to the time limitation of this thesis, further attempts to improve the Hall instrumentation had to be given up.

The transverse magnetoresistance was measured on the samples ($\phi > \phi_c$) with the

length-to-width ratio of 1/6 at room temperature. The data acquisition was computerized so that the measurement could be repeated ~10 times at each field to improve the signal to noise ratio. For the experimental details, see Section 3.4.

The magnetic field induced a change of conductivity, i.e. magnetoconductivity. It is observed that -$\triangle\sigma$(H= 1.5T) tends to vanish as the percolation threshold ϕ_c = 0.150 is approached from above, as shown on a log-log scale in Fig. 4.13. The solid line is the result of a least squares fit of the equation -$\triangle\sigma \propto (\phi - \phi_c)^{t_m}$ to the data, which yields the critical exponent $t_m = 3.07 \pm 0.06$, using the ϕ_c of 0.150 found from the DC conductivity measurements. Fig. 4.14 shows that the relative magnetoresistance $\triangle R(1.5\text{T})/R$ also decreases with decreasing graphite volume fraction ϕ, and varies as $(\phi - \phi_c)^{g_c}$, with the critical exponent g_c=0.28±0.01. The difference between the exponent t_m (=3.07±0.06) and t (=2.68±0.13) is 0.39±0.19, which is consistent with the observed value of the exponent g_c, within the quoted experimental errors.

As discussed in Subsection 2.3.4, the magnetoconductivity or relative magnetoresistance of random metal-insulator percolation composites has been investigated theoretically by Bergman (1987). In this pioneering work, he used scaling arguments to predict the behavior of $\triangle\sigma$ and $\triangle R/R$ near a percolation threshold. As Rohde and Micklitz (1989) pointed out, this calculation gives a critical exponent t_m for the magnetoconductivity which is same as the t for the conductivity. Consequently $g_c = t_m - t = 0$, implying that $\triangle R/R$ does not vary near the percolation threshold. These theoretical predictions are in disagreement with the measurements made on the G-BN samples, shown in Fig. 4.14, where the relative magnetoresistivity exhibits a dependence upon $(\phi - \phi_c)$.

The only other experimental study of magnetoconductivity and relative magnetoresistivity was made *in situ* on granular Sn-Ar films with a thickness of 800 — 1000Å at a temperature of 4.2K, by Rohde and Micklitz (1989). The films were fabricated by coevaporating the metal and the rare gas on a sapphire substrate. They found the critical volume fraction ϕ_c to be 0.26 and the critical exponents t, t_m and g_c to be 1.6±0.1, 1.90±0.15 and 0.30 respectively. This value of g_c is consistent with

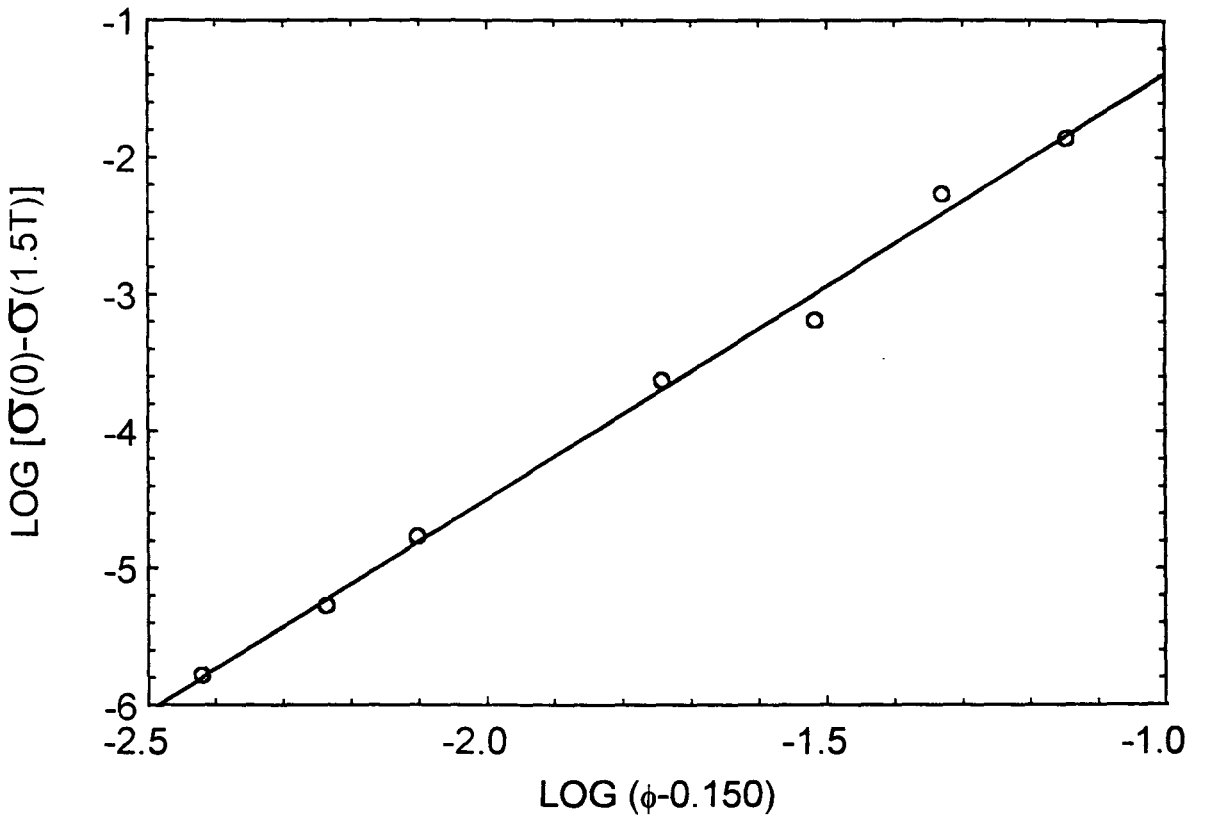

Fig. 4.13 The magnetoconductivity plotted against $(\phi - \phi_c)$ for $\phi > \phi_c$ on a log-log scale. Here $\phi_c = 0.150$. A least squares fit yields t_m=3.07±0.06(note t =2.68±0.13).

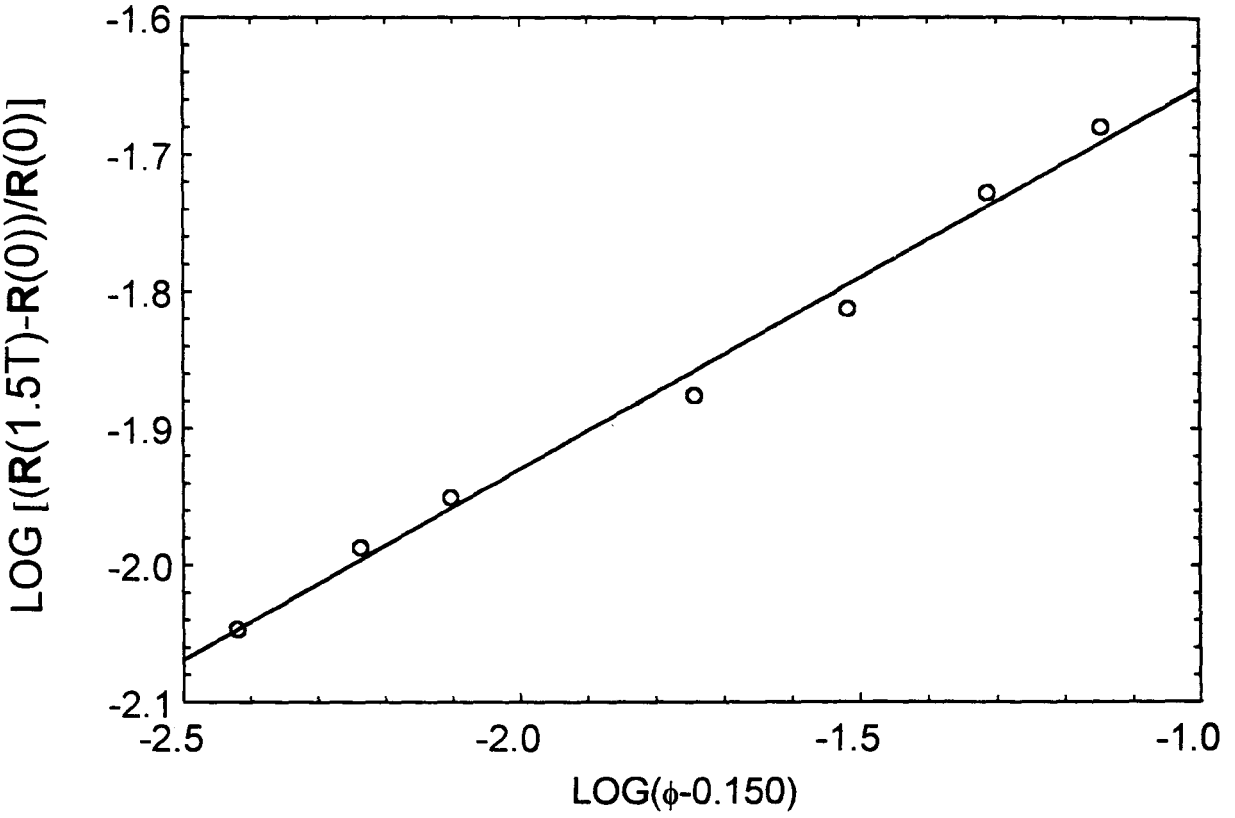

Fig. 4.14 The relative magnetoresistance $\triangle R/R$ plotted against $(\phi - \phi_c)$ for $\phi > \phi_c$ on a log-log scale. Here ϕ_c =0.150. A least squares fit to the data yields the exponent g_c of 0.28±0.01.

the one obtained from the G-BN system. Comparing the experimental observations from the percolation systems G-BN and Sn-Ar, the values of g_c are very similar, but the values of the exponent t_m are very different for the two systems and disagree with the theoretical prediction that $t_m = t$. The G-BN composites and Sn-Ar mixture are physically very different percolation systems, as indicated by the different conductivity exponents and the different percolation thresholds. The Sn-Ar mixtures gave the critical exponent $t = 1.6 \pm 0.1$, slightly lower than the generally accepted range of 1.7 — 2.0, while the observed conductivity exponent $t = 2.68 \pm 0.13$ for the G-BN parallelepiped samples is much larger and definitely nonuniversal. Because they have the same crystal structures and densities, the graphite and hexagonal boron-nitride phases in the composites are indistinguishable by topological methods, in contrast to that of the Sn-Ar mixtures [Rohde and Micklitz 1989]. The agreement in the critical behavior of the magnetoresistivity in such very different systems indicates that the observed discrepancy between theory and experiments could be fundamental. Further measurements of the magnetoresistivity are necessary to check if a g_c of 0.28 — 0.30 is "universal" for all disordered systems.

4.5 Summary

Critical volume fractions ϕ_c=0.150 and 0.153 were observed for two sets of G-BN disc samples, which are close to the "random" value of 0.16±0.02. For the powders, the measured values of ϕ_c are from 0.11 to 0.12, smaller than the random value in three dimensions. This difference is attributed to the presence of a large number of cavities, as the packing fraction is about 0.25 at ϕ_c in the G-BN powders undergoing compression. Nonuniversal t values were obtained in all three G-BN percolation systems. For the disc samples, the observed t values are about 2.6 and 2.7 in the axial and transverse directions respectively. For the powders, the values of exponent t are found to be 4.8 and 6.1 in the axial and transverse direction respectively, which are approximately three times the universal value in three dimensions. The observed $\bar{s}$ and s values distributed in a rather broad range 0.4 — 1.1. The observed nonuniver-

sal exponent t, $\overline{s}$ and s cannot be explained by the existing models for non universal exponents, e.g. the Swiss-cheese model and the inverted Swiss-cheese model with tunnelling.

For the AC conductivity, all the measured exponents x and y for the G-BN discs and powders have been interpreted in a satisfactory way, using the intercluster polarization model and the measured values of t and s. Above the percolation threshold, the scaling law $\omega_c \propto \sigma^q(\phi, 0)$ is observed. Although the measured values of the exponent q are smaller than their theoretical predictions using the observed exponents t and s for the G-BN systems, these somewhat lower than expected values are consistent with other experimental observations. Below the percolation threshold, the crossover frequency ω_c is found to be unity and consequently $q \sim 0$, which cannot be explained using existing percolation theories. A nearly constant or frequency-independent loss tangent $\tan \delta_c$ near the critical volume fraction on the insulating side is observed, and the exponents y derived from the plots of loss tangent versus frequency agrees with those obtained from $\omega \cdot \varepsilon(\phi, \omega)$ versus frequency plots on a log-log scale. The global minimum in $\tan \delta$ as a function of frequency below ϕ_c cannot be accounted for by the intercluster polarization model.

The magnetoresistivity exponent (0.28) obtained from the G-BN system at room temperature and in a magnetic field of 1.5T agrees with the value (0.30) obtained at $4.2K$ in a field of 2T for the three-dimensional granular films of Sn-Ar mixtures [Rohde and Micklitz 1989]. Both these experimental results are in disagreement with the theoretical prediction made by Bergman (1987). This discrepancy between experiment and theory shows the necessity of further experimental and theoretical magnetoconductivity studies.

Chapter 5

THE $1/f$ NOISE

5.1 Introduction

The purpose of the study of $1/f$ noise in the G-BN compressed conducting samples (discs and parallelepipeds) close to the percolation threshold is twofold. First, to verify the power-laws $S_V/V^2 \propto R^w$ and $(\phi - \phi_c)^k$ in the critical region, which may assist in the identification of the conduction mechanism on the conducting side of the percolation threshold. Secondly, to investigate the inhomogeneous structure of the samples near ϕ_c, since the voltage fluctuations are more sensitive than the resistance because the voltage fluctuation is a fourth order moment of the local current whereas the resistance is of second order [Rammal et al. 1985b].

There are several theoretical models dealing with the $1/f$ noise in percolation systems. These models include lattice resistor networks, Swiss-cheese and inverted Swiss-cheese models, and two component effective-medium theories. However, it must be noted that there is no single $1/f$ noise model, which can explain all the experimental results obtained from all measurements to date of continuum percolation systems. Also many models are designed to explain the results for a single experimental system.

As previously stated in Section 3.5, the $1/f$ noise in the conducting G-BN disc samples near the percolation threshold was measured in both the axial and transverse

directions in the frequency range $1Hz \sim 1000Hz$ at room temperature. Six or seven different DC currents were used to check the I^2—dependence. The noise power spectra measured as a function of the frequency are found to be close to $1/f$ in all the G-BN conducting samples measured and at all current levels used. The measured noise spectrum can be characterized by the Hooge's empirical formula (2.48), which is rewritten here for convenience as

$$S_V = \frac{\alpha}{N^\eta} \frac{V^\vartheta}{f^\gamma}, \tag{5.1}$$

where the symbols are already defined in Section 2.3.3.

Using the fractal structure of infinite percolation cluster near ϕ_c, Rammal and his co-workers (1985b) predicted that near the percolation threshold the normalized $1/f$ noise power scales as $S_V/V^2 \propto L^{-b}$, where L $(>\xi)$ is the linear dimension of the sample and b=1.18~1.26 in a three dimensional resistor network lattice. Unfortunately, this theoretical prediction still lacks experimental support. This chapter will give the experimental results of the sample size dependence of the $1/f$ noise in the compressed G-BN samples. The measurements of size dependence of normalized $1/f$ noise power were, to a certain extent, to try to reveal the fractal structure of the percolation cluster in the G-BN disc samples. The $1/f$ noise was measured on several conducting samples near the percolation threshold, where the sample volume was decreased in such a way that the thickness of sample was kept constant, while the length and width were decreased with the same length-to-width ratio for each sample.

The rest of this chapter is organized as follows. The experimental results, with constant sample volume, are presented and discussed in Section 5.2. The sample size dependence of the normalized $1/f$ noise is given in Section 5.3. The chapter is concluded in Section 5.4.

5.2 S_V/V^2 as a Function of Sample Resistance

Figs. 5.1a and b show the normalized noise power spectra $S_V(f)/V^2$ (with the background noise subtracted off) against the frequency for seven samples both in the axial direction (disc-shaped) and in the transverse direction (parallelepipeds of the same dimensional size) respectively. These figures show that the noise spectrum can be fitted to the relation $S_V(f)/V^2 \propto f^{-\gamma}$. The values of the exponents γ are obtained by using least squares fits, and the values are summarized in the columns 2 and 3 of Table 5.1. The exponent γ varied in the range 0.95—1.08 with a weighted mean (see Section 3.7) of 1.01±0.01 in the axial and 1.06±0.01 in the transverse direction respectively. It is seen from these plots that, within the experimental error, there is no significant difference in the values of the exponent γ in the transverse and axial directions.

The current dependences of noise power magnitude at $10Hz$ for each sample are illustrated on a log-log scale in Figs. 5.2a and b. The lines drawn through each sample data points are the results of least squares fits to the data. The columns 4 and 5 of Table 5.1 list all the values of exponent ϑ determined by the slopes of lines through the data points. Similar results are obtained at other fixed frequencies in the range $1Hz \sim 1000Hz$. In general the noise varies with I, for small currents and independent of frequency, with a power just less than 2. The averaged values of the exponents ϑ are found to be 1.96±0.01 and 1.93±0.02 in the axial and transverse directions respectively. From Equation (5.1) an I^2-dependence is expected for noise generated by resistance fluctuations in the composites probed by DC current, and is usually found for "$1/f$ " noise systems

Fig. 5.3 shows the normalized noise power at $10Hz$, as a function of the sample resistance, near the percolation threshold, in the axial and transverse directions. The least squares fits of a straight line to the relevant data yield two exponents

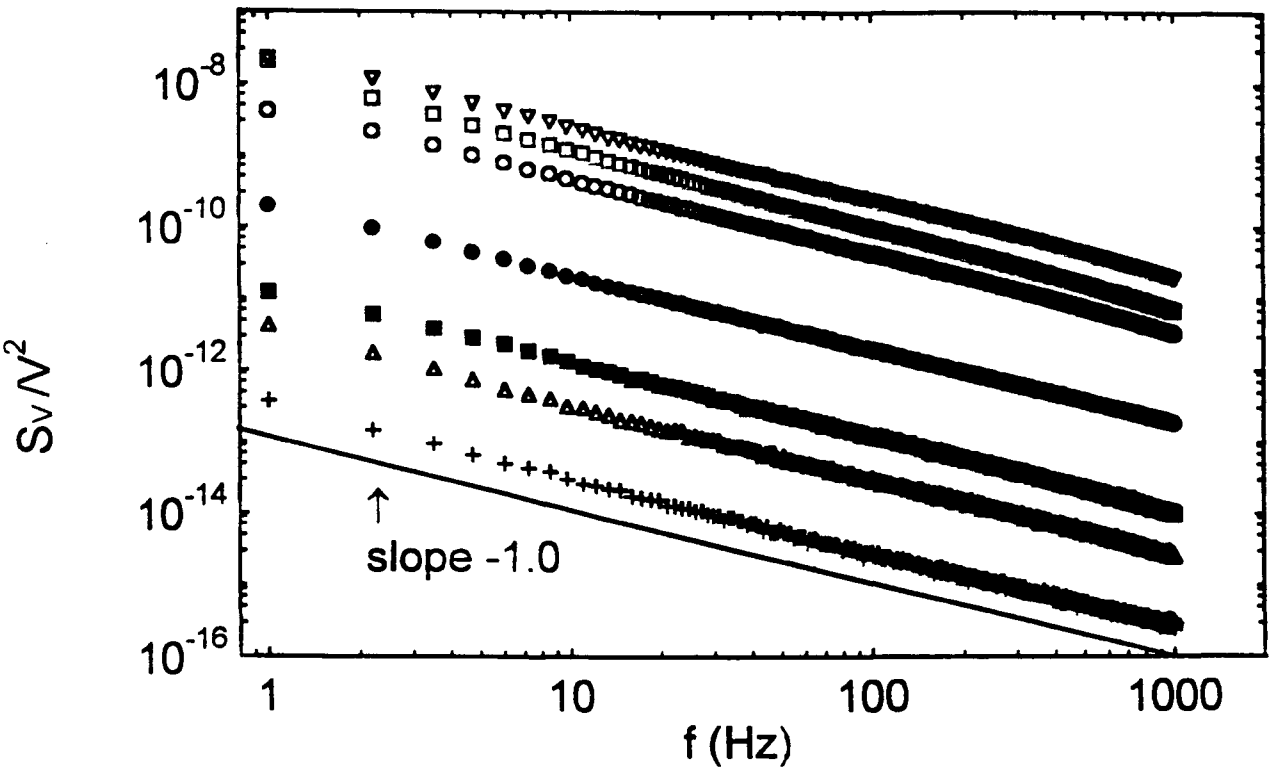

Fig. 5.1a The normalized noise power against the frequency in the axial direction. The volume fractions from top to bottom are ϕ =0.152(∇), 0.158(□), 0.156(o), 0.168(•), 0.180(■), 0.197(△), 0.221(+). The values of the exponents γ are given in Table 5.1.

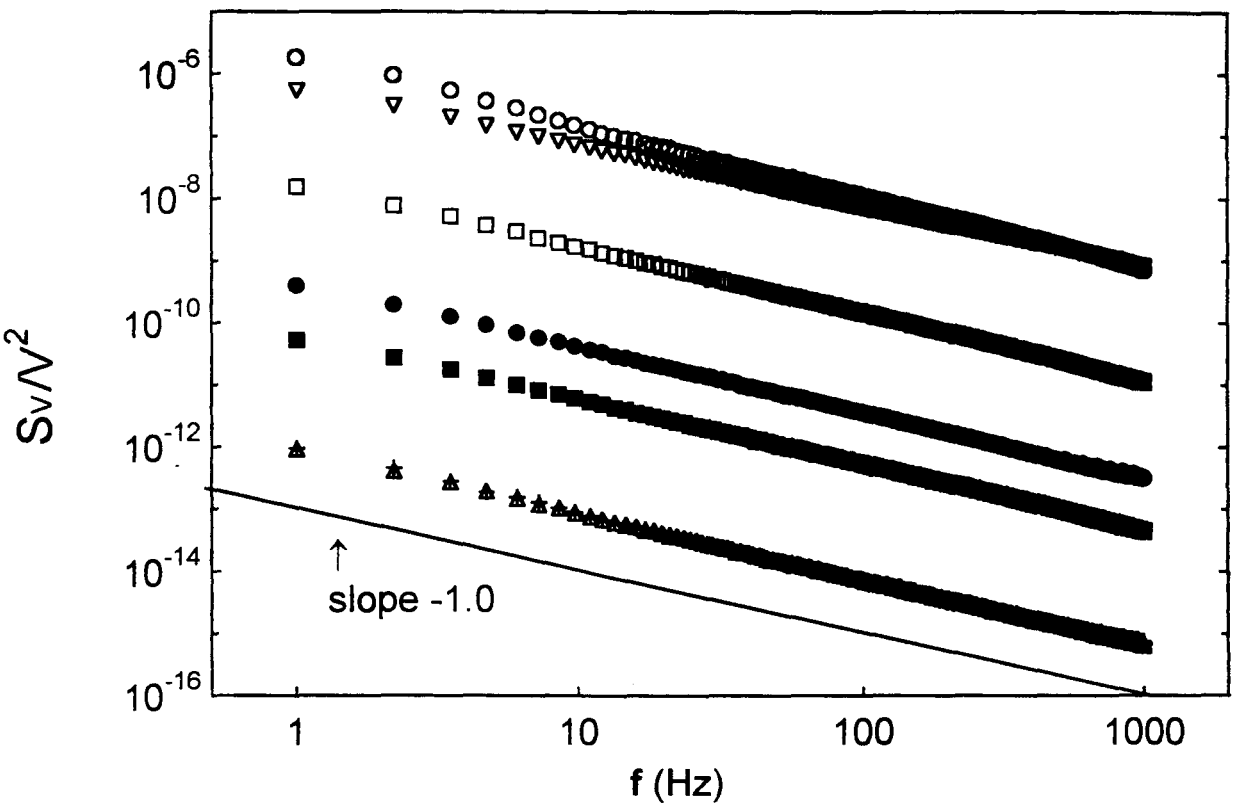

Fig. 5.1b The normalized noise power against the frequency in the transverse direction. The volume fractions from top to bottom are ϕ =0.152(o), 0.156(∇), 0.158($\square$), 0.168($\bullet$), 0.180($\blacksquare$), 0.221(+), 0.197($\triangle$). The values of the exponents γ are given in Table 5.1.

Table 5.1 The observed values of the exponents γ and ϑ in the axial and transverse directions respectively.

ϕ	γ	uncertainty in γ	ϑ	uncertainty in ϑ
Axial				
0.152	1.024	0.002	1.977	0.045
0.156	0.976	0.002	1.868	0.035
0.158	1.019	0.002	1.940	0.038
0.168	1.018	0.002	1.990	0.020
0.180	1.027	0.003	2.020	0.031
0.197	1.015	0.002	1.952	0.032
0.221	1.039	0.005	1.980	0.035
Transverse				
0.152	1.134	0.004	1.817	0.055
0.156	1.047	0.003	1.826	0.044
0.158	1.045	0.003	1.804	0.082
0.168	1.045	0.002	2.068	0.056
0.180	1.029	0.003	2.093	0.053
0.197	1.065	0.002	1.980	0.037
0.221	1.095	0.004	1.810	0.066

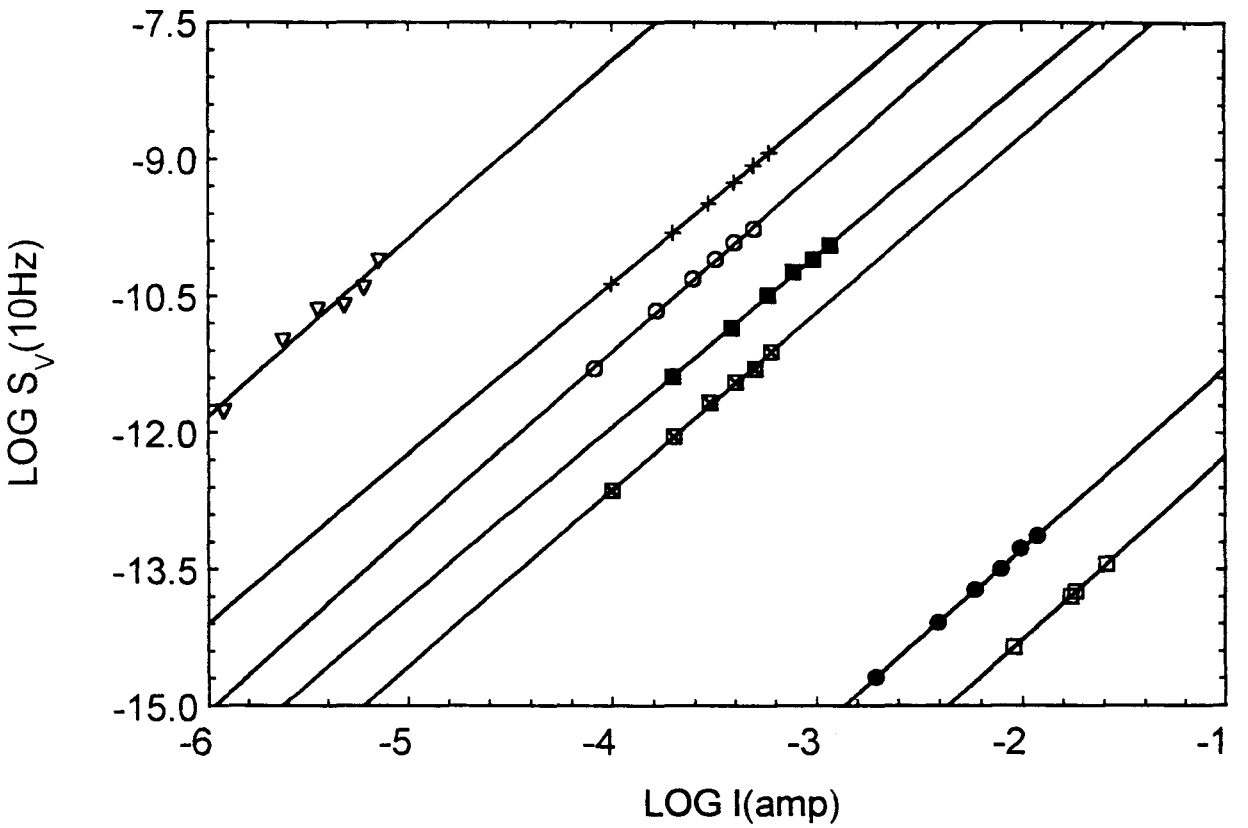

Fig. 5.2a The noise power in the axial direction against the DC current on a log-log scale. The solid lines are least squares fits to the data. From right to left ϕ =0.221, 0.197, 0.180, 0.168, 0.158, 0.156, 0.152. The slopes are given in Table 5.1.

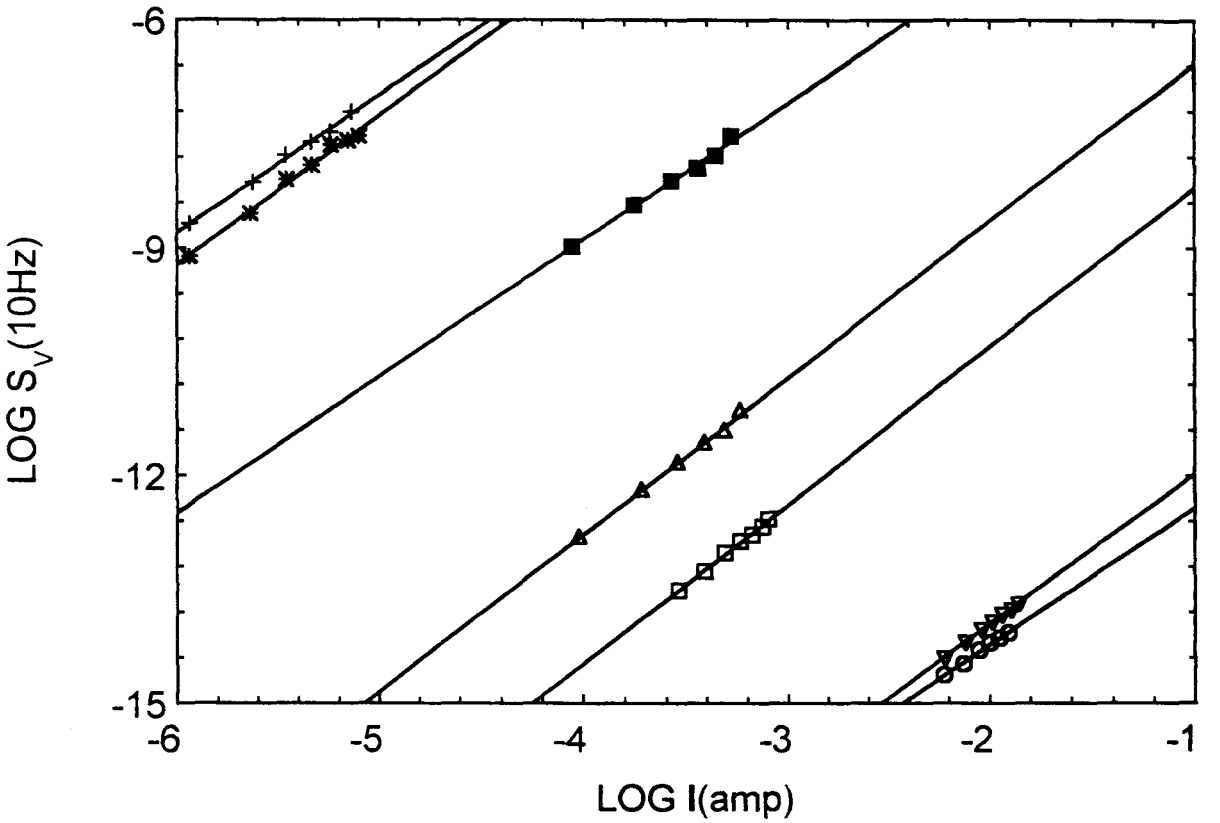

Fig. 5.2b The noise power in the transverse direction against the DC current on a log-log scale. The solid lines are least squares fits to the data. From right to left ϕ =0.221, 0.197, 0.180, 0.168, 0.158, 0.156, 0.152. The slopes are given in Table 5.1.

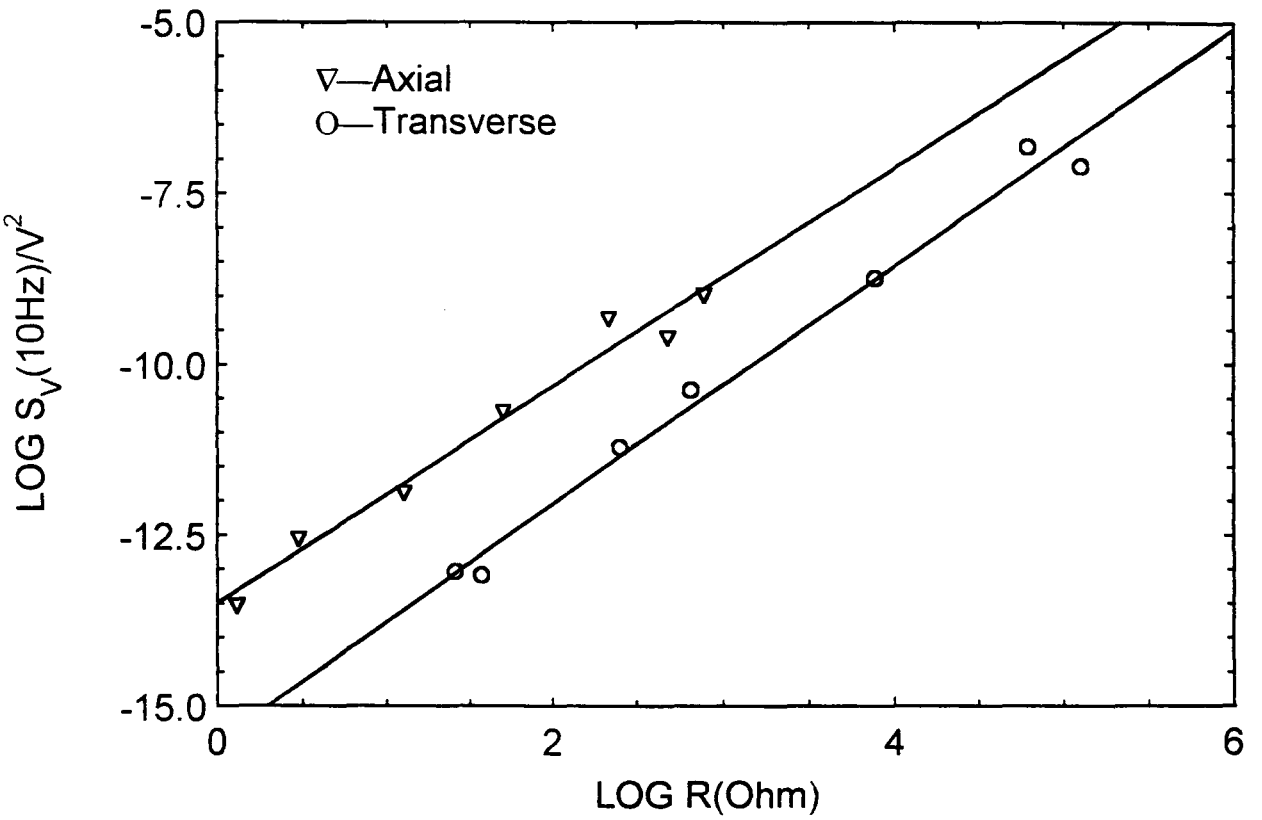

Fig. 5.3 The normalized noise power against the sample DC resistance on a log-log scale. The solid lines are least squares fits to the data. The slopes are 1.47±0.05 and 1.72±0.08 in the axial and transverse directions respectively.

w =1.47±0.08 in the axial and 1.72±0.08 in the transverse direction. The difference between these two exponents is probably due to the anisotropy of the sample microstructures. The two values of the exponent κ are obtained using the relation $w = \kappa/t$, and the results are κ=3.87±0.31 ($t = 2.63 \pm 0.07$) in the axial and 4.61±0.43 (t=2.68±0.13) in the transverse direction.

The discrete lattice model was the first to be developed to explain $1/f$ noise in percolation systems. In calculating the noise in a percolation lattice model of resistors, Tremblay et al. (1989) assumed that the spatial correlation length of $1/f$ noise is much shorter than the lattice spacing, as has been experimentally observed in many situations of interest [Tremblay et al. 1989 and references therein], and that the resistance of each resistor fluctuates around an average value, independent of all the other resistances. Computer simulations of the noise using this model system gave that $1.0 \leq \kappa \leq 1.56$ in three dimensions. This model gives too weak a $(\phi - \phi_c)$ dependence for the noise power to account for the results shown in Fig. 5.3, where two values of the exponent w correspond to κ=3.9 and 4.6 respectively. The reason for this inconsistency is probably the so-called continuum correction [Rammal 1985] for the G-BN samples.

The present results for the noise exponents are close to those obtained by Chen and Chou (1985) on three dimensional carbon powder and wax mixtures. Their samples were made by mixing the two components at a temperature slightly higher than the melting point of wax. The resistance and $1/f$ noise were measured at room temperature, and it was found that the isotropic DC conductivity could be fitted to $(\phi - \phi_c)^t$, where t=2.3, and that the magnitude of the $1/f$ noise followed the power-law $S_V/V^2 \propto (\phi - \phi_c)^\kappa$. The two critical noise exponents κ and w were found to be 5 and 1.7 respectively. To try to explain Chen and Chou's data, Rammal (1985) calculated these exponents using the Swiss-cheese model and obtained $t = 2.38$ and $\kappa = 5.14$ for three dimensional systems, yielding $w = \kappa/t = 2.2$, which agrees fairly well with Chen and Chou's data. The exponents t, κ, and w obtained from the G-BN samples are not in good agreement with the calculation made by Rammal. Chen and

Chou (1985) claimed that inter granular tunneling is responsible for the noise process in their samples. Indeed the wax may form thin layers between the carbon clusters in these samples near the critical volume fraction. Thus the tunneling of electrons between the carbon clusters, separated by a very thin wax layer, could play a major role in conduction and noise generation.

Garfunkel and Weissman (1985) studied the $1/f$ noise power as a function of sample resistance for Al, In and Cr foils. The metal volume fraction of films was changed by sand-blasting. Most of the samples were found to have exponents between 3.4 and 6.0 in the rather limited range of resistances measured. These high values of w were explained by the authors using a Swiss-cheese continuum percolation model, in which the size δ_m of the smallest neck scales as $(\phi - \phi_c)^2$ to minimize the power dissipation in the Links-Nodes-Blobs (LNB) model [Garfunkel and Weissman, 1985]. This version of the Swiss-cheese model makes the prediction that the exponent w, after taking into account the nonuniformities of the samples, should be in the range 3.5 — 6.5, in contrast to 2.0 — 3.8 for the original Swiss-cheese model in which δ_m is taken to be proportional to $(\phi - \phi_c)$ [Halperin et al., 1985].

Rudman et al. (1986) observed a noise exponent $w \simeq 3$ in their three dimensional granular AgPt-TFE samples near the percolation. In an effort to explain this large exponent w, they modified in a straightforward way the ideal Swiss-cheese model, where the insulating spheres in a conducting matrix are replaced by interpenetrating conducting spheres in an insulating matrix (i.e. inverted Swiss-cheese model). In this case, with the assumption that the interpenetration cutoff length (the smallest neck size) δ_m varies as $(\phi - \phi_c)^2$, they obtained $t = 1.88$, $\kappa = 5.64$ and correspondingly $w = \kappa/t = 3$. Note that all the Swiss-cheese and the inverted Swiss-cheese models discussed above assume a single conduction mechanism, that also generates the noise.

Pierre and his collaborators (1990) observed a $R^{1.5}$ dependence in copper-particle-polymer samples on conducting side of ϕ_c. For high resistances (>1MΩ and $\phi < \phi_c$), their data can be fitted to a $R^{1.0}$ law, which is characteristic of tunneling through a

metallic oxide barrier [Mantese and Webb 1985]. Pierre et al. (1990) then proposed a two component effective-medium theory to explain their experimental results. This model showed that the values of the noise exponent above and below ϕ_c are consistent with a transition from metallic conduction to tunneling conduction in their samples, as they pass from above to below the critical volume fraction. Note that only a single value of the noise exponent in both the axial and transverse directions, which fits the data over five decades of resistances, was observed in the G-BN samples. This observation indicates that, if the noise in the G-BN system is due to the inter contact noise only, a single type of metal-metal contact in the backbone probably dominates the noise process in the G-BN sample system. This observation is also consistent with the DC conductivity data where the volume fraction varies from 0.150 to 0.82, as shown in Fig. 4.4, and the conductivity data can be fitted with the single conductivity exponent $t = 2.7$ (in the axial direction), implying a single conduction mechanism both near to and far from the percolation threshold above ϕ_c.

The measured noise exponent w=1.47 in the axial direction agrees very well with the two component effective-medium theory proposed by Pierre et al. (1990) in the metal-metal contact noise regime, in which the Sharvin contact prevails. The value of $w = 1.5$ predicted by this model is also only just outside the error bars of the observed value of $w = 1.72$ in the G-BN system in the transverse direction. This small discrepancy in w can probably be explained qualitatively using the following extension of the metal-to-metal contact model. The metal-to-metal (G-G) contact bonds in transverse direction are slightly and mechanically weaker than those in axial direction, along which the pressure was applied during the making of the discs. For these weaker transverse bonds the contact resistances are higher than those of the bonds in the axial direction, resulting in a relatively large noise amplitude, since the noise exponent w for single contact resistor is never less than unity [Takagi et al. 1986 and Vandamme 1987]. Taking into account the noise contribution from these weaker bonds, the sample (averaged) noise power would increase faster (i.e. a larger value of the w) in the transverse direction than that in the axial direction. Unfortunatly, models based on this idea have not yet been explored.

Another effective-medium model for the $1/f$ noise in percolation systems, proposed by Mantese et al. (1986), was used to model the normalized $1/f$ noise as a function of the conductor volume fraction for Pt-Al_2O_3 metal-oxide composites. In these composites, above the percolation threshold, the electrical conduction is dominated by metallic conduction along the backbone, while below the percolation threshold, electron tunneling between the metal clusters is the primary conduction mechanism. However, Mantese et al. (1986) proposed that the noise is dominated by tunneling resistance fluctuations over the entire range of volume fractions. Therefore, according to their model, the conduction and noise in the composites above ϕ_c stem from completely different mechanisms. As the tunnel junctions are always in parallel with some metal contacts, the tunneling eliminates the divergence of the noise power at ϕ_c and there is no change in noise mechanisms as ϕ goes from above to below ϕ_c in the Pt-Al_2O_3 system. A saturation of the normalized $1/f$ noise magnitude below ϕ_c was also observed in these composites [Mantese and Webb 1985 and Mantese et al. 1986], and explained by Mantese et al. (1986), using the same effective-medium theory. This model does not give explicit quantitative predictions of the noise exponent κ or w, even though there only is a single noise mechanism (tunnelling) in the percolation system above and below ϕ_c. As tunneling does not occur in the G-BN samples, it cannot be the source of the $1/f$ noise in the G-BN samples above ϕ_c. Therefore, Mantese et al.'s model probably does not apply to the present study.

Many authors observed a R^2-dependence of the normalized $1/f$ noise power in thin film systems. Koch et al. (1985) reported that, at room temperature, the $1/f$ noise source changed from metallic to hopping in the ion-milled thin gold films near the percolation threshold. Over a resistance range between 1kΩ and 100kΩ on conducting side, the exponent w that they observed was 2.0. This result fits neither the lattice nor the Swiss-cheese percolation models, because in this system the microscopic metallic islands are connected by both necks and hopping paths, which is not the case for either a lattice system or a Swiss-cheese type continuum. A R^2-dependence of the normalized $1/f$ noise power has also been observed by Octavio et al. (1987) for

ion-milled silver films at liquid-nitrogen temperature and by Williams and Burdett (1969) for evaporated thin gold films. However, the latter interpreted their results as coming from noisy tunneling conduction. The similarity in the experimental results, obtained from the thin films, suggests that some important considerations have been neglected in the various calculations for the exponent w for the noise in these systems. Since there is no oxide layer or thin polymer coating between the graphite grains in the G-BN samples, the $1/f$ noise source from the electron tunneling and thermally activated hopping can probably be ruled out in the present study.

5.3 Dependence of S_V/V^2 on Sample Size

The compressed disc samples used in this experiment were made using exactly the same procedures as all the other compressed disc samples previously used, and then cut into parallelepipeds of ever decreasing size. The full experimental details have been described in Section 3.5. The noise powers of these samples, with both different sizes and compositions, were successfully checked for $1/f$—like and I^2—dependence. Fig. 5.4 is a log-log plot of the normalized noise power at 10 Hz, in the transverse direction, versus the sample volumes. The straight lines in the figure are the best linear fits to the data for each sample. The broken lines and the corresponding data have been shifted up or down to avoid overlap. The slopes and corresponding volume fraction from top to bottom are -0.49±0.09[ϕ=0.156], -0.65±0.04[ϕ=0.164], -0.50±0.03[ϕ=0.164], -0.58±0.02[ϕ=0.168], -0.41±0.07[ϕ=0.164], -0.52±0.17[ϕ=0.172], and -0.64±0.09[ϕ=0.168]. The weighted average of the slopes, obtained by using (3.4) and (3.5), is -0.56±0.02. Therefore a nearly inverse square root dependence of the normalized $1/f$ noise power on the sample volume is observed such that

$$\frac{S_V(10Hz)}{V^2} \propto (Volume)^{-0.56}. \tag{5.2}$$

Since the mean grain size is about 10μm (=a_o), the maximum correlation length

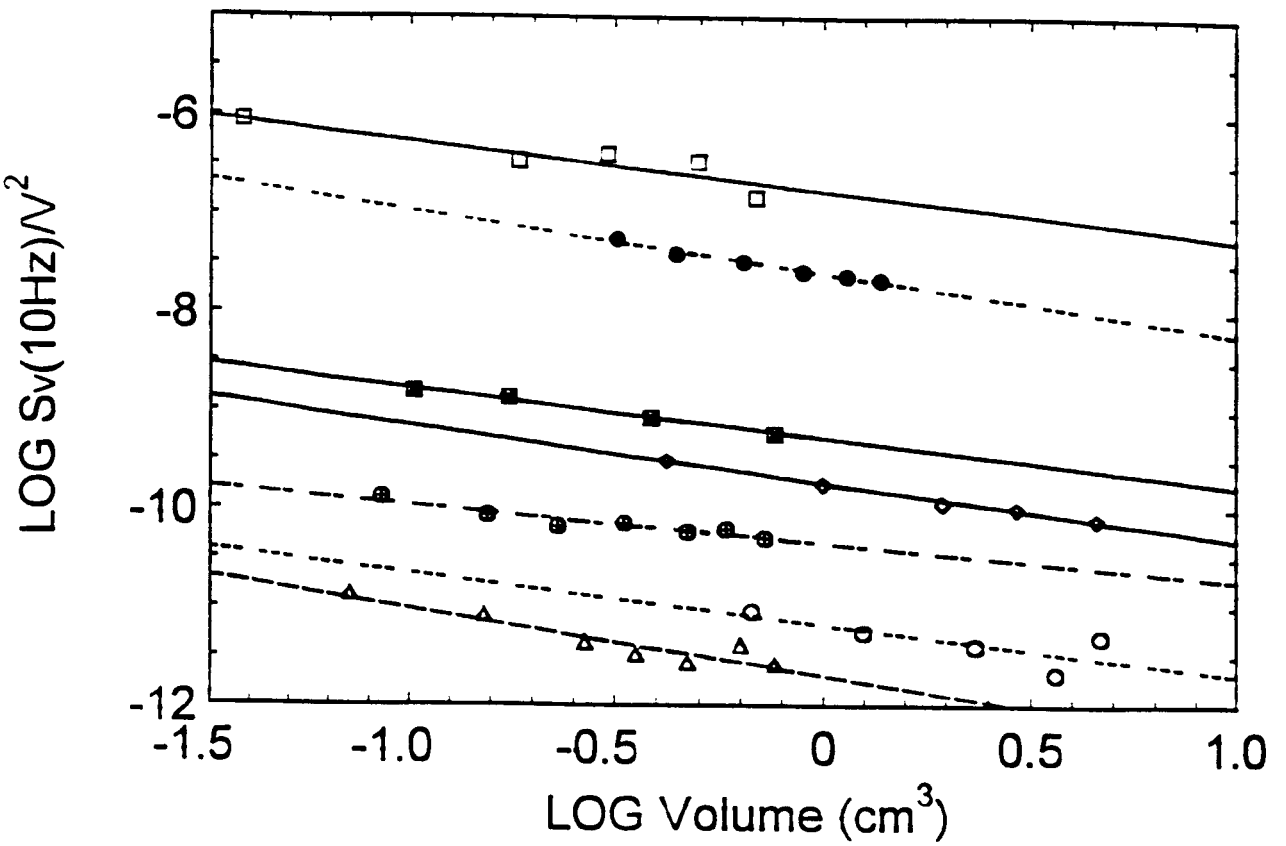

Fig. 5.4 The normalized noise power as a function of the sample volume on a log-log scale for the G-BN parallelepipeds near the percolation threshold. The slopes from top to bottom are -0.49±0.09 [ϕ =0.156], -0.65±0.04 [ϕ =0.164], -0.50±0.03 [ϕ =0.164], -0.58±0.02 [ϕ =0.168], -0.41±0.07 [ϕ =0.164], -0.52±0.17 [ϕ =0.172], -0.64±0.09 [ϕ =0.168]. The weighted average of the slopes is -0.56±0.02. The broken lines and corresponding data points have been shifted in the vertical direction to avoid overlap.

ξ for all the G-BN samples used in the sample size experiments can be estimated as $\xi_{max}= a_o/(\phi - \phi_c)^{0.85}_{min} \simeq 10\mu m/(0.156\text{-}0.150)^{0.85} \simeq 1mm$, which is smaller than and at the same order of magnitude of the thickness of the samples and the minimum length and width in decreasing sample volumes. In addition it is obvious (see Section 3.5) that $L >> 1$ (measured in the grain size) in the sample size dependent experiments. Therefore it can be assumed that the samples were approximately three dimensional and in the region from the crossover ($L \sim \xi$) to macroscopic homogeneous ($L > \xi$). This implies that (5.2) should correspond to a $L^{-1.68}$-dependence. However, one could make the argument that the sample volume was decreased in two dimensions. This means that $Volume \propto L^2$, which results in a $L^{-1.12}$–dependence from (5.2). The argument, leading to the value of $b = 1.12$, is very debatable and suspect, but is given, because the value of b=1.12 obtained in this way is very close to the lower bound obtained from computer simulations on discrete lattice networks in three dimensions (see the next paragraph). If this were correct it would contrast with the other critical exponents from the G-BN systems where, as often stated, the values of these critical exponents are obviously different from the ones for discrete lattices, probably due to a continuum correction.

These appear to be the first measurements where the size dependence of the $1/f$ noise power near the percolation threshold has been obtained experimentally for a three dimensional percolation continuum system. Computer simulations on the three dimensional standard discrete percolation networks give a lower and upper bounds of the exponent b to be $-\beta_L = 1.1$ and $-2\beta_L - 1/\nu = 1.26$ respectively [Tremblay et al. 1986]. Therefore the observed exponent $b = 1.68 \pm 0.06$ for the G-BN samples is much larger than those permissible for discrete lattice networks according to Tremblay et al. (1986). This fact suggests that the continuum correction in the G-BN samples could also play a significant role in the size dependence of noise exponent b. But there are, to the author's best knowledge, no previous experimental result and existing theoretical model for the exponent b in continuum percolation systems.

The existing predicted values of the noise exponent b are strictly speaking only

applicable to conducting samples for which $L < \xi$ [Rammal et al. 1985b]. This implies that the measured value of the noise exponent b would be higher if sample is in the region $L > \xi$. Hence the value of b=1.68 seems quite reasonable because the G-BN samples, with volume fractions ϕ from 0.156 to 0.172, which were measured to study the size dependence of the $1/f$ noise, all have $L >$ or $L >> \xi$, depending on ϕ and the direction. However, these samples could all lie in a transition region from a fractal character ($S_V/V^2 \propto L^{-b}$) to a homogeneous one where the Hooge's law applies ($S_V/V^2 \propto L^{-3}$). Therefore the observed anomalous size dependence of S_V/V^2, which deviates from the Hooge's empirical formula, could still be due to the fractal geometry of the backbone in all the samples ($0.156 \leq \phi \leq 0.172$). The value 1.68 of the exponent b is very close to the exponent D_B of 1.74 in three dimensions. Here the D_B is defined as [Chapter 5, Stauffer and Aharony 1994]

$$M_B(L) \propto L^{D_B} \tag{5.3}$$

where M_B is the backbone mass. This could mean that only the mass of graphite on the backbone gives contributions to the $1/f$ noise. This implies that, similar to most cases where the $1/f$ noise is a bulk effect and inversely proportional to the sample volume [Dutta and Horn 1981 and Weissman 1988], the relation $S_V/V^2 \propto (Volume)^{-0.56}$ observed in the G-BN samples could still suggest a bulk source of $1/f$ noise on the backbone.

It has been shown in the previous section that the metal-to-metal (G-G) contacts on the backbone were possibly responsible for the $1/f$ noise in the compacted conducting G-BN samples. Therefore, if this is the case, the $1/f$ noise and resistance in the G-BN samples measured come from different mechanisms, both involving the graphite grains on the backbone. These are intergranular contacts between neighbouring graphite grains on the backbone for the former and bulk resistivity for the later.

The only other experimental study of size effects on the $1/f$ noise has been made

by Girand et al. (1987) for a two dimensional deterministic fractal lattice. They measured the $1/f$ noise on a special hierarchical network, built from capacitors, with immeasurable $1/f$ noise, and selected carbon layer resistors, all with the same normalized noise power. With n=0,1,2,3 experimental iterations, they found the exponent b to be 1, which is half of the value of the exponent b=2 expected from the Hooge's law for two dimensional Euclidean networks. Moreover, the value of b observed in this discrete model system is consistent with numerical calculations which gave lower and upper bounds for the exponent b, in two dimensional lattice percolation models, of 0.97±0.01 and 1.19±0.01 respectively [Tremblay et al. 1986]. Exact values for the exponent b for two dimensional continuum percolation systems cannot be obtained from the above experimental result, because the system studied is a discrete percolation network and, as mentioned in the last paragraph, percolation exponents for a continuum system and for a discrete lattice model can be considerably different. Therefore, one cannot directly relate these two observed values of the exponent b for the G-BN system and for the hierarchical network to each other due to their different dimensionality [two and three dimensions] and characteristics [discrete and continuum]. The above hierarchical network study was, nevertheless, an important step in characterization of size dependence of $1/f$ noise in percolation systems.

5.4 Summary

The experimental results for the $1/f$ noise in G-BN compressed conducting samples near the percolation threshold have been presented in this chapter. The noise power spectra were measured in both the axial and transverse directions and have typical $1/f$ behavior. The I^2- law of the noise power is evidence of the ohmic behavior of the resistance of the samples and that the noise originates from resistance fluctuations. The normalized noise powers follow a power-law $R^{1.47}$ in the axial direction and $R^{1.72}$ in the transverse direction, where R is the sample DC resistance. These results can best be explained using a model involving intergranular metal-to-metal (G-G) contact resistance noise in the Sharvin regime, derived using a self-consistent

effective-medium approximation. The most important new result from the $1/f$ noise experiments on the G-BN samples is probably the $(Volume)^{-0.56}$–dependence of the normalized $1/f$ noise magnitude, which applies from near to far from the percolation threshold on the conducting side. The value of the noise exponent b has been found to be 1.68 ± 0.04, which is considerably larger than the predictions made for discrete lattice models.

Chapter 6

THE THERMOELECTRIC POWER

6.1 Introduction

While the conductivity, dielectric constant and $1/f$ noise have been studied extensively in percolation systems, the behavior of thermoelectric power near the percolation threshold has not been extensively investigated for binary percolation composites. As mentioned in Section 2.3, Levy and Bergman (1992) proposed a scaling scheme for the thermoelectric power in percolation systems. Their expressions for the thermoelectric power near the percolation threshold are quite complex and depend in part on the relation between the electrical and thermal conductivity ratios. In order to obtain their analytic results, both the ratio σ_i/σ_c and k_i/k_c must be very small compared to unity. The physical meaning of these requirements is that the good electrical conductor is also a good thermal conductor and *vice versa*. Since $k_i > k_c$ for the graphite and hexagonal boron nitride, Levy and Bergman's scaling results are not applicable to the G-BN percolation system. On the experimental side, only one experimental study on the Al-Ge percolation thin films has been reported and analyzed [Hurvits, Rosenbaum and McLachlan 1993] following the two theoretical papers [Bergman and Levy 1991; Levy and Bergman 1992]. As an extension to these previous works, new power-laws for the thermoelectric powers in binary continuum percolation systems

are proposed, and measurements of the thermoelectric power were made on the G-BN parallelepiped samples. The new power-laws for the thermoelectric power near the percolation threshold are developed in Section 6.2. The experimental results for the thermoelectric power in the G-BN composites are given and analyzed, using the newly proposed power-laws, in Section 6.3. The thermoelectric data obtained from the Al-Ge films [Hurvits et al. 1993] is also re-analyzed in this section. The results are summarized in Section 6.4.

6.2 New Power-Laws for the Thermoelectric Power

The Milgrom-Shtrikman-Bergman-Levy (MSBL) formula for thermoelectric power in binary composites is an analytic result [Milgrom and Shtrikman 1989 and Bergman and Levy 1991] and has previously been used to develop power-laws for thermoelectric power in percolation systems [Levy and Bergman 1992]. As stated in Subsection 2.3.6, the power-laws proposed by Levy and Bergman are very complex and are not applicable to the percolation systems in which the electrical insulator is a better thermal conductor than the another component. In an attempt to improve the Levy and Bergman's scaling scheme, new power-laws for the thermoelectric power near the percolation threshold are proposed and will be presented in this section. For convenience, the MSBL formula is re-written here

$$S_m = S_c + (S_i - S_c)\frac{\frac{K_m/K_c}{\sigma_m/\sigma_c} - 1}{\frac{K_i/K_c}{\sigma_{i/\sigma_c}} - 1}, \tag{6.1}$$

where the symbols have been defined in Subsection 2.3.6.

To obtain simple and well-defined scaling form for the thermoelectric power in percolation systems, the terms on the right-hand side of Equation (6.1) have to be rewritten in the following way

$$S_m = S_c - (S_i - S_c)\frac{1}{\frac{K_i}{\sigma_i}\frac{\sigma_c}{K_c} - 1} + (S_i - S_c)\frac{1}{\frac{K_i}{\sigma_i} - \frac{K_c}{\sigma_c}} \cdot \frac{K_m}{\sigma_m}$$

$$\equiv M_1(S_c,S_i,K_c/\sigma_c,K_i/\sigma_i) + M_2(S_c,S_i,K_c/\sigma_c,K_i/\sigma_i) \cdot \frac{K_m}{\sigma_m},$$

(6.2)

where $M_1(S_c, S_i, K_c/\sigma_c, K_i/\sigma_i)$ and $M_2(S_c, S_i, K_c/\sigma_c, K_i/\sigma_i)$, abbreviated as M_1 and M_2 respectively, are defined by

$$M_1 \equiv S_c - (S_i - S_c)\frac{1}{\frac{K_i}{\sigma_i}\frac{\sigma_c}{K_c} - 1} \tag{6.3}$$

$$M_2 \equiv (S_i - S_c)\frac{1}{\frac{K_i}{\sigma_i} - \frac{K_c}{\sigma_c}} \tag{6.4}$$

For a given set of composites, both M_1 and M_2 are constant since they depend only on the electrical and thermal properties of the two components but do not on the composition of samples. Equation (6.2) shows that the thermoelectric power S_m of binary composites should be linear function of the ratio of thermal conductivity and electrical conductivity, i.e. the Wiedeman-Franz ratio K_m/σ_m and *vice versa*. Furthermore, of the three composite variables S_m, K_m and σ_m, only two of them are independent. Equation (6.2) also shows that, at a fixed temperature, the variation of S_m in binary continuum percolation composites is entirely determined by their Wiedeman-Franz ratio, which depends on the compositions of sample. Therefore the problem of how to describe the thermoelectric power in binary continuum percolation systems can be reduced to how to describe the behavior of the Wiedeman-Franz ratio in the percolation systems. Before proceeding further in this direction, it is worthy to recall some fundamental results for the Wiedeman-Franz ratio in homogeneous materials [Busch and Schade 1976 and references therein]. For homogeneous metals and at high temperature ($T>\theta_D$, θ_D=Debye temperature), the Wiedeman-Franz ratio varies as

$$\frac{k_c}{\sigma_c} = \hat{L}T \tag{6.5}$$

where T is the absolute temperature, and $\hat{L} = \frac{\pi^2}{3}(\frac{k_B}{e})^2 = 2.45 \times 10^{-8}(V/k)^2$ is the universal Lorenz number. The physical requirement for $T \gtrsim \theta_D$ is that the relaxation time must be unchanged when an electrical field and temperature gradient are acting, that is, the same scattering processes must be responsible for both the electrical resistance and the thermal resistance. This condition is satisfied for temperatures above the Debye temperature, when inelastic scattering is dominant. However, these considerations do not apply to a semi-metal, such as graphite, where the thermal conductivity due to the electrons is low compared to that due to the phonons. The Wiedeman-Franz ratio for an insulator will be defined as K_i/σ_i, which is a very large number and is completely unrelated to free electron theory. Note that the Wiedeman-Franz ratio for percolation systems varies drastically with the compositions of samples as K_m and especially σ_m vary strongly close to the percolation threshold. But there is, to the author's knowledge, no theoretical model dealing with the ratio K_m/σ_m for binary continuum percolation composites.

In order to use the scaling theory to describe the Wiedeman-Franz ratio near percolation threshold, consider the case where

$$\frac{K_c}{\sigma_c} \cdot \frac{\sigma_i}{K_i} \ll 1 \text{ and } \sigma_i \neq 0. \tag{6.6}$$

Near the percolation threshold and at constant temperature, the Wiedeman-Franz ratio K_m/σ_m is assumed to have the scaling form [Straley 1976, Efros and Shklovskii 1976, and Bergman and Imry 1977]

$$\frac{K_m}{\sigma_m} = \frac{K_i}{\sigma_i} |\phi - \phi_c|^{h_1} \Lambda(\frac{K_c}{\sigma_c}\frac{\sigma_i}{K_i} |\phi - \phi_c|^{-(h_1+h_2)}), \tag{6.7}$$

where the scaling function $\Lambda(z)$ has the following asymptotic forms

$$\Lambda(z) \sim \begin{cases} A + Bz + \cdots & \text{for } |z| \ll 1,\ \phi > \phi_c \quad \text{Regime I} \\ B'z + \cdots & \text{for } |z| \ll 1,\ \phi < \phi_c \quad \text{Regime II} \\ A'' z^{\frac{h_1}{h_1+h_2}} & \text{for } |z| \gg 1 \quad \text{Regime III} \end{cases} \tag{6.8}$$

The parameters A, B′ and A″, that appear in (6.8), can only be determined experimentally. From the asymptotic forms of $\Lambda(z)$, and using the relation (6.2), one can deduce the following power-laws for the thermoelectric power

$$S_m - M_1 \propto \frac{M_2 K_i}{\sigma_i} \cdot (\phi - \phi_c)^{h_1} \qquad \text{for } \phi > \phi_c \tag{6.9}$$

$$S_m - M_1 \propto \frac{M_2 K_c}{\sigma_c} (\phi_c - \phi)^{-h_2} \qquad \text{for } \phi < \phi_c \tag{6.10}$$

$$S_m - M_1 \propto M_2 \left(\frac{K_i}{\sigma_i}\right)^{h_1/(h_1+h_2)} \left(\frac{K_c}{\sigma_c}\right)^{h_2/(h_1+h_2)} \qquad \text{for } \phi \simeq \phi_c \tag{6.11}$$

where h_1 and h_2 are two, probably new, critical exponents. Note that the power-laws (6.9) and (6.10) are similar in form to the percolation equation for the magnetoconductivity given in (2.42). This similarity is probably attributed to "two field" coupling in both these cases: the electrical and external magnetic fields for the magnetoconductivity, and the electrical and temperature fields for the thermoelectric power. Therefore "field coupling" would appear to lead to a difference (off-set), rather than a directly measured physical quantity, obeying a power-law. One advantage of the newly proposed percolation equations (power-laws) for thermoelectric power is that the electrical conductivity and thermal conductivity data for the composites need not be known or modelled separately when one uses (6.9) and (6.10) to fit the thermoelectric data. It is important to note that the condition (6.6), which is necessary to use the scaling theory, should apply to the present experimental study of the graphite and hexagonal boron-nitride composites in which K_i and K_c are at the same order of magnitude, but $\sigma_i/\sigma_m <<< 1$. Note that (6.11) shows that the data for a system obeying (6.9), (6.10) and (6.11) will go smoothly through the $\phi = \phi_c$ point, if $K_c\sigma_i/K_i\sigma_c$ is not zero.

6.3 Experimental Results and Discussion

The thermoelectric power for conducting G-BN parallelepiped samples, with graphite volume fractions from 0.154 to 0.82, was measured in an evaporation plant at a pressure of less than 1×10^{-5}Torr. The sample was mounted between two copper blocks, of which one was warmed up to $45°C$ by a heater and the other was cooled down to $5°C$ by cold water. Because of the very large resistance of samples on the insulating side of the percolation, the thermoelectric power for these samples could not be measured using the existing instruments. More experimental details are given in Section 3.6.

The measured thermoelectric power as a function of the graphite volume fraction is shown in Fig. 6.1, where the solid line is a best fit to the percolation equation (6.9). From this figure it is observed that the thermoelectric power over a large range of the graphite volume fractions on the conducting side is nearly constant and equal to that of $\phi = 0.82$ graphite sample. Very near the percolation threshold, the thermoelectric power shows a sudden upturn. These results are qualitatively in good agreement with the predictions made by Webman et al. (1977), using the self-consistent effective-media approximation. The thermoelectric power for the G-BN samples above the percolation threshold ϕ_c can be estimated by using the MSBL formula (6.1). In fact the following approximation holds

$$\frac{K_i}{\sigma_i}\frac{\sigma_c}{K_c} - 1 = \frac{K_i/K_c}{\sigma_i/\sigma_c} - 1 \approx 10^{17} \tag{6.12}$$

Note that $\mathbf{Min}\{K_i, K_c\} \leq K_m \leq \mathbf{Max}\{K_i, K_c\}$ for any binary composites and $1 \leq K_i/K_c \leq 10$ [Lide 1994] for the G-BN system, so that one has

$$K_m/K_c \leq 10 \tag{6.13}$$

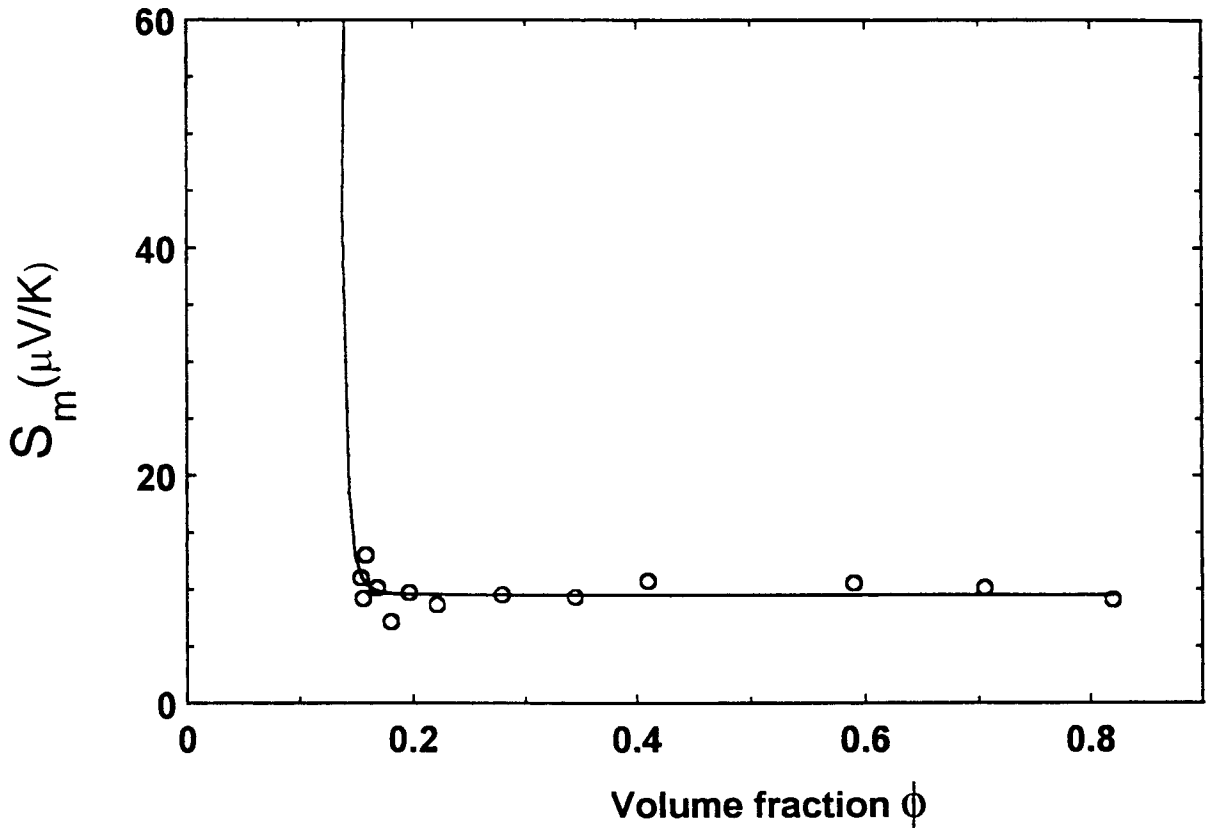

Fig. 6.1 The thermoelectric power against the volume fraction ϕ for the G-BN parallelepipeds. The solid curve is a best fit to data, using ϕ_c =0.150±0.001 and the power-law (6.9). The best fit parameters are given in the text.

On the conducting side, from Fig. 4.2a,

$$\sigma_m/\sigma_c \geq 10^{-7}/(3.5 \times 10^2) \approx 2.9 \times 10^{-9} \tag{6.14}$$

Inserting (6.12), (6.13) and (6.14) into (6.1) or (6.2), one concludes that, to first order, there is no significant change in S_m on the conducting side for the G-BN system.

As mentioned early in this section, the thermoelectric power data could be fitted to the percolation equation $(S_m - M_1) \propto (\phi - \phi_c)^{h_1}$. Since only the data on the conducting side are available, the critical volume fraction ϕ_c is fixed at 0.150±0.001, which was obtained from the electrical conductivity data (see Section 4.2), in the fitting program, while M_1, pre-factor and exponent h_1 are allowed to vary to give the best result. Note that for the G-BN system, M_1 is equal to the thermoelectric power of pure graphite sample, according to its definition given in the previous section and using the approximation (6.12). The best fit values of the parameter M_1, pre-factor and exponent h_1 are (9.51±0.01)$\mu V/K$, (0.0035±0.001)$\mu V/K$, and -1.13±0.05 respectively. The theoretical curve through the data points can thus be written as $S_m = 9.51 + 0.0035(\phi - 0.150)^{-1.13}$. This relation gives the value of S_c for graphite to be 9.51$\mu V/K$ in agreement with the measured value on the ϕ=0.82 graphite parallelepiped of (9.10±0.07)$\mu V/K$.

In order to test the MSBL equation (6.1), Hurvits, Rosenbaum and McLachlan (1993) measured the thermoelectric power and electrical conductivity at room temperature on the Al-Ge films with varying aluminum volume fractions in the range 0.20 ~1.0. As the thermal conductivity for the Al-Ge films on glass substrates cannot be measured experimentally, they used both the GEM equation and another effective medium equation to calculate the K_m from K_c(Al) and K_i(Ge). Using this data and the fitted and experimental data for σ_m, σ_i and σ_c ($\sigma_i/\sigma_c \simeq 10^{-7}$), together with a fixed value of $\phi_c = 0.56$ obtained from superconducting measurements, they found that the MSBL formula described their experimental thermoelectric power data reasonably well. Shown in Fig. 6.2a is the data of Hurvits et al. (1993) for the Al-Ge

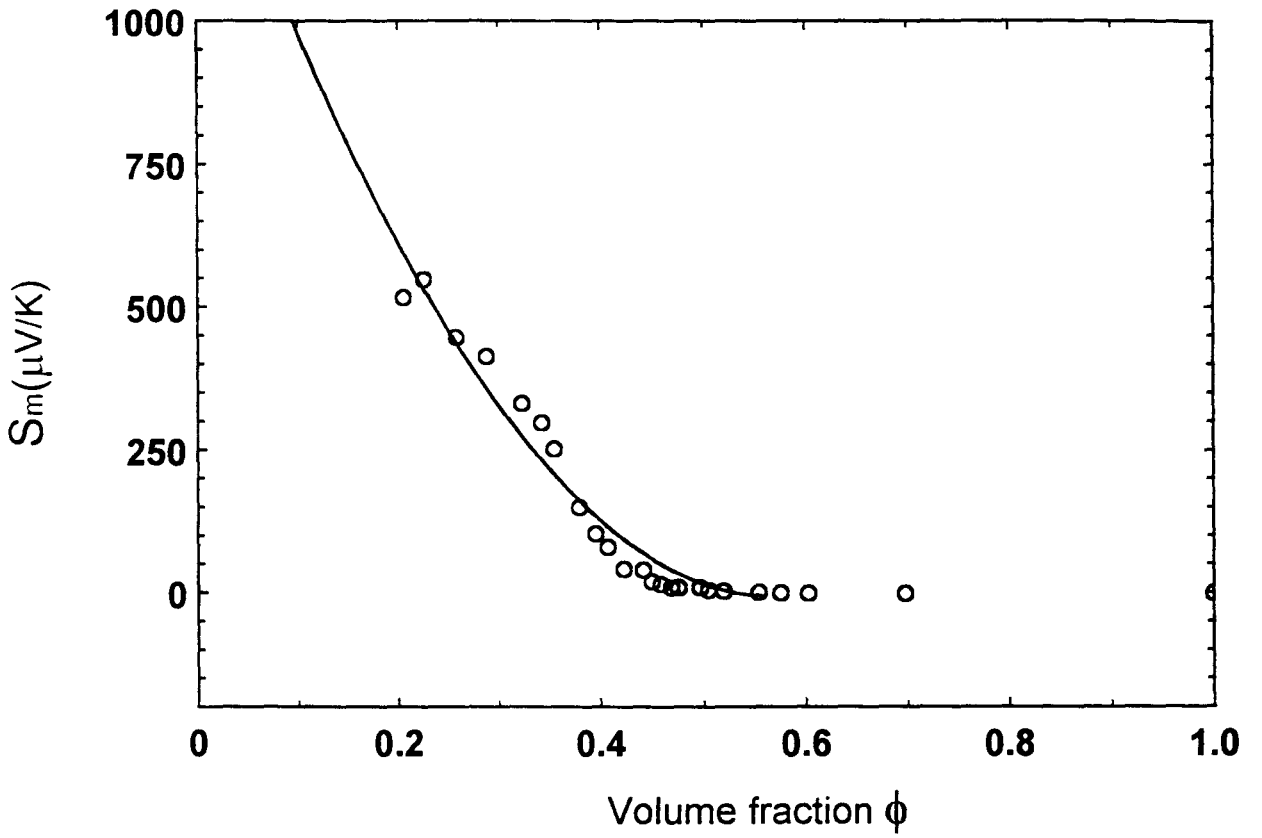

Fig. 6.2a The thermoelectric power against the volume fraction ϕ for $Al-Ge$ system. The solid curve is a best fit to data, using a fixed ϕ_c of 0.56 and the power-law (6.9). The experimental data were taken from Hurvits et al. (1993). The best fit parameters are given in the text.

system. Since $K_i(\mathrm{Ge})/K_c(\mathrm{Al}) \simeq 0.12$, the Levy and Bergman's power-laws for thermoelectric power are not applicable to the Al-Ge system. Equation (6.10) can be fitted to the data, using a fixed ϕ_c of 0.56. The best fit is S_m=-5.61+4290(0.56-ϕ)$^{1.90}$, which is plotted in Fig. 6.2a. A visual comparison of this fit to that made by Hurvits et al. (1993) shows that these two best fit theoretical lines are virtually identical. The advantage of using (6.9) and/or (6.10) is that full details of $\sigma_m(\phi)$ and $K_m(\phi)$ do not have to be known or modelled.

An alternative is to fit the thermoelectric data for the Al-Ge films simultaneously using equations (6.9) and (6.10), where the critical volume fraction ϕ_c, the parameter M_1, the prefactors and the two exponents h_1 and h_2 are all allowed to vary to give a best fit. The two solid curves through the data in Fig. 6.2b show the best fit. The common parameters in (6.9) and (6.10) are ϕ_c=0.427±0.001 and M_1=-(2.56±0.14)$\mu V/K$. On the conducting side, the exponent h_1 and pre-factor are found to be -1.19±0.02 and (0.28±0.04)$\mu V/K$ while on the insulating side, h_2 and pre-factor are determined to be -0.74±0.01 and (1702±23)$\mu V/K$, respectively. In summary, their thermoelectric power data can also be fitted to the relations S_m=2.56+0.28(ϕ-0.427)$^{-1.19}$ for $\phi > 0.427$ and S_m=2.56+1702(0.427-ϕ)$^{0.74}$ for $\phi < 0.427$. It is noted that the apparent critical volume fraction ϕ_c of 0.427 obtained here is smaller than that of 0.56 from the electrical conductivity and superconductivity data. This discrepancy is qualitatively consistent with computer simulations made by Webman et al. (1977) and Levy and Bergman (1992), who found that the thermoelectric power at ϕ_c, or even slightly smaller than it, is still nearly equal to that of the conducting component. These results imply that the percolation threshold ϕ_c, obtained directly from fitting experimental thermoelectric power data, as given above in this paragraph , could be smaller than those obtained from the measurements for other percolation physical properties, such as electrical conductivity.

These measurements of thermoelectric power on the systems G-BN and Al-Ge seem to be the only experimental studies of the critical behavior of thermoelectric power in percolation systems. The good agreement between theory and experiment

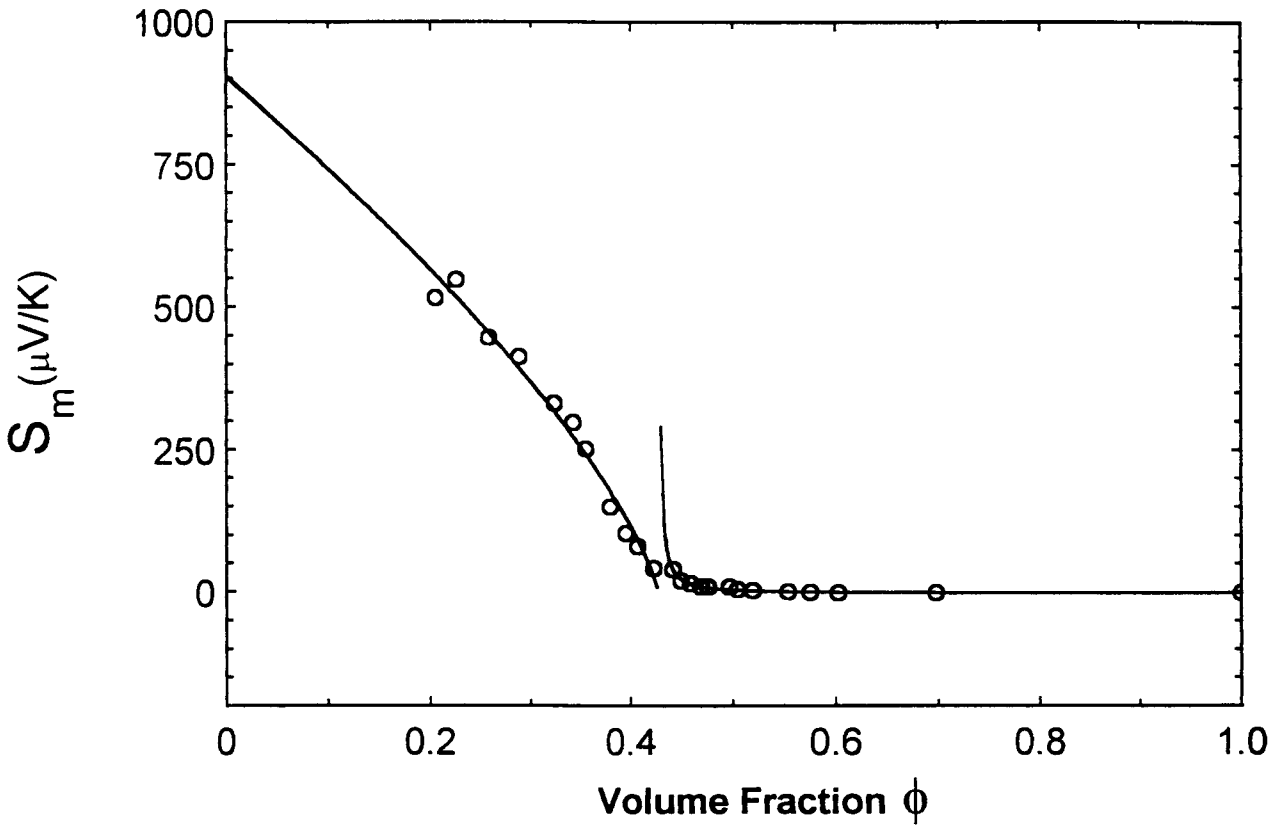

Fig. 6.2b The thermoelectric power against the volume fraction ϕ for $Al-Ge$ system [Hurvits et al. 1993]. The solid curves are a least squares fit of the power-laws (6.9) and (6.10) to data: S_m =-2.56+0.281(ϕ-0.427)$^{-1.19}$ for ϕ >0.427 and S_m=-2.56+1702(0.427-ϕ)$^{0.74}$ for ϕ <0.427. Note that the critical volume fraction ϕ_c determined by this method is 0.427.

in both these two cases shows the validity of the two percolation equations (6.9) and (6.10) derived from the MSBL formula (6.1). However, the two percolation equations (6.9) and (6.10) for the thermoelectric power on both sides of percolation threshold, proposed in this thesis, need to be tested by more accurate experimental investigations, preferably with very good data on both sides of ϕ_c.

6.4 Summary

Based on the MSBL formula, it has been shown that the thermoelectric power of binary continuum composites is a linear function of the Wiedeman-Franz ratio. A scaling scheme for the Wiedeman-Franz ratio near the percolation threshold in binary continuum percolation systems has been proposed. When incorporated into a modified MSBL formula, this scaling hypothesis results in the two new percolation equations (power-laws) for the thermoelectric power near and on both sides of the percolation threshold. The new power-laws for thermoelectric power have a form similar to the one for the magnetoconductivity, probably due to "two field" coupling in these two cases. The thermoelectric power data obtained from the G-BN samples on the conducting side are in accordance with the self-consistent effective-media approximation due to Webman et al. (1977), and the MSBL formula. The newly proposed percolation equations for thermoelectric power can fit the experimental thermoelectric data obtained both from the G-BN percolation system and from the Al-Ge one very well. Levy and Bergman's percolation equations are not suitable for fitting the data for these two systems.

Chapter 7

SUMMARY, CONCLUSION AND PROPOSALS FOR FUTURE WORK

The G-BN compressed disc system and powder mixtures undergoing compression have proved to be very good continuum percolation systems, upon which a number of typical percolation measurements have been made, and many theoretical percolation models have been tested. The various critical exponents measured for the G-BN systems cannot be explained using a single percolation model.

The critical volume fraction ϕ_c=0.150 for the G-BN disc samples can be explained by the existing models [Kusy 1977 and Balberg et al. 1984]. The slightly smaller value of $\phi_c \approx 0.12$ obtained from the four different types of power experiments (in axial direction: DC and AC; in transverse direction: DC and AC) are attributed to the presence of cavities of approximately 7 times the size of the graphite grains. The conductivity exponents are found to be $t = 2.63$ and 2.68 in the axial and transverse directions, respectively, for the disc samples, and $t \simeq 4.8$ and 6.1 in the axial and transverse directions for both the 50%G-50%BN and 55%G-45%BN powders. As one can fit the conductivity data with a single conductivity exponent of t=2.74 over entire volume fraction range on the conducting side (0.150 $\sim$ 0.82), a single metallic con-

duction mechanism must be responsible to the electrical conduction for all the disc samples with $\phi > \phi_c$. The exponent $\bar{s}$ obtained from the conductivity measurements on the insulating side does not appear to be related to the dielectric constant exponent s. However, the values of exponent $\bar{s}$, which describes the divergence behavior of conductivity for $\phi < \phi_c$, are not well understood [Chpater 15, Deutscher et al. (Ed.) 1983].

Close to the percolation threshold it has been observed that the AC conductivity and dielectric constant vary with frequency as $\sigma(\phi,\omega) \propto \omega^x$ and $\varepsilon(\phi,\omega) \propto \omega^{-y}$. The measured exponents x and y for the disc system and two powders are in excellent agreement with the predictions of intercluster polarization model in spite of the unusual large values of conductivity exponent t obtained from the DC conductivity data. Unfortunately, the anomalous diffusion model cannot be checked quantitatively due to the lack of knowledge of exponents ν and θ for the G-BN systems. The exponent q, which describes the power-law behavior of the crossover frequency ω_c against the DC conductivity, has also been measured. On the conducting side, the measured q values are all less than the predictions of the intercluster polarization model, even using the observed exponents t and s. Furthermore, the observed values of ω_c for the powders undergoing compression are several orders of magnitude larger than the theoretically predicted ones. On the insulating side, the frequency response of the imaginary part of the AC complex conductivity, $\omega \cdot \varepsilon(\phi,\omega)$ against ω, collapsed into a single straight line when normalized by the DC conductivities for the same sample. This behavior results in a measured $\omega_c \sim 1$ and consequently $q \sim 0$, for all the insulating samples. This result can not be explained using any of the existing percolation models and there is no published experimental result available for comparison. The shallow global minima in the loss tangent $\tan\delta$ as a function of frequency for the insulating samples near the percolation threshold are not in agreement with computer simulations based on the R-C model [Clerc et al. 1990]. These two anomalies cannot be resolved in this study.

The magnetoconductivity exponent t_m in a field of 1.5T is found to be 3.08. This

value is clearly larger than the measured conductivity exponent of t=2.68. This result contradicts the only existing theoretical model [Bergman 1987], which predicts the same value for the conductivity exponent t and magnetoconductivity exponent t_m. The observed relative magnetoresistivity exponent g_c of 0.28 is in agreement with that obtained from granular percolation Sn-Ar films [Rohde and Micklitz 1989]. Since the microstructures of the G-BN and Sn-Ar are topologically very different, the same magnetoresistivity exponent suggests that the difference between the two experimental results and the single theoretical prediction is a fundamental one.

The excess noise measured in the G-BN conducting disc and parallelepiped samples is typically $1/f^{\gamma}$ with the exponent γ ranging from 0.98 to 1.08. Near the percolation threshold the normalized $1/f$ noise power diverges as $S_{V^2}/V^2 \propto R^w$ with exponents $w = 1.47$ and 1.72 in the axial and transverse directions respectively. These two exponents are close to the prediction of a metal-metal contact noise model in the Sharvin regime and using the self-consistent effective medium approximation.

The relation $S_V/V^2 \propto (Volume)^{-0.56}$ for the samples near the percolation threshold is the first experimental investigation in binary continuum percolation systems, and the results could be used to test the theoretical models developed by Rammal et al. (1985b). The noise exponent b, appeared in the relation $S_V/V^2 \propto L^{-b}$, is found to be 1.68. This value for b is outside the estimated range $1.1 \sim 1.26$, obtained from computer simulations on three dimensional discrete lattices [Rammal et al. 1985a, Tremblay et al. 1986].

The thermoelectric power in a binary composite has been shown to be a linear function of the Wiedeman-Franz ratio. A scaling scheme for the Wiedeman-Franz ratio in percolation systems has been proposed in this thesis. This scaling hypothesis, when used in conjunction with the MSBL formula, results in two new power-laws for the thermoelectric power, one on each side of the percolation threshold. These two power-laws can be written as $(S_m - M_1) \propto (\phi - \phi_c)^{h_1}$ on the conducting side of the percolation and as $(S_m - M_1) \propto (\phi_c - \phi)^{-h_2}$ on the insulating side. One advantage of

these two percolation equations is that the electrical conductivity and thermal conductivity data for the composites do not have to be known separately when one uses these equations to fit experimental thermoelectric data.

The thermoelectric power data obtained from the G-BN samples with $\phi \geq \phi_c$ are in good agreement with predictions based on the self-consistent effective-medium approximation [Webman et al. 1977] and the MSBL theory. The new power-laws for thermoelectric power fit the experimental data, obtained from the G-BN percolation system and from a series of Al-Ge granular films [Hurvits et al. 1993].

The studies of percolation phenomena associated with the G-BN systems point out that several investigations still need to be done. For example, on experimental side, a systematic study of grain size dependence of conductivity exponent t is required as this dependence has been noted by Chen and Jonhson (1991). This suggestion is motivated and imitated by the investigations carried out by Kusy (1977) and Dovzhenko and Zhirkov (1995) in which it is found that the critical volume fraction varies with the ratio of the conducting grain size to the insulating grain size.

As only two experiments on the magnetoconductivity of percolation systems have been performed up till now, more data, using different percolation systems, is needed to resolve the fundamental differences between the two observations and the single theory.

The power-laws for the thermoelectric power in percolation systems, proposed in this thesis, need to be tested using more and more accurate experimental data.

On the theoretical side, it has been noted in Chapter 5 that, for the Swiss-cheese model the scaling behavior of the smallest neck width, $\delta \propto(\phi - \phi_c)^{\varphi}$, determines the conductivity exponent t and noise exponent w [Halperin et al. 1985, Garfunkel and Weissman 1985]. Only two cases, with $\varphi = 1$ and 2, have been studied. Neither of these calculations can explain the t and w values that have been observed in the G-BN

systems. Further investigation on the relation between the values of the exponents t and w and that of the exponent φ is needed.

Bibliography

[1] Albers A., Ph.D thesis, University of the Witwatersrand (1994).

[2] Alexander S. and Orbach R., J. Physique Lett. (Paris), **43**, L625 (1982).

[3] Balberg I. and Bozowski S., Solid St. Commun. **44**, 551 (1982).

[4] Balberg I., Anderson C. H., Alexander S. and Wagner N., Phys. Rev. B**30**, 3933 (1984).

[5] Balberg[a] I., Phys. Rev. Lett. **59**, 1305 (1987).

[6] Balberg[b] I., Phil. Mag. **B56,** 991 (1987).

[7] Benguigui L., J. Physque Lett. **46**, L-1015 (1985).

[8] Bergman D. J. and Imry Y., Phys. Rev. Lett. **39**, 1222 (1977).

[9] Bergman D. J. and Stroud D., Phys. Rev. B**32**, 6097 (1985).

[10] Bergman D. J., Phil. Mag. B**56**, 983 (1987).

[11] Bergman D. J. and Stroud D., in *Solid State Physics* **46,** edited by Ehrenneich H. and Turnbull D., Academic Press, San Diego (1992).

[12] Bergman D. J. and Levy O., J. Appl. Phys. **70**, 6821 (1991).

[13] Broadbent S. R. and Hammersley J. M., Proc. Camb. Philos. Soc., **53**, 629 (1957).

[14] Busch G. and Schade H., *Lectures on Solid State Physics*, Pergamon (1976).

[15] Carmona F., Prudhon P., and Barreau F., Solid St. Commun. **51**, 255 (1984).

[16] Chakrabarty R. K., Bardhan K. K. and Basu A., J. Phys.: Condens. Matter **5**, 2377 (1993).

[17] Chen C. C. and Chou Y. C., Phys. Rev. Lett. **54**, 2529 (1985).

[18] Chen I. G. and Johnson W. B., J. Mat. Science **26**, 1565 (1991).

[19] Chou Y. C. and Jaw T. S. , Solid St. Commun. **67**, 753 (1988).

[20] Clarkson M. T. and Smedley S. I., Phys. Rev. A **37**, 2070 (1988).

[21] Clerc J. P., Giraud G., Laugier J. M. and Luck J. M., Adv. Phys. **39**, 191 (1990).

[22] Dai U., Palevski A. and Deutscher G., Phys. Rev. B**36,** 790 (1987).

[23] Deprez N. and McLachlan D. S., J. Phys. D.: Appl. Phys. **21,** 101 (1988).

[24] Deptuck D., Harrison J. P. and Zawadski P., Phys. Rev. Lett. **54**, 913 (1985).

[25] Deutscher G. and Rappaport M. L., J. Phys. Lett. (Paris) **40**, L219 (1979).

[26] Deutscher G., Zallen R. and Adler J. (editors), *Percolation Structures and Processes,* Annals of the Israel Physical Society, Vol.5 (1983).

[27] Dovzhenko A. Y. and Zhirkov P.V., Phys. Lett. A**204**, 247 (1995).

[28] Dutta P. and Horn P. M., Rev. Mod. Phys. **53**, 497 (1981).

[29] Efros A. L. and Shklovskii B. I., Phys. Stat. Sol. (b) **76**, 475 (1976).

[30] Essam J. W., Rep. Prog. Phys., **43**, 833 (1980).

[31] Feng S., Halperin B. I. and Sen P. N., Phys. Rev. B**35**, 197 (1987).

[32] Fisher M.E., Physics, **3**, 255 (1961).

[33] Fitzpatrick J. P., Malt R. B. and Spaepen F., Phys. Lett. A**47**, 207 (1974).

[34] Fizazi A., Moulton J., Pakbaz K., Rughooputh S. D. D. V., Smith P. and Heeger A. J., Phys. Rev. Lett. **64**, 2180 (1990).

[35] Frisch H. L. and Hammersley J. M., J. Soc. Indust. Appl. Math. **11**, 894 (1963).

[36] Garfunkel G. A. and Weissman M. B., Phys. Rev. Lett. **55**, 296 (1985).

[37] Gefen Y., Aharony A. and Alexander S., Phys. Rev. Lett. **50**, 77 (1983).

[38] Girand G., Clerc J. P., Orsal B. and Laugier J. M., Europhys. Lett. **3**(8), 935 (1987).

[39] Grannan D. M., Garland J. C. and Tanner D. B., Phys. Rev. Lett. **46**, 375 (1981).

[40] Grave I., Deutscher G. and Alexander S., Phys. Rev. Lett. **48**, 1497 (1982).

[41] Halperin B. I., Feng S. and Sen P. N., Phys. Rev. Lett. **54**, 2391 (1985).

[42] Harris A. B., Phys. Rev. B**28**, 2614 (1983).

[43] Herring C., J. Appl. Phys. **31**, 1939 (1960).

[44] Hooge F. N., Phys. Lett. A**29**, 139 (1969).

[45] Hooge F. N., Kleinpenning T. G. M. and Vandamme L. K. J., Rep. Prog. Phys., **44**, 480 (1981).

[46] Hundley M. F. and Zettl A., Phys. Rev. B**38**, 10290 (1988).

[47] Hurvits G., Rosenbaum R. and McLachlan D. S., J. Appl. Phys. **73**, 7441 (1993).

[48] Kang W. N., Kim D. H., Park J. H., Hahn T. S., Choi S. S. and Gray K. E., Physica C**233**, 402 (1994).

[49] Kirkpatrick S., Rev. Mod. Phys. **45**, 574 (1973).

[50] Kirkpatrick S., in *Proceedings of Les Houches Summer School on Ill-Condensed Matter* (edited by Balian R., Maynard R. and Toulouse G.), North-Holland, Amsterdam (1979).

[51] Koch R. H., Laibowitz R. B., Alessandrini E. I. and Viggiano J. M., Phys. Rev. B**32**, 6932 (1985).

[52] Kogut P. M. and Straley J. P., J. Phys. C.: Solid State Phys. **12**, 2151 (1979).

[53] Kolek A. and Kusy A., Phys. Rev. B**43**, 11274 (1991).

[54] Kusy R. P., J. Appl. Phys. **48**, 5301 (1977).

[55] Laibowitz R. B. and Gefen Y., Phys. Rev. Lett. **53**, 380 (1984).

[56] Laugier J. M., Thèse de Troisième cycle, Universitè de Provence, Marseille (1982).

[57] Laugier J. M., Thèse d'Etat, Universitè de Provence, Marseille (1987).

[58] Laugier J. M., Clerc J. P. and Girand G., in *Proceedings of International AMSE Conference*, edited by Mesnard G., Lyon: AMSE (1986).

[59] Lee J.-W., See S. K., Kim J.-J. and Kim H. C., J. Korean Phys. Soc. **26**, 683 (1993).

[60] Lee S., Song Y., Noh T., Chen X. and Gaines J. R., Phys. Rev. B**34**, 6719 (1986).

[61] Leeman C., Skove M. J. and Stillwell E. P., Solid State Commun. **35**, 97 (1980).

[62] Levinshtein M. E., Shur M. S. and Efros A. L., Zh. Eksp. Teor. Fiz. **69**, 2203(1975)(Sov. Phys. -JETP, **42**, 1120 (1976)).

[63] Levy O. and Bergman D. J., J. Phys. A: Math. Gen. **25**, 1875 (1992).

[64] Lide D. R. (editor-in-chief), *CRC Handbook of Chemistry and Physics,* CRC Press (1994).

[65] Lin J. J., Phys. Rev. B**44**, 789 (1991).

[66] Lynch R. W. and Drickamer H. G., J. Chem. Phys. **44**, 181 (1966).

[67] Malliaris A. and Turner D. T., J. Appl. Phys. **42**, 614 (1971).

[68] Mantese J. V., Curtin W. A. and Webb W. W. Phys. Rev. B**33**, 7897 (1986).

[69] Mantese J. V. and Webb W. W., Phys. Rev. Lett. **55**, 2212 (1985).

[70] McLachlan D. S., J. Phys. C**19**, 1339 (1986).

[71] McLachlan D. S., Electrically Based Microstructural Characterization, edited by Gerhardt R. A., Taylor S. R., and Garboczi E. J., MRS Proceedings **411** (1996).

[72] McLachlan D. S., Blaskiewicz M. and Newnham R. E., J. Am. Ceram. Soc. **73**, 2187 (1990).

[73] McLachlan D. S., J. Appl. Phys. **70,** 3681 (1991).

[74] Michels M. A. J., Brokken-Zijp J. C. M., Groenewoud W. M. and Knoester A., Physica A **157**, 529 (1989).

[75] Milgrom M. and Shtrikman S., Phys. Rev. Lett. **62**, 1979 (1989).

[76] Moha-Ouchane M., Peyrelasse J. and Boned C., Phys. Rev. A **35**, 3027 (1987).

[77] Nan Ce-Wen, Prog. in Mat. Science **37**, 1 (1993).

[78] Nitsch K., Dziedzic A. and Golonka L., Int. J. Electronics **69,** 515 (1990).

[79] Octavio M., Gutierrez G. and Aponte J., Phys. Rev. B**36**, 2461 (1987).

[80] Peyrelasse J., Moha-Ouchane M. and Boned C., Phys. Rev. A**38**, 904 (1988).

[81] Pierre C., Deltour R., Van Bentum J., Perenboom J. A. A. J. and Rammal R., Phys. Rev. B**42**, 3386 (1990).

[82] Pike G. E., in *Electrical Transport and Optical Properties of Imhomogeneous Media,* Edited by Garland J. C. and Tanner D. B., AIP Conf. Proc. **40**, 366 (1978).

[83] Putley E. H., *The Hall Effect and Related Phenomena,* Butterworths, London (1960).

[84] Rajab M. and Coleman D. S., Powder Metall. **28**, 207 (1985).

[85] Rammal R. and Toulouse G., ibid, **44**, L13 (1983).

[86] Rammal R., Phys. Rev. Lett. **55**, 1428 (1985).

[87] Rammal[a] R., Tannous C., Breton P. and Tremblay A. M. S., Phys. Rev. Lett. **54**, 1718 (1985).

[88] Rammal[b] R., Tannous C. and Tremblay A. M. S., Phys. Rev. A**31**, 2662 (1985).

[89] Reynolds W. N., *Physical Properties of Graphite,* Elsevier Materials Science Series (1968).

[90] Rohde M. and Micklitz H., Physica A**157**, 120 (1989).

[91] Rudman D. A., Caladreze J. J. and Garland J. C., Phys. Rev. B**33**, 1456 (1986).

[92] Scher H. and Zallen R., J. Chem. Phys. **53**, 3759 (1970).

[93] Schirmacher W., J. Phys. A: Math. Gen. **27**, L727 (1994).

[94] Skal A. S. and Shklovskii B.I., Fiz. Tekh. Poluprov., **8**, 1586(1974)(Sov. Phys.-Semicond., **8**, 1029 (1975)).

[95] Smilauer P., Contemporary Physics, **32**, 89 (1991).

[96] Song Y., Lee S.-I. and Gaines J. R., Phys. Rev. B**46**, 14 (1992).

[97] Song Y., Misra A., Cao Y. Querubin A., Chen Xiao-Deng, Crooker P. P. and Gaines J. R., Physica C**172**, 1 (1990).

[98] Song Y., Noh T. W., Lee S. I. and Gaines J. R., Phys. Rev. B**33**, 904 (1986).

[99] Stauffer D. S. and Aharony A., *Introduction to Percolation Theory,* 2nd Ed., Taylor and Francis (1994).

[100] Stephen M. J., Phys. Rev. B**17**, 4444 (1978).

[101] Straley J. P., J. Phys. C: Solid St. Phys. **9**, 783 (1976).

[102] Straley J. P., Phys. Rev. B**15**, 5733 (1977).

[103] Straley J. P., J. Phys. C: Solid St. Phys. **13**, L773 (1980).

[104] Straley J. P., J. Phys. D**14**, 2101 (1981).

[105] Stroud D. and Bergman D. J., Phys. Rev. B**25**, 2061 (1982).

[106] Takagi K., Mizunami T., Suzuki J. I. and Masuda S., IEEE Trans. Components, Hybrids, Manuf. Technol., Vol. CHMT-9, 141 (1986).

[107] Testa J. A., Song Y., Chen X. D., Golben J., Lee S. I., Patton B. R. and Gaines J. R., Phys. Rev. B**38,** 2922 (1988).

[108] Tremblay A. M. S., Feng S. and Breton P., Phys. Rev. B**33**, 2077 (1986).

[109] Tremblay A. M. S., Fourcade B. and Breton P., Physica A**157**, 89 (1989).

[110] Van Dijk M. A., Phys. Rev. Lett., **55**, 1003 (1985).

[111] Van Dijk M. A., Casteleijn G., Joosten J. G. H., and Levine Y. K., J. Chem. Phys. **85**, 626 (1986).

[112] Vandamme L. K. J., IEEE Trans. Components, Hybrids, Manuf. Technol., Vol. CHMT-10, 290 (1987).

[113] Webman I., Jortner J. and Cohen M. H., Phys. Rev. B**16**, 2959 (1977).

[114] Webman I., Phys. Rev. Lett. **47**, 1496 (1981).

[115] Weissman M. B., Rev. Mod. Phys. **60**, 537 (1988).

[116] Wilkinson D., Langer J. S. and Sen P. N., Phys. Rev. B**28,** 1081 (1983).

[117] Williams J. L. and Burdett R. K., J. Phys. C **2**, 298 (1969).

[118] Yoon S. and Lee S.-I., Physica B**167**, 133 (1990).

[119] Zallen R., *The Physics of Amorphous Solids,* Wiley, New York (1983).